Development and Evaluation of a Thermophoretic Personal Sampler for Nanoparticle Exposure Studies

Von der Fakultät für Ingenieurwissenschaften, Abteilung Maschinenbau der
Universität Duisburg-Essen
zur Erlangung des akademischen Grades

DOKTOR-INGENIEURIN/
DOKTOR-INGENIEUR

genehmigte Dissertation

von

Nkwenti Azong-Wara
aus
Victoria, Kamerun

Referent: Prof. Dr.-Ing. Dieter Bathen
Korreferent: Prof. Dr. Jing Wang
Tag der mündlichen Prüfung: 26.02.2013

"…For to be free is not merely to cast off one's chains, but to live in a way that respects and enhances the freedom of others…"

Nelson Mandela in: *Long Walk to Freedom*

Dedicated to my parents Pauline and Andrew Azong-Wara for showing me the way

Acknowledgment

I would like to acknowledge the following people who have supported me in the past years not only with regards to this thesis.

Thank you Prof. Dr.-Ing. Dieter Bathen and Prof. Dr. Jing Wang for accepting to review my thesis.

Very special thanks to Prof. Dr.-Ing. Heinz Fissan for introducing me to research and for helping me realize my potential. For the many scientific discussions which have pushed me to develop and improve as a scientist.

My unending gratitude to Dr.-Ing. Christof Asbach for holding my hand and walking with me throughout these past five years. Without your encouragement, input and support, this work would never have been possible

To Dr. rer. nat. Burkhard Stahlmecke, I say thank you for all the work you put in for me. Your expertise and energy especially concerning SEM were found to be invaluable in the realization of this work. Words alone cannot fully express the extent of my gratitude

Thank you Dr. rer. nat. Thomas Kuhlbusch and the LUNANA Team (Carmen Nickel, Dr. Ulrich Quass, Dr. Astrid John, Dr. Brian Hellack, Dr. Lavanya Ravi, Heike Glaser, Heinz Kaminski, Uwe Rating, Till van de Zwaag) at IUTA for being like a family to me.

To my friends in Germany, Cameroon, UK and USA as well as my team mates at Duisburg United e.V., I say thank you for all the support.

To my extended family in Germany, Awa'ah, Ngekwi and Sis. Patience, you are the reason why I am able to get up in the morning and push on.

To my brothers and sisters, Tabe, Ayuk, Ngenjang, Nchotie, Ebot, family is everything.
Thank you to my father and mother for always believing. In the rough tides, you were always my anchor.

To my wife Bonjeh and to my children, Tamasang, Madiba and Awu, life only makes sense because you are in it. You give me joy and hope and without you, I am nothing. I thank you for being part of my life. Every success I enjoy is motivated by you.

Lastly, I would like to thank the Federal Institute for Occupational Safety and Health (Bundesanstalt für Arbeitsschutz und Arbeitsmedizin), BAuA for financially supporting this work.

Abstract

Some Nanoparticles have been shown to cause adverse health effects. Assessment of personal exposure to these nanoparticles is a major step towards evaluating this potential risk. Assessment measurements of fine and coarse particles have been carried out mainly with samplers consisting of a miniaturized impactor with a defined cut off size followed by a filter for off-line weighing. This approach is unsuitable for nanoparticles due to their low mass. One applicable way of sampling nanoparticles is by employing the principle of thermophoresis.

In this thesis, a personal sampler (Thermal Precipitator, TP) which thermophoretically samples particles, was developed based on CFD-modelling. The objective was to uniformly deposit a representative sample of nanoparticles on a substrate to simplify the subsequent off-line Scanning Electron Microscopy (SEM) analysis by minimising the analysis time. Numerical simulations provided information about the deposition characteristics and this was used as the basis to develop the sampler.

Laboratory tests were carried out with the TP using monodisperse PSL particles of 95,6 nm and 305 nm in diameters as well as polydisperse soot particles in the size range of about 14 – 98 nm. The particles were sampled with the TP on substrates and later analysed by SEM. Different locations along the entire length of the substrate were investigated. A more detailed analysis was made of the evaluation region on the substrate, where a uniform deposition of particles is expected according to the prior modelling.

Experimental results show a homogeneous deposition of particles up to a size range of 300 nm in the evaluation region independent of particle material type as well as the orientation of the device during sampling. Independence of deposition is important since the worker is mobile in all directions

Unlike with an older version of the TP where up to 32 SEM images of its non-uniform particle deposition had to be evaluated to obtain an average particle size distribution, an evaluation of the uniform deposition with the new TP is much more simplified, remarkably reducing the time and cost of the evaluation, while improving the statistics of the results.

Table of Contents

List of Tables

List of Figures

Nomenclature

Symbol (Unit)	**Meaning**
C_c	Cunningham slip correction factor
$C\ (1/m^3)$	Particle number concentration
$D_p\ (m)$	Particle Diameter
N	Total number of particles counted on all SEM images of TP1 substrate(s)
$\overline{N}$	Mean number of particles counted on TP2 SEM images
$A_1\ (m^2)$	Area of first deposition stripe of a TP1 substrate
$A_2\ (m^2)$	Area of second deposition stripe of a TP1 substrate
$A_{14}\ (m^2)$	Combined area of 28 SEM images from TP1 substrates
$A_S\ (m^2)$	Area of an SEM image from TP2 substrates
$\beta\ (m/s)$	Correction factor for calculating particle number concentration from the mean particle count on TP2 substrates
$t\ (s)$	Sampling times with TP
$Q\ (m^3/s)$	Flow rate
$v_g\ (m/s)$	Terminal gravitational velocity
$g\ (m/s^2)$	Gravitational acceleration
$\eta\ (Kg/ms)$	Dynamic viscosity of the carrier gas
$\rho_g\ (Kg/m^3)$	Density of the carrier gas
$\rho_p\ (Kg/m^3)$	Density of the particle
Kn	Knudsen number
$\lambda\ (m)$	Mean free path of gas molecules
$v_T\ (m/s)$	Thermophoretic velocity
$\nabla T\ (K/m)$	Temperature gradient
H_T	Thermophoretic coefficient
$v\ (m^2/s)$	Kinematic viscosity
$T\ (K)$	Absolute temperature of particle
C_s	Thermal creep coefficient
C_t	Thermal jump coefficient
C_m	Velocity jump coefficient

k_g *(W/mK)*	Thermal conductivity of carrier gas
k_p *(W/mK)*	Thermal conductivity of particle
L (m)	Worst case deposition distance
x (m)	Gap distance between plates
v_f *(m/s)*	Flow velocity in the TP
ΔT	Temperature difference
Z_P *(m²/Vs)*	Electrical mobility of particle
α *(1/K)*	Linear temperature coefficient
N_{cf}	Number of particle tracks investigate for TP2 inlet simulations
N_{TP}	Analytically calculated number of particle tracks into the inlet of the TP2
N_{mod}	Numerically modelled number of particle tracks into the inlet of the TP2

1 Introduction and motivation

The use of nanoparticles in new applications and products has continued to increase rapidly over the last decade. Nanoparticles here denote all particles < 100 nm diameter in at least one dimension independent of their state of agglomeration. Their unique properties which include high surface area to volume ratio enable new and previously unknown applications. According to the Woodrow Wilson database (*www.nanotechproject.org*, March 2011), the enlisted number of nanotechnology-based consumer products has continued to rise at a regular pace from about 50 enlisted products in 2005 to over 1300 in 2011. These products come from all sections of the industry from health and fitness, to automotive, food and electronics.

Some nanoparticles have however also been reported to potentially induce adverse health effects (Donaldson et al, 1998, 2002; Oberdörster, 2001; Oberdörster et al., 2002; Gilmour et al., 2004; Borm et al., 2006) and the need for thorough risk assessment has been identified (Maynard and Kuempel, 2005). The risk of nanoparticles is not only a function of their potential hazard, but also of the exposure thereto. Minimizing any risk from nanomaterials, including nanoparticles will enhance the acceptance of nanoproducts and therefore contribute to a sustainable development of this emerging technology. Assessing the exposure to nanoparticles, e.g. at workplaces during nanoparticle production or handling, is therefore one important step towards a sustainable nanotechnology (Fissan, 2008).

In general there are several ways of assessing exposure to nanoparticles. Exposure can be measured by stationary measurements, using established aerosol monitoring equipment. Kuhlbusch et al. conducted one of the first thorough studies on particle characteristics in bag filling areas (2004) as well as in reactor and pelletizing areas (2006) of soot production. The measured particle and aerosol quantities included number size distribution, mass concentration and chemical composition of the particles. Exposure measurements with high spatial resolution can be performed by mapping, whereby the particle number concentration and/or size distribution is measured with mobile instruments, while at the same time the exact measurement location is recorded. As a result, maps can be constructed of the area of interest, showing the spatially resolved particle number concentration. Peters et al. (2006) used condensation particle counters and optical particle counters to map both the number and mass concentration in an engine machining and assembly facility. In a later study, Evans et al. (2008) used the same technique to map number and mass concentrations in an automotive grey iron foundry. In both studies this technique allowed the investigators to

identify particle sources within the respective investigated facility. Most of these on-line methods for assessing the exposure to nanoparticles make use of equivalent properties such as the electrical mobility or the aerodynamic diameter of the particles. The morphology and diffusion equivalent size of the measured nanoparticles can be at best approximated with such methods. All these methods do not take the movement of the worker and change in particle concentration into account. These types of exposure measurements are therefore not suitable in determining the exposure of a mobile worker.

Another big challenge in assessing nanoparticle exposure is the ever-present (sometimes in very high concentration) background ultrafine particles which may be as a result of e.g. combustion, evaporation and/or condensation processes. These high background concentrations can sometimes overwhelm the concentration of the present engineered nanoparticles such that an accurate measurement of the released nanoparticles is very difficult especially using on-line measurement techniques. The process which leads to the release of ultrafine background particles is also more often synchronous with the activation of the potential nanoparticle source. Kuhlbusch et al. (2004) tried to distinguish the ever-present background particles from the released particles in bag filling of soot production in the workplace, by performing a secondary simultaneous measurement at a location representative for the background. They showed that butane gas powered forklift can be a dominant source of ultrafine particles. In an engine machining and assembly facility, Peters et al. (2006) found very high concentrations in the order of 10^6 1/cm^3 in supply air heated by natural gas burners compared to the ultrafine particle number concentrations attributed to metal-working operations ranging from $2.5*10^5$ to $7.5*10^5$ 1/cm^3.

A way of assessing the personal exposure of workers to (nano-) particles is by the use of personal particle samplers, taking samples in the breathing zone of the worker. Especially in the context of epidemiological or risk assessment studies, personal sampling methods provide a more accurate picture of the exposure of a worker to nanoparticles. Due to the off-line analysis method of most personal samplers, background particles can be differentiated from engineered nanoparticles through subsequent electron microscopic analysis of the sample. The morphology and chemical composition of the measured particles can be evaluated more accurately with similar off-line techniques. Personal particle samplers have been widely used in a large variety of versions. Most common versions consist of a miniaturized impactor with a defined cut off size and an after filter. In an impactor, particles are deposited according to their inertia. An impactor can be designed to deposit all particles above a certain cut off size and let all smaller particles penetrate e.g. to be collected on an after filter for consecutive analysis.

Common commercial personal impactor samplers (e.g. Model 200 Personal Environmental Monitor, MSP Corp., Shoreview, MN, USA) use single stage impaction with cut off sizes in the micrometer size range, in case of the MSP impactors either 2.5 µm or 10 µm. Sioutas et al. (1999) designed two impactors with cut off sizes of 2.5 µm and 1.0 µm, respectively. Other personal impactor samplers use several stages with different cut off sizes to further differentiate the size fractions (Rubow et al., 1987; Misra et al., 2002; Lee et al., 2006; Wu and Vincent, 2007; Tsai et al., 2008). The deposited material on each stage can further be analyzed for its mass and chemical composition. All these impactor samplers have the common characteristic that the particles collected on the impaction stages are much larger in size compared with nanoparticles because of the very low inertia of nanoparticles. While sampling nanoscale particles by impaction is generally possible by reducing the pressure (Hering et al., 1978, 1979; Keskinen et al., 1992), this is not feasible for personal samplers because of the requirement of a larger pump causing significantly increased power consumption.

Another way of sampling particles for consecutive analysis is by electrostatic precipitation. Cardello et al. (2002) presented a personal wire-tube electrostatic precipitator (ESP) and showed that the collection efficiency is $\geq$ 95 % for all particles $\geq$ 15 nm if an appropriate flow rate was chosen. In the ESP, particles are charged by a corona discharge surrounding a wire electrode. This corona discharge is known to produce ozone and oxides of nitrogen (Viner et al., 1992; Martinez and Brandvold, 1996; Boelter and Davidson, 1997; Asbach et al., 2005), which may be irritant if used in a personal sampler. Furthermore such an ESP requires the use of a high voltage, which may reduce its acceptance.

If time resolution is considered in addition to the spatial resolution, the possibilities get very limited. Patashnick et al. (1980) developed a personal oscillating microbalance (TEOM series 3600 personal dust monitor) to monitor the time-resolved personal exposure to the total particle mass concentration of miners. The unit has been specifically designed for coal mines and shown to be in good agreement with the US coal mine respirable dust sampler (Page et al., 2008). Particle number concentrations prevailing in coal mines are usually very high and the instrument was therefore specified to have a mass concentration sensitivity of 50 µg/m³ for 30 minute averaging time, according to the manufacturer. For a 100 nm soot particle for example this sensitivity equals a very high number concentration of about $5.3*10^4$ 1/cm³ and therefore makes this instrument insensitive to nanoscale particles.

Qi et al. (2008a) recently presented a sophisticated personal sampler system to monitor the time resolved particle size distribution. The system comprises an electrical mobility based

classifier and a miniaturized particle charger (Qi et al, 2008b). If the two devices are used along with a particle counting device downstream of the classifier, the system delivers particle size distributions of particle sizes between 10 nm and 200 nm. However, the instrument is still in a rather infant state and also uses high voltage as well as a corona discharge that produces ozone and NO_x.

Another personal sampler which has been effectively used to collect nanoparticles is a Thermal Precipitator (TP). In general, a TP is a device that collects particles by applying the principle of thermophoresis which arises from inhomogeneous thermal diffusion of aerosol particles against a temperature gradient in a gas. TPs have the advantage that the particle deposition is independent of electrical charges. This means that for a sufficiently high temperature gradient all particles within the required size range will be deposited. Furthermore due to the very low thermophoretic velocity in comparison with an electrophoretic velocity for example, the particles are deposited rather gently thereby retaining the morphology of agglomerates which for higher velocities may be otherwise dispersed on collision with the collection surface (substrate). This characteristic of gentle particle deposition also best simulates the deposition of particles in the lungs. TPs have been used for decades already to sample aerosol particles (Orr and Martin, 1958; Gonzalez et al., 2005; Lee et al., 2008). They have also been designed for occupational exposure monitoring or personal exposure measurements in the micrometer size range (Roach, 1959; Sherwood and Greenhalgh, 1960; Cherrie, 2003). The difficulty with such methods of exposure measurement which involve particle sampling and subsequent analysis is the complexity of the analysis routines. In some personal samplers, where the deposition is size dependent or inhomogeneous, quantitative Scanning Electron Microscopic (SEM) analysis of such a sample becomes very difficult and time consuming due to the many SEM images which have to be examined in order to get a complete picture regarding the morphology and size distribution of the sample.

This thesis describes the development of a new Thermal Precipitator (TP) as a personal sampler built to effectively sample particles homogeneously on a substrate, with a known and constant temperature gradient and flow rate, in order to simplify subsequent analysis routines. Chapter 2 of this thesis gives a summary of available exposure measurement techniques and instruments and also describes why and where thermophoretic particle sampling is advantageous with respect to the other measurement techniques described. Chapter 3 describes the TP in detail and chapter 4 outlines the analytical and numerical modelling which forms the basis for the design and construction of the new TP. The design and construction of

the TP is also described in this chapter 5. In Chapter 6, the new TP is experimentally evaluated and validated in the laboratory with defined monodisperse particles and with polydisperse soot particles in the smaller size ranges up to about 98 nm. Chapter 7 then summarizes the thesis while giving an outlook of future applications using the TP.

2 Background on exposure measurement techniques and instrumentation

Measurement methods for detection of airborne nanoparticles can be categorised as on-line or off-line assessment methods. These methods may be used for different exposure metrics such as number concentration (total and size-resolved), mass, surface area and chemical composition. Most exposure measurements have used either on-line techniques to determine particle size distribution (Wake et al., 2002; Kuhlbusch et al., 2004, 2006; Möhlmann, 2005) or offline techniques like thermal or electrostatic precipitation, diffusion/impaction or filtration and subsequent particle characterisation (Plitzko, *BIA Report 7/2003e*; Gnewuch et al., 2008). Basically, various physical and/or chemical properties of aerosols can be determined with especially particle size distribution and number concentration being physical properties of particular importance in the case of nanoparticles. For the choice of exposure measurement instrumentation, the following scheme (Fig. 2.1) was introduced by Borm et al. (2006).

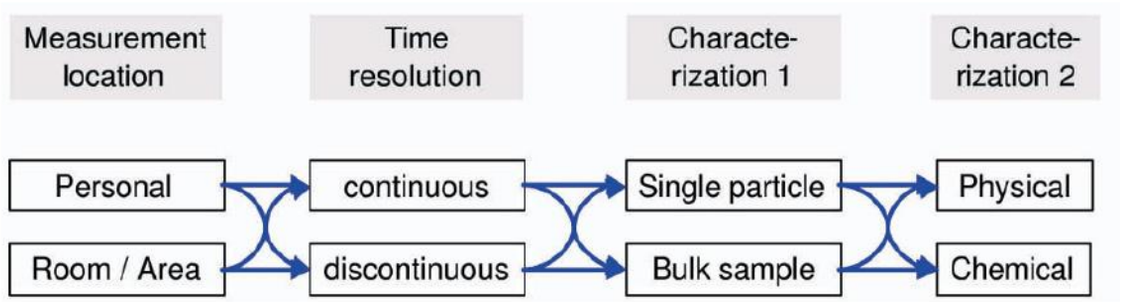

Fig. 2.1 Scheme of particle characterisation for exposure measurements (Borm et al., 2006)

The scheme indicates the different possibilities that should be considered when choosing exposure assessment instrumentation. The ideal method of assessing airborne nanoparticle exposure would certainly be the use of a personal sampler that determines in real time, all relevant physical and chemical properties of all single particles (primary particles and agglomerates) as well as their concentrations entering the measurement system. Since this is currently not possible, one has to consider the task to perform in combination with available measurement technology. The various available techniques are described in this chapter.

2.1 Stationary and portable measuring equipment

The choice of stationary and/or portable measuring technology can depend on several factors. If for example there is a need to determine whether primary particles or agglomerates of a specific nanoparticle product are present in a workplace, a device which determines particle number size distribution may be sufficient. If on the other hand, exposure should be determined in the interest of epidemiological studies, certain aerosol properties such as lung deposited particle surface area become important and therefore particle surface area measuring equipment such as the TSI Nanoparticle Surface Area Monitor (NSAM) may be used (Fissan et al., 2007). An array of stationary instruments and measurement technologies has been used to study exposure to nanoparticles. There is commercially available online instrumentation for determination of several aerosol properties e.g. particle number concentration, surface area concentration as well as particle size distribution. Mass concentration is impractical for nanoparticle detection due to the low mass and low sensitivity of mass measuring devices. Some of these measuring equipment and areas where they have been employed for exposure assessment measurements are described below.

The total particle number concentrations of airborne ultrafine and nanoparticles are usually determined using a Condensation Particle Counter (CPC). In a CPC, due to vapour condensation on particles, the particles become larger and can thereby be optically detected. The lower detection limit reaches down to 3 nm for n-butanol-based and 2.5 nm for water-based CPCs (Hermann et al., 2007) and an upper size limit of about 3000 nm. CPCs have been built as stationary as well as portable battery-powered equipment. Peters *et al.* (2006) used portable CPCs and optical particle counters to map both the number concentration in an engine machining and assembly facility. In a later study, Evans *et al.* (2008) used the same technique to map number and mass concentrations in an automotive grey iron foundry. In both studies this technique allowed the investigators to identify particle sources within the respective investigated facility.

A major limitation of a CPC however is its lack of size discrimination. A CPC alone is therefore not suitable for detailed exposure measurement of nanoparticles. As part of a Scanning Mobility Particle Sizer (SMPS) – system, a CPC can be used for concentration measurement of size selected samples.

Kuhlbusch *et al.* (2004) used an SMPS system to measure the particle size distribution of released particles in bag filling areas as well as in reactor and pelletizing areas (2006) of soot production. In an SMPS, aerosol particles are given a known charge distribution in a neutralizer which is based on radioactive decay and then the particles are passed into a

Differential Mobility Analyzer (DMA) where they are classified according to their electrical mobility which is a function of particle size and charge state. In a DMA, charged particles are deflected in an electric field between an outer and an inner electrode. Particles with a high electrical mobility (small and/or highly charged particles) move faster towards the inner electrode where they are eventually deposited. Particles of a similar size with an opposite charge are consequently deposited on the outer electrode. At the end of the inner electrode, particles of a particular lower electrical mobility are sampled through a slit and the number concentration of that particular electrical mobility size is measured with a CPC. The electrical mobility sampled is a function of the strength of the electric field. Particles with a lower electrical mobility than the particles sampled, are carried out with the flow. By continuously ramping up the voltage applied to the electrodes, particles of different electrical mobilities can be sampled and counted. The measured concentration is related to the electrical mobility with an algorithm and with knowledge of the charge distribution, a number size distribution as a function of electrical mobility diameter is determined. Typically an SMPS can classify particles in the electrical mobility size range of 3 nm to 1000 nm depending on the DMA which is used and covers a concentration range of about 20 1/cm³ to 10^7 1/cm³.

Electrical mobility analysis has also been implemented in a Fast Mobility Particle Sizer (FMPS) according to a work performed by Mirme et al. (1984). With an FMPS, simultaneous detection of particles can be performed for its entire covered size range of 5.6 – 560 nm with a time resolution of 1 s in comparison with at least 2 minutes for the same size range with an SMPS. Contrary to an SMPS where the different sizes are sequentially measured, the FMPS is based on an array of 22 electrometers, placed along the outer electrode of a DMA. The FMPS can be used in workplace measurements with rapidly changing work processes and size distribution fluctuations thus making use of its very small time resolution. The downside of the FMPS is however its lower size resolution of 16 channels per decade compared to up to 64 size channels per decade with the SMPS. Electrical mobility analysis has become the standard for submicron size distribution measurements. Kuhlbusch et al. (2008a) have provided extended information on aerosol measurement techniques.

An Optical Particle Counter (OPC) is another instrument which can be used to measure the size distribution of aerosols. Görner et al. (2011) used an OPC to measure the workplace mass concentration of a known aerosol. An OPC takes advantage of the light scattering phenomenon to count particles in the size range of about 300 nm to 20 µm. Most OPCs work with visible or near infra-red wavelengths in the range of about 500 nm – 1100 nm. Due to this larger wavelength in comparison with the diameter of nanoparticles, the scattering intensity of

these particles is too small to be detected. This therefore makes OPCs unsuitable for measurement and size classification of nanoparticles.

Another device used for nanoparticle exposure measurements is an Electrical Low Pressure Impactor (ELPI). Keskinen et al. (1992) developed an ELPI which measures size selective number concentrations in real-time. In an ELPI, inflowing particles are unipolarly charged by corona discharge and a 13 stage low pressure impactor classifies the particles in different aerodynamic diameters (D_{50} cut-off range 6.8 nm to 10 µm) and each charged particle is detected upon impaction. Due to the fact the ELPI collects these particles, gravimetric and other analysis can be performed on the collected sample.

Many stationary measuring equipment can provide online values of number size distribution and particle number concentration. However, due to the spatial difference in aerosol concentration and size distribution, attributed to dilution and/or agglomeration, the exposure of a mobile worker to nanoparticles cannot be effectively measured using stationary measuring equipment. For such personal exposure measurements, personal sampling methods are more suitable.

2.2 Personal samplers

In order to assess particle properties such as morphology and chemical composition, mainly off-line methods, are required, with single particle analysis following particle deposition being the most complete method Personal samplers operating on different physical concepts such as thermophoresis, electrophoresis, filtration or diffusion/impaction have been employed. Of the personal particle samplers existing, majority of them consist of a miniaturized impactor with a defined cut off size and an after filter. Particles are deposited according to their inertia in an impactor which can be designed to deposit all particles above a certain cut off size and let all smaller particles penetrate e.g. to be collected on an after filter for consecutive analysis. Sioutas *et al.* (1999) designed two impactors with cut off sizes of 2.5 µm and 1 µm, respectively. Wu and Vincent (2007) have designed an improved version of a cascade impactor which uses several impaction stages with different cut off size to further differentiate the size fractions. The deposited material on each stage can further be analyzed for its mass and chemical composition. For all of these impactor samplers, the particles collected are usually much larger than nanoparticles. Sampling nanoparticles by impaction is possible for low pressures, but the use of a large pump requiring large batteries to achieve this goal, makes this method unsuitable for personal sampling.

Electrophoresis has been successfully employed in sampling nanoparticles. An Electrostatic Precipitator (ESP) employs the principle of electrophoresis to sample charged particles on suitable surfaces for consecutive physical and chemical analysis. Inside an ESP, charged particles (from a corona discharge) are exposed to an electric field which directs particles of one polarity towards a suitable plate or grid, placed on a sample electrode. Particles of the other polarity are pushed towards the (grounded) walls of the ESP. Uncharged particles which are unaffected by the electric field, are directed out by the flow. Dixkens and Fissan (1999) designed an ESP which has been commercialised (TSI Model 3089) as stand-alone sampler. This device is bulky and mains powered and therefore unsuitable for personal sampling. It is possible to reduce the size of the sampler so it can be used as a personal sampler, even though sampling efficiency may fall as a result. A personal wire-tube ESP was developed by Cardello *et al*. (2002) with a sampling efficiency of ≥95% for all particles ≥15 nm if an appropriate flow rate is chosen. The corona discharge which is mostly used to unipolarly charge particles before being sampled in an ESP has been shown to produce ozone and oxides of nitrogen. This together with the use of a high voltage makes this method unsuitable to be employed in a personal sampler.

Filtration has also been used to separate particles from the gaseous phase. Furuuchi *et al.* (2010) developed a personal sampler based on inertial filtration to sampling ultrafine particles around the breathing zone. They placed inertial filters which consist of fibres with diameters ranging from 5.6 to 13.5 µm in circular nozzles (3 – 6 mm in diameter and 4.5 mm in length). Under the permissible pressure drop of 5.7 kPa at 6 L/min, a cut-off diameter of 140 nm and 200 nm were achieved for fibre diameters of 5.6 µm and 9.8 µm respectively. This device however does not effectively cover the entire range of nanoparticles as especially the smaller particles are removed at the filtration stage by Brownian diffusion. Moreover this device was developed to collect particles for chemical analysis. Single particle and size distribution analysis are not feasible.

Another device which effectively samples nanoparticles irrespective of their charge state is a thermal precipitator (TP). The TP is described in detail in the next chapter.

3 Thermal Precipitator (TP)

A Thermal precipitator (TP) is a device that samples particles using the principle of thermophoresis, defined as the thermal diffusion of aerosol particles due to collision with gas molecules, when a temperature gradient is present in the gas. In a gas where a temperature gradient exists, the gas molecules on the side with a higher temperature have a higher kinetic energy than the gas molecules on the side with a lower temperature. On collision with gas molecules on the warmer side, a particle obtains a higher momentum transfer than with collisions with gas molecules on the colder side. The particle is therefore diverted towards the colder side. Tyndall (1870) first described this phenomenon when he observed that in a chamber filled with dust-laden air, particle free regions formed around hot bodies. This phenomenon has been extensively studied and experimentally verified (e.g. Epstein 1929; Brock 1962; Waldmann and Schmitt 1966; Montassier et al. 1991; Stratmann et al. 1994; Romay et al. 1998; Tsai et al. 2004). There have been wide-ranging studies using the principle of thermophoresis to sample micrometer and nanometer particles (Kodas and Hampden-Smith 1999; Zheng 2002). Green and Watson (1935) developed the first known TP. This TP comprised of an electrically heated nichrome wire placed midway between two parallel glass microscope cover slips, mounted on brass heat sinks. This device was used extensively to examine dust particle number concentrations in mines in conjunction with optical microscopy (Watson, 1937).

A number of different TPs have been developed over the years, many of them focused especially on achieving uniform particle deposition (Kethley et al., 1952; Wright, 1953). These TPs based on plane-to-plane deposition, allowed for lower operating temperatures since particles have a long stretch on which the thermophoretic force acts on them. More recently, with the emerging interest in nanotechnology, new TPs were constructed to sample nanoparticles (Tsai et al. 1995; Maynard 1995; Bang et al. 2003; Gonzalez et al. 2005; Wang et al. 2012).

The Federal Insititute for Occupational Safety and Health (Bundesanstalt für Arbeitsschutz und Arbeitsmedizin - BAuA) developed a TP as a personal sampler to collect particles in the size range of a few nanometers up to about one micrometer for subsequent analysis using microscopic methods such as SEM. These sampled particles are usually evaluated with respect to their size, shape, number concentration as well as chemical composition.

3.1 First version of Thermal Precipitator (TP1)

The first version of the thermal precipitator (TP1) built by BAuA, samples particles in the size range of a few nanometers up to about 1 µm. The TP1 has been used to sample nanoparticles at workplaces where such particles are used and may be released (Plitzko, *BIA Report 7/2003e*). The TP1 was investigated with respect to its deposition properties.

3.1.1 Description of TP1 and method of sampling

The TP1 comprises mainly of a sampling component in combination with a controller unit containing a small fan responsible for the suction of aerosol into the TP1 and a power supply for creating a temperature gradient in the device. In the sampling component, particles are thermophoretically deposited on two round substrates lying parallel to the direction of flow as shown in Fig. 3.1.

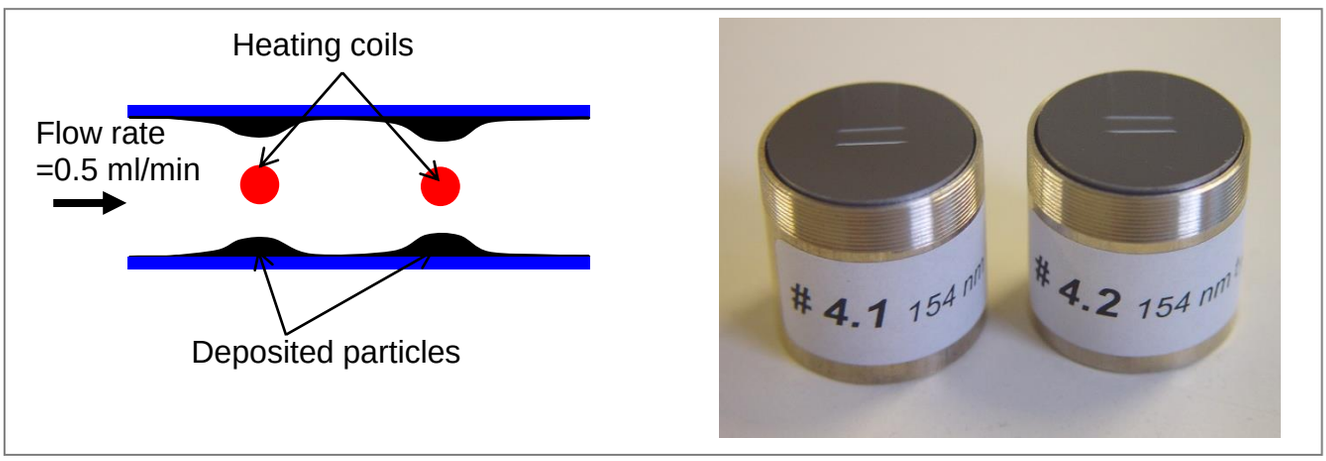

Fig. 3.1 2D Schematic of the TP1 showing its deposition characteristics and image of TP1 substrates after sampling

A temperature gradient is established by means of two centrally placed heating coils between the substrates, perpendicular to the direction of flow. The plates are placed 0.3 mm apart by a spacer and the heating coils have a diameter of 56 µm. Two round shaped silicon plates each with a diameter of 20 mm are used as substrates for particle deposition. A small fan in the controller unit in connection with a capillary of 0.45 mm in diameter and 16 mm in length, placed at the exit of the sampling component, creates by means of a pressure drop, a small flow rate of 0.5 ml/min which is equal to an inlet flow velocity of 5.5 mm/s. The heating current is provided by the controller unit which is powered by one 9V block battery. The sampling component has an outer diameter of 36 mm and is about 20 mm thick.

Before sampling the sampling component is dismantled and the two silicon substrates are placed with the polished side on both sides of a copper spacer (Fig. 3.2). Both sides are then closed by lids which are held in place by two spring elements. The controller unit of the TP1 is switched on and thereby providing power to the heating coils as well as turning on the pump. When a temperature gradient is established, particles are deposited on the substrates in the region near the heating coils as shown in Fig. 3.1.

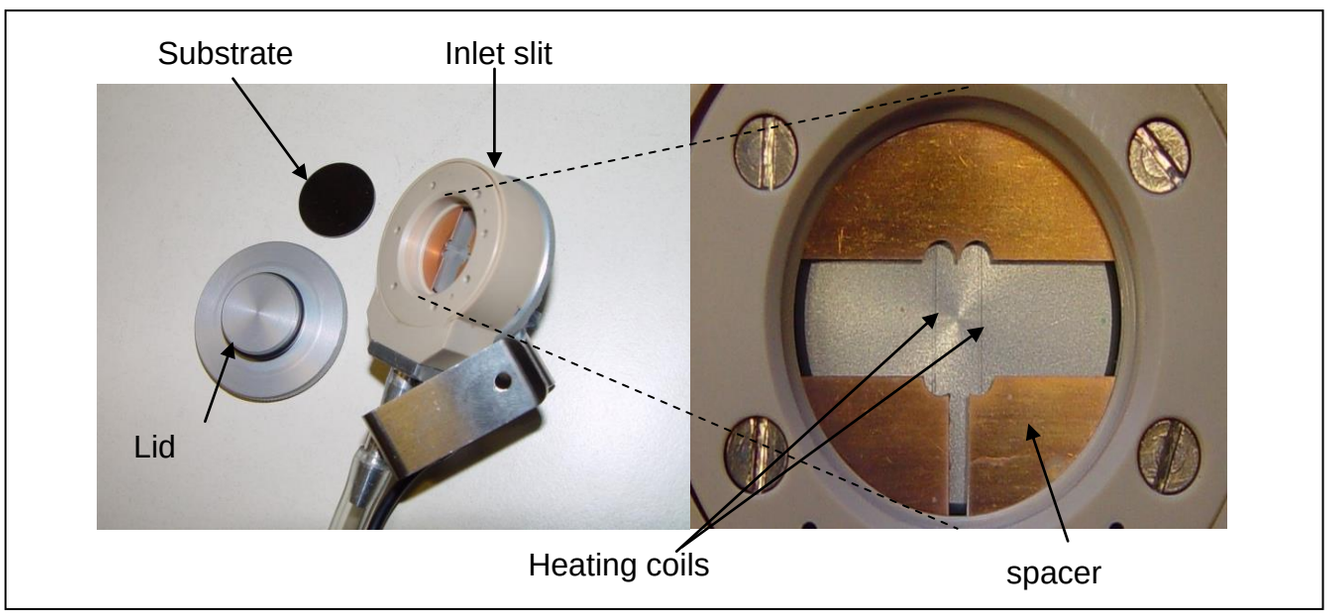

Fig. 3.2 Sampling component of the TP1

An image of the sampling component and controller unit of the TP1 is shown in Fig. 3.3.

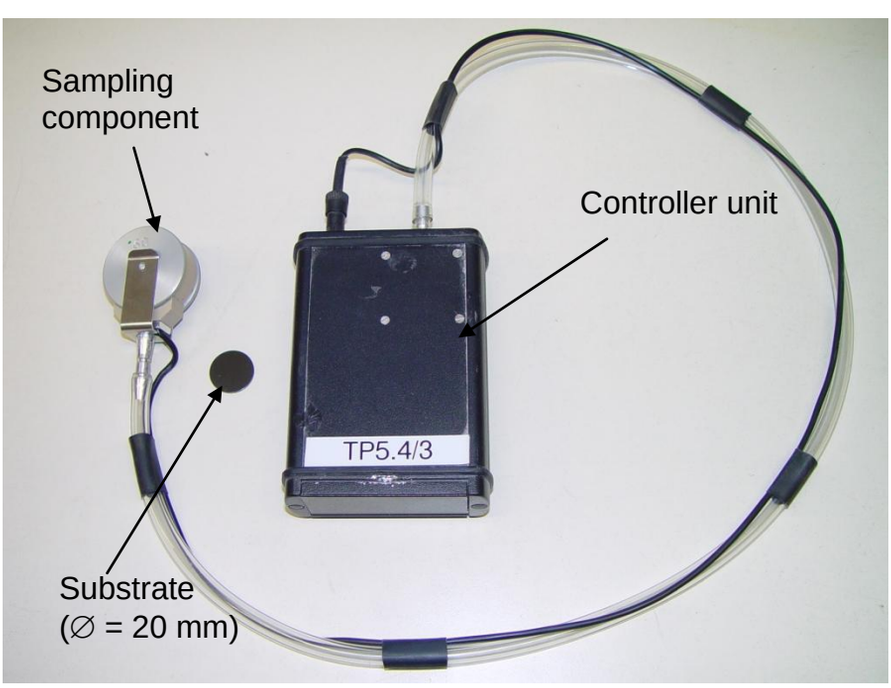

Fig. 3.3 Picture of a thermal precipitator (TP1) built by BAuA

3.1.2 Experimental evaluation of the TP1

A performance evaluation of the TP1 was experimentally performed to investigate its deposition characteristics, i.e. the pattern of particle deposition on the substrate. Initially, the TP1 was used to sample distilled water to investigate its purity. Monodisperse Polystyrene Latex (PSL) particles of different sizes which were dispersed in this distilled water prior to aerosolisation were then sampled with the TP1. Additionally polydisperse diesel soot aerosol and ambient air were also sampled. Table 3.1 shows a summary of the evaluation experiments carried out with the TP1. For all experiments, comparative measurements were performed in parallel with an SMPS system.

Table 3.1 Evaluation experiments with the TP1

Experiment	Aerosol	Sampling period [h]	Mean SMPS-Particle number concentration [1/cm^3]
1	Distilled water	8.00	3.725
2	PSL 390 nm	2.50	103.397
3	PSL 390 nm	6.00	34.001
4	PSL 153.5 nm	2.30	388.171
5	PSL 153.5 nm	7.00	75.374
6	PSL 75 nm	6.00	20.504
7	PSL 75 nm	7.00	106.394
8	Diesel soot	3.166	1.374.725
9	Diesel soot	6.083	516.614
10	Ambient air	42.50	18.986

The particles were found to be deposited mainly as two stripes on each substrate around the region of the heating coils (Fig. 3.1). The two dimensional schematic in Fig. 3.1 further illustrates the inhomogeneous deposition characteristic in the TP1. Since the particles were deposited primarily around the region of the heating coils, it was supposed that the inhomogeneous temperature gradient in these regions is responsible for the inhomogeneous particle deposition.

3.1.2.1Analysis routines of the TP1 samples

Evaluation of the TP1 substrates was performed by Scanning Electron Microscopy (SEM), according to the standard operating procedure of BAuA. It was assumed that all particles are deposited on the two stripes on both substrates as shown in the image in Fig. 3.1. The edges of the stripes were established and one overview image of each stripe was taken in the middle of the stripe. An example of such an overview image is shown in Fig. 3.4. It had been shown that the particles are deposited homogeneously along the length of the stripe and therefore the deposition in the middle was considered as representative for the whole stripe.
For each stripe of deposited particles, seven equally spaced images were taken with the boundaries of the first and seventh images corresponding to the boundaries of the overview image. A total of 28 detailed images were therefore taken for both substrates, which are considered as representative of the deposition in the TP1. An example of a detailed image is shown in Fig. 3.5.

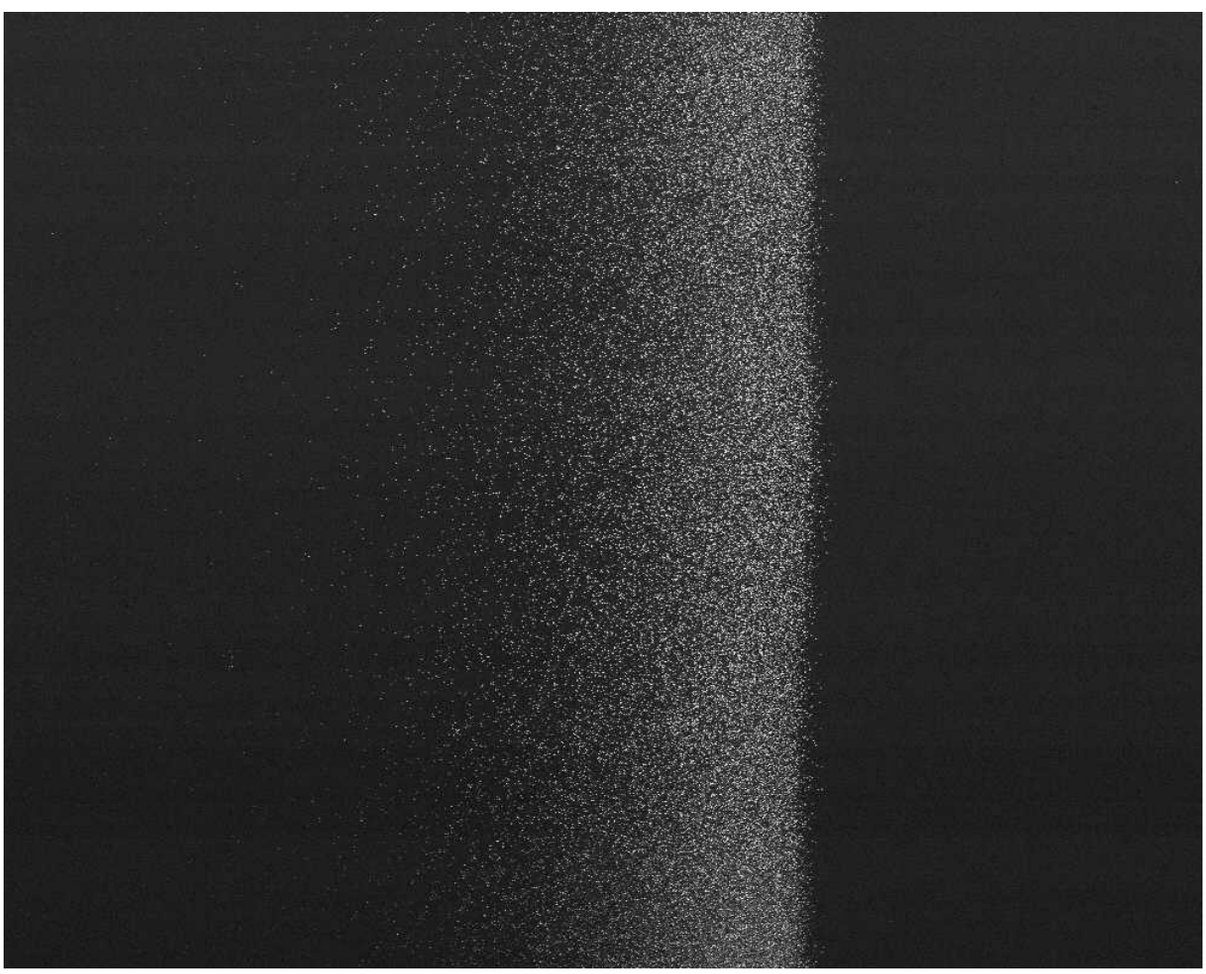

Fig. 3.4 Example of an overview image of a stripe of deposited 390 nm monodisperse particles on a substrate taken with a magnification of 80.

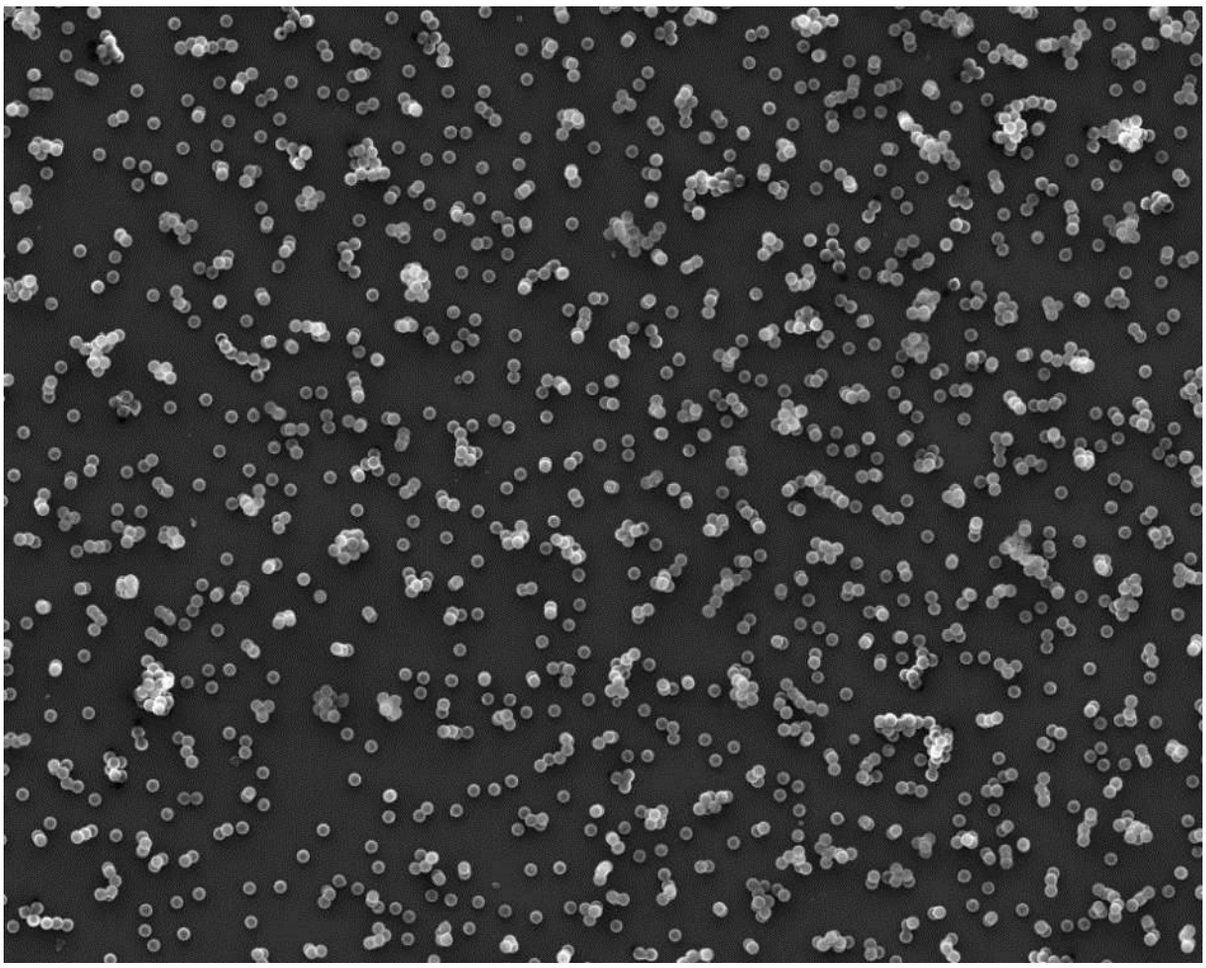

Fig. 3.5 Example of a detailed image of a stripe of deposited 390 nm monodisperse particles on a substrate taken with a magnification of 3000

The images were then analysed using image analysis software. The particle number concentration was calculated from the particle count on the 28 images as follows:

$$C = \frac{1}{t \cdot Q} \cdot N \cdot \frac{2 \cdot (A_1 + A_2)}{A_{28}} \tag{3.1}$$

Where

C is the Particle number concentration,

t is the sampling time,

Q is the flow rate,

N is the total number of particles counted on the 28 SEM images,

A_1 and A_2 are the areas of the first and second stripes on each substrate and

A_{28} is the area of all 28 SEM images.

Typically, analysis on a single detailed SEM image may take several hours. In the case of monodisperse PSL particles the analysis maybe much simpler since the size of the particles

is already known and only the number of deposited particles is of interest. At work places where product particles may be released, these particles usually have different morphologies. Analysing an image of such particles with image analysis software is sometimes very cumbersome and there is usually a need for manual analysis which can take several hours per image. Analysis of so many SEM images is necessary due to the inhomogeneous deposition of particles as well a overloading of particles on the TP1 substrates. A homogeneous deposit should lead to a reduction in the number of images needed to be analysed and thereby enhance the efficiency of the analysis routines.

3.1.3 Numerical modelling of the TP1

Numerical modelling was carried out in order to further understand the temperature and flow profiles in the TP1 as well as the resulting deposition characteristic of the TP1. Numerical simulations were carried out with the CFD software FLUENT (ANSYS, version 6.1.22) in connection with the Fine Particle Model (FPM, Particle Dynamics version 1.0.1). Results from the numerical modelling confirmed experimental results with an inhomogeneous deposition of particles found around the region of the heating coils, caused by the inhomogeneous temperature gradient in these regions. Detailed results of the numerical modelling of the TP1 can be found in Appendix A.

3.1.4 Need for optimisation

Due to the inhomogeneous and overlaid deposition of particles in a small area of the substrate in the TP1, SEM analysis of the sample becomes very difficult and time consuming. The need for optimisation stemmed primarily from the need for a less time-consuming examination of the substrate. With the TP1, a total of at least 32 SEM images are needed in order to evaluate the inhomogeneous deposition of the particles on the substrates. In a case where a homogeneous deposition is guaranteed, only about five SEM images should be sufficient to obtain a quantitative evaluation of the deposition. The inhomogeneous deposition in the TP1 was caused primarily by the inhomogeneous temperature gradient around the region of the heating coils. A homogeneous deposition is therefore achieved by creating a homogeneous temperature gradient.

Numerical modelling results also showed that many, particularly small particles, are deposited in the inlet region of the TP1 due to Brownian diffusion. There is therefore a need to improve the inlet region of the TP in order to reduce the number of particles which are deposited in this section.

The exact temperatures of the heating coils were unknown. Measurement of the temperatures was not possible without influencing the temperatures. The true value of the temperature gradient in the TP1 is therefore unknown and this causes an uncertainty in the analysis as well as comparison of the deposition. For a more exact evaluation of the deposition, it is required that the deposition rate stays constant for the entire sampling period. This can be done by ensuring a constant temperature gradient in the TP throughout this period. It is also important to ensure that the temperature of the substrate is kept as close as possible to the ambient temperature in order to avoid condensation. The size of the TP should be kept similarly small for handling purposes and the energy consumption maintained low.

3.2 Development of a new Thermal Precipitator (TP2)

A new thermal precipitator (TP2) was developed with the TP1 as the basis and taking the points of optimisation into account. The TP2 was developed to deposit particles homogeneously in order to simplify subsequent off-line SEM analysis. To create a homogeneous temperature gradient in the TP2, two parallel plates with different but constant temperatures were introduced with the colder surface acting as a substrate for particle deposition. A homogeneous temperature gradient is thereby guaranteed and by so doing, a homogeneous particle deposition is achieved (see Fig. 3.6).

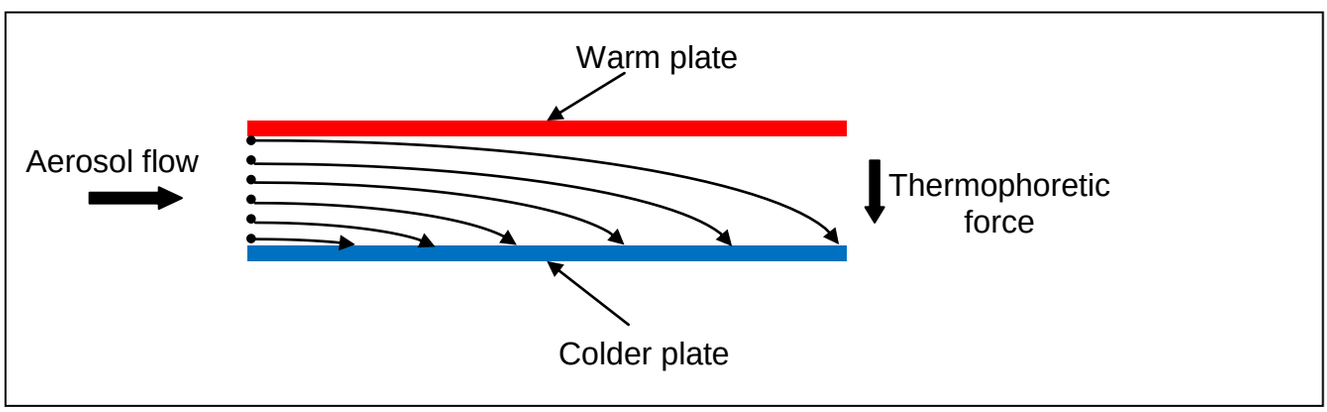

Fig. 3.6 Deposition properties of optimised TP (TP2)

In order to create a uniform flow tunnel and thereby create a more uniform flow profile in the TP2, a rectangular flow tunnel was envisaged. The substrates were also made rectangular in shape. The size of the TP1 was however considered to be appropriate for a personal sampler and therefore the size of the substrates was maintained at a length of 20 mm which is the diameter of the round shaped substrates in the TP1. Moreover, the rectangular substrates are cheaper than round substrates used in the TP1.

For a more exact evaluation of the deposition, it is required that the flow rate and temperature gradient in the TP2 stay constant for the entire sampling period. The development of the TP2 was done by modelling. Through modelling, optimal conditions for the flow and temperature as well as the general geometry of the TP2 can be obtained for an effective homogeneous deposition of nanoparticles and thereby achieving the stated optimisation goals. A simplified analytical model was developed to estimate optimal boundary conditions which are set in a more complex numerical model for a more detailed evaluation of the deposition pattern in the TP2.

4 Modelling

4.1 Analytical modelling of the TP2

The feasibility of the abovementioned approach for the TP2 design using 20 mm long substrates was studied by a simplified analytical model. The resulting parameters were then used for setting up the simulation grid for numerical modelling that allows for a more extensive study of the particle deposition. In order to fully analyse the deposition pattern in the TP and thus determine the characteristics of an optimised TP, it was important to understand the interaction and effectiveness of the various forces acting on particles in the TP. In this case where two parallel plates are introduced for the creation of a homogenous temperature gradient, the thermophoretic force acts in the direction of the colder plate and therefore perpendicular to the direction of flow.

Thermophoresis is primarily a function of the temperature gradient that a particle experiences in gas as well as the size of the particle. Different thermophoretic expressions have been described for different particle size regimes. The Knudsen number, Kn, is a measure of the various particle size regimes from free molecular to continuum regimes. The Knudsen number is a dimensionless number which represents the ratio of the mean free path of air molecules to a representative physical length scale (particle radius). The mean free path is the average distance between consecutive collisions of a moving particle with molecules in a gas.

$$Kn = \frac{2\lambda}{D_p} \tag{4.1}$$

Where λ is the molecular mean free path and D_p is the particle diameter. At standard temperature and pressure, λ has the value of about 67 nm at atmospheric pressure (Hinds, 1999). The free molecular regime exists for Kn >> 1, i.e for very small particles (< 10 nm). Waldmann and Schmitt (1966) presented an expression for the thermophoretic force in the free molecule regime as follows:

$$\vec{F}_{T,mol} = -\frac{\pi}{2} \cdot \frac{\eta^2 \cdot {D_P}^2}{\rho_g \cdot \lambda} \cdot \frac{\nabla T}{T} \tag{4.2}$$

Where η is the viscosity of the carrier gas, ρ_g is the density of the gas, ∇T is the temperature gradient and T is the absolute temperature of the particle. The negative sign in equation 4.2 indicates that the force acts in the direction of decreasing temperature. In the continuum

regime (kn << 1 or D_p > 200 nm) as well as the intermediary transition regime, it becomes more complicated to derive an expression for the thermophoretic force due to the presence of a temperature gradient within the particle. In this case the thermophoretic force is affected by the thermal conductivity of the particle relative to the thermal conductivity of the surrounding gas. Many studies have been carried out to derive an equation for the thermophoretic force in the transition and continuum regimes. Talbot et al. (1980) derived an expression for the thermophoretic force in these regimes as follows:

$$\vec{F}_{T,cont} = -3\pi \cdot \frac{\eta^2}{\rho_g} \cdot D_P \cdot H_T \cdot \frac{\nabla T}{T} \tag{4.3}$$

Where H_T is the thermophoretic coefficient, given by Talbot (1980) to be tolerably accurate in all regimes from free molecular to continuum.

$$H_T = 2C_s \frac{\left(k_g / k_p + C_t Kn\right)}{\left(1+3C_m Kn\right)\left(1+2k_g / k_p + 2C_t Kn\right)} \tag{4.4}$$

C_s = 1.147, C_t = 2.2 and C_m = 1.146 are the thermal creep coefficient, the thermal jump coefficient and the velocity jump coefficient respectively, which were empirically determined by Batchelor and Shen (1985). k_g and k_p are the thermal conductivities of the gas and the particle. The ratio of thermal conductivities, k_g/k_p, only becomes important for low Knudsen numbers (large particles) and/or high pressure, whereas for high Knudsen numbers, the effect of thermal conductivity can be neglected.

Particles which are displaced by a thermophoretic force always experience an opposing drag force. When no other forces are present, the effective thermophoretic velocity of a particle can be obtained by solving the force balance between the thermophoretic and the drag force. The thermophoretic particle velocity in still gas can then be described as:

$$\vec{v}_T(t) = \frac{C_c \cdot \vec{F}_T}{3\pi \cdot \eta \cdot D_P} \cdot \left[1 - exp\left(\frac{3\pi \cdot \eta \cdot D_P}{C_c \cdot m_P} \cdot t\right)\right] \tag{4.5}$$

Where $\vec{F}_T$ is the applicable thermophoretic force as in equation 4.3. The Cunningham slip correction factor C_c (Cunningham, 1910; Kim, 2005) has been derived as:

$$C_c = 1 + Kn\left(1.165 + 0.483 exp\left(-\frac{0.997}{Kn}\right)\right) \tag{4.6}$$

The resulting velocities calculated using equation 4.5 for 10 nm and 300 nm as well as for 10 µm particles with different thermal conductivities are shown in Fig. 4.1.

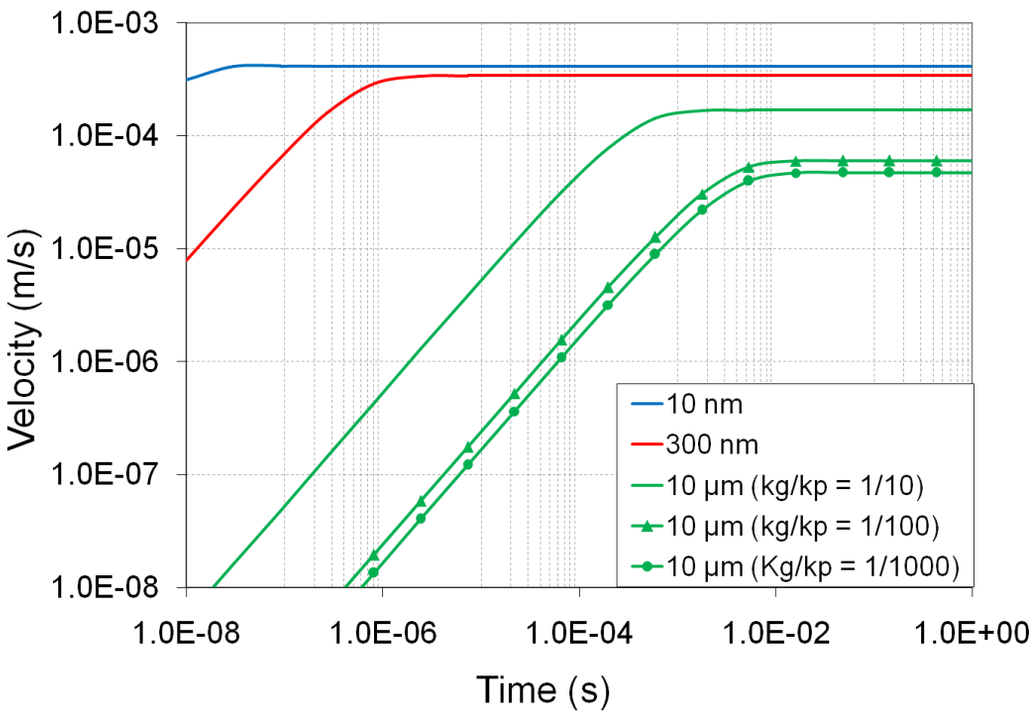

Fig. 4.1 Thermophoretic velocity as function of time for 10 nm, 300 nm, and 10 µm particles in air at atmospheric pressure and a temperature gradient of 15 K/mm; ratio of thermal conductivities, k_g/k_p, assumed to be 1/1000 for 10 nm and 300 nm at atmospheric pressure; three different exemplary ratios for 10 µm particles at atmospheric pressure.

Considering the case of 300 nm particles for example, a particle in a gas, experiencing a temperature gradient of 15 K/mm, reaches its terminal velocity of about $3.4*10^{-4}$ m/s after less than $3*10^{-6}$ seconds. This means that the particle attains its terminal velocity after moving for less than 1 nm. The relaxation time and distance for smaller particles are even much smaller. It can therefore be assumed that the particles in the TP instantly reach terminal velocity. The linear relationship between the terminal thermophoretic velocity v_T of a particle and the temperature gradient ∇T it experiences can be described by the following expression (Batchelor and Shen, 1985).

$$v_T = \frac{-H_T C_c \eta \nabla T}{\rho_g T} \qquad (4.7)$$

Similarly to thermophoresis, it can be shown that airborne particles arrive rather instantaneously at their terminal gravitational velocity with the magnitude of the terminal

velocity, a direct proportion to the particles' mass. The terminal gravitational velocity v_g of a particle is given by the following expression (Hinds, 1999):

$$v_g = \frac{g D_p^{\,2} C_c}{18\eta}\left(\rho_p - \rho_g\right) \tag{4.8}$$

where g is the gravitational acceleration and ρ_p is the density of the particle. Depending on the orientation of the TP during sampling, the effective deposition velocity of (nano-) particles would be the vector additive of the thermophoretic and gravitational velocities. The gravitational velocity however plays a significant role only for particles of larger size and/or density.

4.1.1 Effect of particle size on deposition velocity

The deposition velocity of the particles in the TP2 is a combination of the thermophoretic velocity, the settling velocity as a result of gravity as well as the effect of Brownian diffusion which will be discussed later. Considering only the thermophoretic velocity, its magnitude decreases with increasing particle size. In the case of the TP2 where a temperature gradient is created between two parallel plates, larger particles which flow into the TP2 will be deposited later than smaller particles which flow in at the same location in the inlet. Fig. 4.2 shows the value of the thermophoretic velocity with respect to particle size. The thermophoretic velocities in Fig. 4.2 were calculated for a temperature gradient of 15 K/mm and an absolute temperature of 293 K. Since the TP2 is built to sample sub-micron particles, a 1 µm particle, with an effective density of 1 g/cm³ is considered as the largest particle size of interest. For 20 mm long plates which were envisaged for the TP2 and for a gap distance of 1 mm, a temperature gradient of 15 K/mm in combination with an inlet flow velocity of 5.5 mm/s (which is maintained from the TP1) is necessary to ensure that a 1 µm particle which enters the TP2 closest to the warm plate, is deposited at the end of the colder plate (substrate). A k_g/k_p value of 0.041 was used in the calculations. It can be assumed that all other sub-micron particles which enter the TP2 further below the warm plate will be deposited on the cold plate under the same conditions.

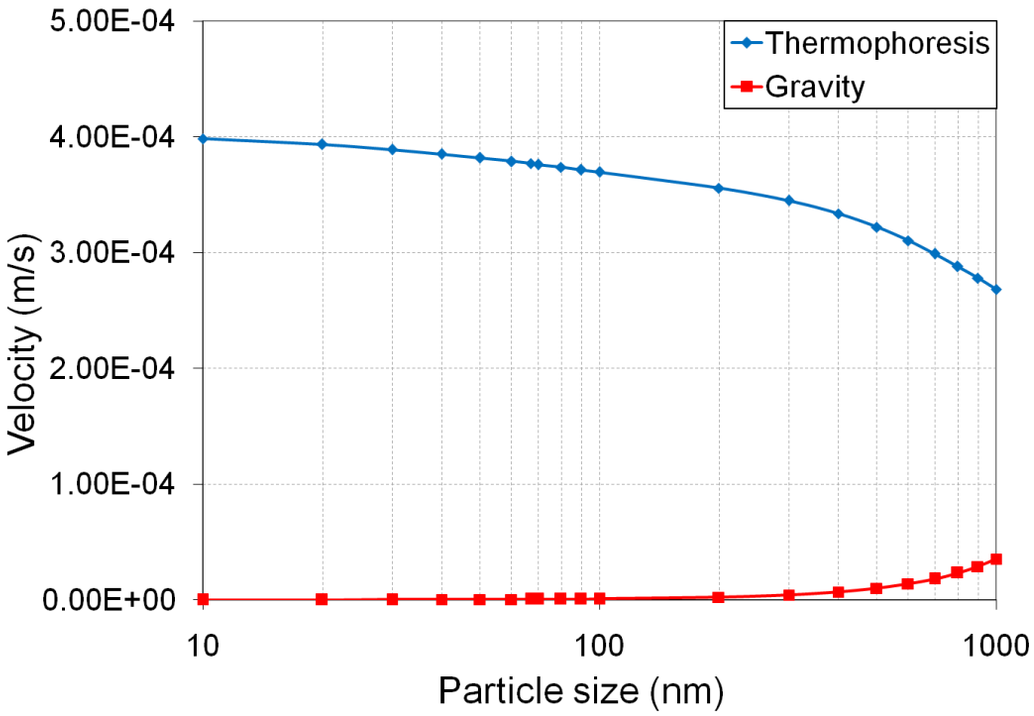

Fig. 4.2 Thermophoretic velocity and settling velocity due to gravity with respect to particle size

Fig. 4.2 also illustrates the increase in the settling velocity due to gravity with increasing particle size. The increase is only noticeable for particle sizes above 300 nm and insignificant for smaller particles.

4.1.2 Effect of device orientation on deposition velocity

The increase in settling velocity for particles larger than 300 nm shows that the orientation of the TP2 during sampling affects the deposition pattern of these larger particles. The TP2 was designed to be carried by a worker on either his chest pocket, over his shoulder or on his helmet. Three different basic orientations were therefore considered depending on how the TP2 was carried by the worker. The TP2 can be hanging on the chest pocket of a worker in an upright position (standing or sitting) with the entrance slit on top, the warmer plate closer to the body and a flow direction pointing vertically downwards (Case 1). The cases where the TP2 is e.g. carried on the helmet of the worker with a horizontal flow and the substrate at the bottom (Case 2) and with the substrate on top (Case 3) were also considered. Fig. 4.3 illustrates these three basic cases of orientation that were considered.

In all three cases, the thermophoretic force always acts perpendicular to the flow direction. For Case 1, gravity works in the direction of the flow. For Case 2, gravity works in the same direction as thermophoresis which may cause larger particles, where the effect of gravity is particularly pronounced, to be deposited faster. For Case 3, gravity works in the opposite

direction to thermophoresis, causing the larger particles to be deposited later or possibly not deposited at all or on the warmer plate depending on the magnitude of the thermophoretic velocity with respect to the gravitational velocity.

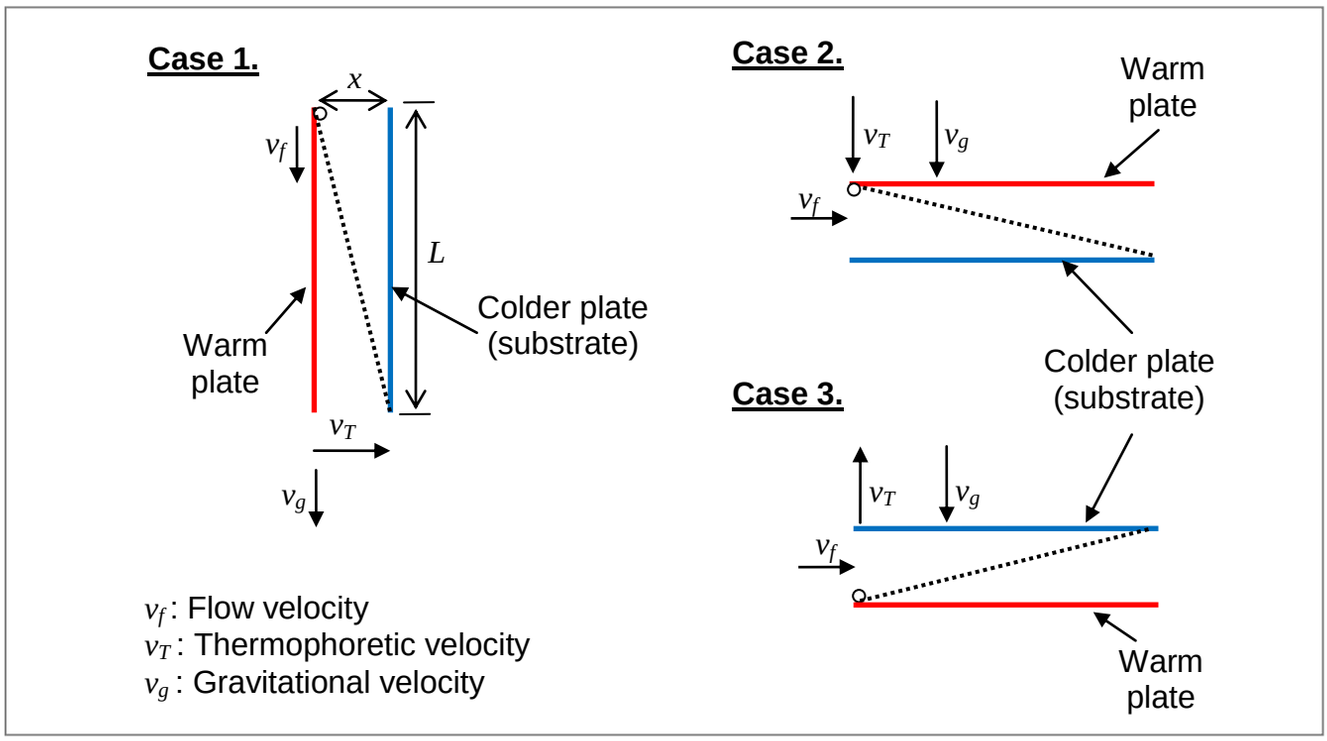

Fig. 4.3 Different orientation cases of a TP2 with a vertically downward aerosol flow (Case 1) and two different horizontal orientations with the substrate at the bottom (Case 2) and with the substrate on top (Case 3).

The deposition velocity is illustrated in Fig. 4.4 for different orientations of the TP2 with respect to particle size. Smaller particles are only very slightly affected by gravity. For larger particles where the effect of gravity is stronger, the particles reach a higher deposition velocity for Case 2 where gravity and thermophoresis act in the same direction and for Case 3, where gravity counteracts thermophoresis, the particles reach a lower deposition velocity. Up to a particle size of about 300 nm, the difference in deposition velocity for Cases 2 and 3 is in the order of ± 1.2 % compared to Case 1. For larger particle sizes the difference becomes more pronounced. This means that subsequent analysis of the TP2 sample especially for particle sizes > 300 nm, has to be done considering the orientation of the device during sampling otherwise the evaluation of the deposition of these larger particles would be done with high inaccuracy.

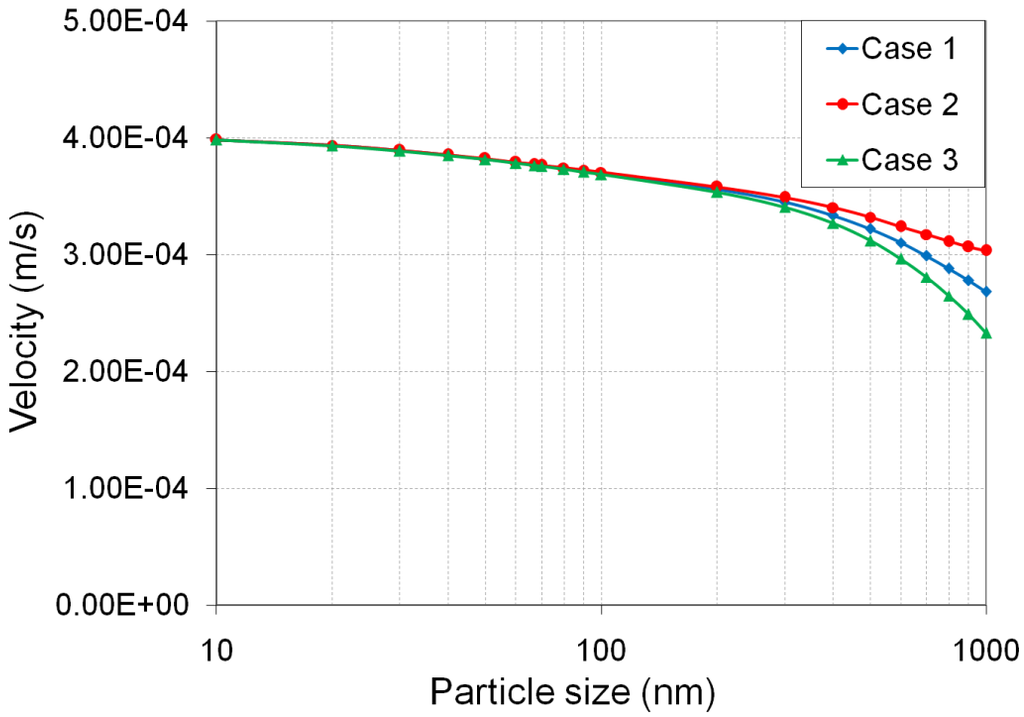

Fig. 4.4 Effect of device orientation on deposition velocity in the TP2. Deposition velocity as a result of thermophoresis and gravity

4.1.3 Effect of particle material type on deposition velocity

The absolute deposition velocity attained by a particle in the TP2 also depends on the particle material type. The thermophoretic coefficient is a function of the thermal conductivity of the particle material k_p as shown by equation 4.4. Generally, the higher the thermal conductivity of the particle material, the lower its thermophoretic velocity. This effect is however more noticeable for larger particles. Particles of different types may also have different densities. The gravitational velocity is a function of the density of the particle according to equation 4.8. Particles with a higher density therefore reach a higher gravitational velocity than particles with lower density. Fig. 4.5 shows the effect of the different material types on the deposition velocity. Iron particles with a density of about 7.9 g/cm³ were used as an extreme case along with particles of unit density to calculate the values shown. It is shown that the particles with a higher density and size reach a much higher deposition velocity for case 2 and a much lower deposition velocity for Case 3. For Case 3 where thermophoresis counteracts gravity, a particle size of about 952 nm is calculated for which the thermophoretic velocity equals the gravitational velocity, using a temperature gradient of 15 K/mm, an absolute particle temperature of 293 K and k_g/k_p of 0.0003 for iron particles. This shows that for Case 3, iron particles which are larger than 952 nm are slightly diverted towards the warm plate under the same conditions. This is illustrated in Fig. 4.5 by the negative deposition velocity. Also shown

in Fig. 4.5 is the effect of the thermal conductivity of the particle on the thermophoretic velocity (Case 1). Iron particles with a higher thermal conductivity (~80 W/mK) reach a lower thermophoretic velocity than unit density water liquid particles with a thermal conductivity of about 0.58 W/mK. The difference is however minimal and only noticeable for larger particles.

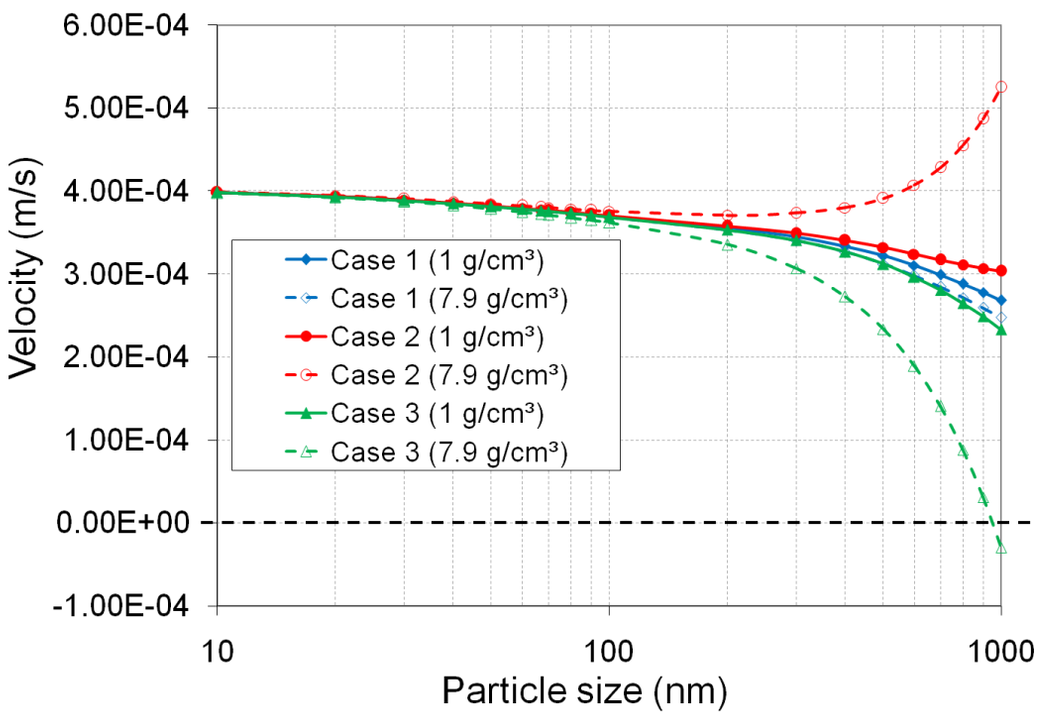

Fig. 4.5 Effect of different particle material types on the deposition velocity in the TP2

4.1.4 Effect of temperature gradient on deposition velocity

The main objective of developing the TP2 was to achieve a uniform deposition of all sub-micron particles along the entire length of the substrate. To achieve this goal, the temperature gradient had to be set so that all particles within the size range of interest that enter the TP2 furthest from the substrate, i.e. close to the surface of the warmer plate, will be deposited before the end of the substrate. For the default orientation (Case 1), where gravity acts in the direction of flow, assuming plug flow with a flow velocity of 5.5 mm/s, the required temperature gradient can be calculated for various gap distances which is necessary to achieve a worst case deposition distance of 20 mm (length of the substrate) for a 1000 nm particle. The worst case deposition distance is defined as the distance between the start of the substrate and the point on the substrate on which the particle is deposited when the particle enters the TP2 furthest away from the substrate (close to the surface of the warm plate). Particles with unit density (1 g/cm³) were assumed and the effect of Brownian diffusion was neglected for these worst case estimates. The worst case deposition distance, L, (see Fig. 4.3) will represent the case where the particle enters the TP2 at the surface of the

warmer plate. For the same temperature gradient, all smaller particles as well as particles which enter the TP2 below the warmer plate will theoretically have a shorter deposition distance.

The temperature gradient required to achieve a worst case deposition distance L for the various orientation cases illustrated in Fig. 4.3 can be calculated by considering that a particle covers exactly the distance, x, in one direction and the distance L in the perpendicular direction. The ratio of these distances will be equal to the ratio of the equivalent velocities acting in the respective directions. For Case 1 for example;

$$\frac{L}{x} = \frac{v_f + v_g}{v_T}$$

$$v_T = \frac{(v_f + v_g)x}{L} \tag{4.9}$$

For Case 2:

$$v_T = \frac{v_f x}{L} - v_g \tag{4.10}$$

For Case 3:

$$v_T = \frac{v_f x}{L} + v_g \tag{4.11}$$

For a worst case deposition distance L = 20 mm (length of substrate) and a chosen gap distance x, the thermophoretic velocity required to achieve a complete deposition of all particles up to the size of 1000 nm was calculated. The corresponding temperature gradient was then calculated by setting equations (4.9) to (4.11) equal to equation (4.7). Various gap distances (x) were considered for the TP2. For the original (TP1) gap distance of 0.3 mm, a temperature gradient of 4.5 K/mm would be necessary to cause a 1000 nm particle of unit density to have a worst case deposition distance of 20 mm. Due to the small gap distance between plates a smaller thermophoretic velocity is needed to match the orthogonal flow velocity such that the worst case deposition distance remains 20 mm. This explains the small temperature gradient of 4.5 K/mm unlike 15 K/mm when the gap distance x = 1 mm. The temperature gradient of 4.5 K/mm corresponds to an effective temperature difference of 1.35 K between the plates. Such a temperature difference would be very difficult to control due to the effect of external temperature fluctuations. Moreover, the effect of gravity becomes

more dominant for smaller gap distances while maintaining the same worst case deposition distance of 20 mm. Considering the different possible orientations of the TP2 during sampling, a too small thermophoretic force (resulting in a small thermophoretic velocity) which is necessary for L = 20 mm, for smaller gap distances, would be more easily overwhelmed by a counteracting gravitational force for Case 3. The effect of the dominant gravitational force is illustrated in Fig. 4.6 by the ratio of gravitational settling velocity to thermophoretic velocity (v_g/v_T). v_g/v_T is very small for smaller particle sizes for all gap distances and temperature gradients and becomes much larger for larger particles which are more affected by gravity, and for lower gap distances with lower counteracting thermophoretic velocities. In the extreme case of iron particles with a density of about 7.9 g/cm³, v_g is almost four times larger than v_T for a 1000 nm particle in an x = 0.3 mm model. In this case, many particles > 600 nm shall be deposited on the warm plate in the TP2 and many particles in the range of about 300 nm – 600 nm shall either be deposited much later on the cold plate or carried out of the TP2 with the flow. The x = 0.3 mm model is therefore inappropriate for the TP2. For particles > 300 nm, v_g is 10% of v_T for x = 1 mm and 14% for x = 0.7 mm (temperature gradient of 10.5 K/mm → ΔT = 7.35 K). This small counteracting gravitational force causes a deviation in the deposition distance of 11% and 16% for x = 1 mm and x = 0.7 mm respectively, with the resulting deposition distances all below 20 mm ensuring that all particles up to this size are deposited on the plate. The gap distance of 1 mm is seen to be more suitable due to the smaller deviation in deposition distance.

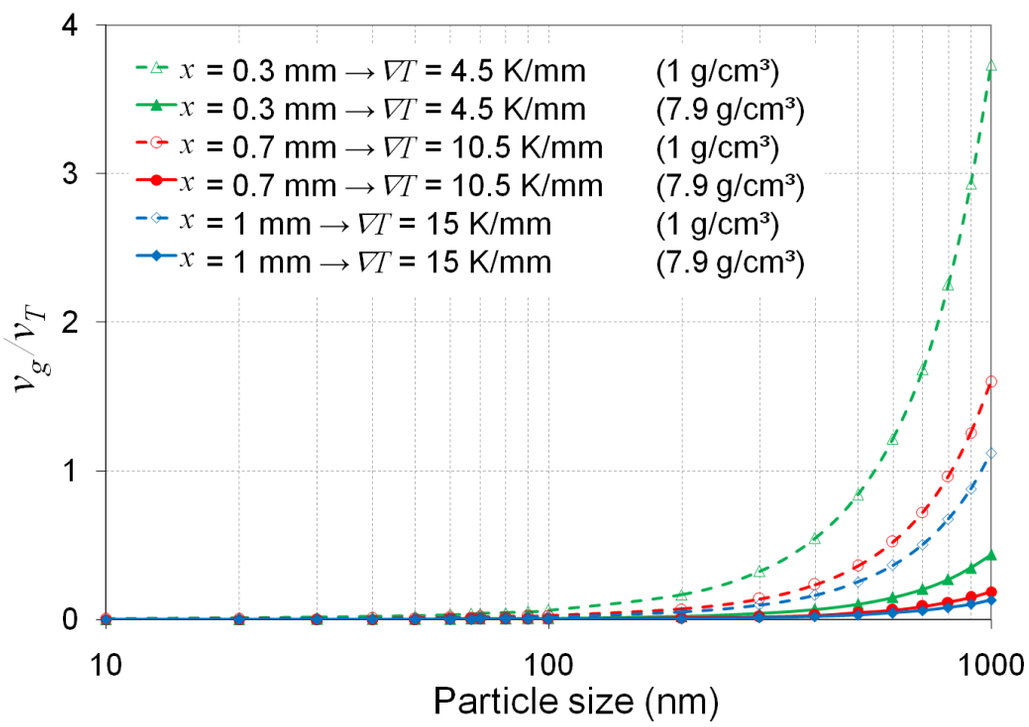

Fig. 4.6 Ratio of gravitational settling velocity to thermophoretic velocity (v_g/v_T) for different gap distances and for particles with unit density as well as iron particles with a density of 7.9 g/cm³. v_g/v_T illustrates the effect of a counteracting v_g to v_T (Case 3). v_T chosen for each gap distance such that a deposition distance of 20 mm is achieved.

The effect of small changes in ambient temperatures which may affect the temperature gradient in the TP2 was modelled by assuming changes of ±1 K. Table **4.1** shows the worst case deposition distances for unit density particles with diameters of 10 nm, 20 nm, 50 nm 100 nm, 300 nm and 1000 nm, calculated for gap distances of 0.7 mm and 1 mm and for changes in the temperature difference between the plates by ±1 K. The temperature gradients used for these calculations were obtained for a worst case deposition distance of 20 mm for 1000 nm particles of unit density for each gap distance.

Table 4.1 Worst case deposition distances calculated for a range of particle sizes, for gap distances of 0.7 mm and 1 mm and for a temperature gradient which gives an approximated worst case deposition distance of 20 mm for 1000 nm particles of unit density. Deposition distances were also calculated for deviations of 1 K from the temperature difference between the plates.

	Worst case deposition distance (L) for TP2 with **0.7 mm** gap distance			Worst case deposition distance (L) for TP2 with **1 mm** gap distance		
Particle size D_P [nm]	L [mm] for ∇T = 10.5 K/mm (ΔT= 7.35 K)	L [mm] ΔT + 1 K	L [mm] ΔT - 1 K	L [mm] for ∇T = 15 K/mm (ΔT = 15 K)	L [mm] ΔT + 1 K	L [mm] ΔT - 1 K
10	13.57	11.95	15.71	13.57	12.72	14.54
20	13.74	12.1	15.91	13.74	12.89	14.73
50	14.16	12.47	16.39	14.16	13.27	15.17
100	14.63	12.88	16.94	14.63	13.72	15.68
300	15.70	13.82	18.17	15.70	14.72	16.82
1000	20.32	17.89	23.52	20.32	19.05	21.77

As with the case of counteracting velocities for Case 3, a smaller deviation in the deposition distance of about -6.2 % and +7.1 % for the different orientation cases is found with a 1 mm gap distance as opposed to -11.9 % and +15.8 % with the 0.7 mm model. For a constant flow velocity of 5.5 mm/s, the total volumetric flow of aerosol into the TP2 is higher for a gap distance of 1 mm than for a gap distance of 0.7 mm. This enables more particles to flow into the TP in the same time period. For these reasons, the model with a gap distance of 1 mm was chosen and thus used for further calculations and modelling.

For a gap distance of 1 mm, deposition distances were calculated for particle sizes from 10 nm up to 1000 nm. All three orientations were considered in the calculations in order to evaluate the effect of gravity on the deposition with respect to particle size. Fig. 4.7 illustrates the difference in the deposition distance calculated for all three orientation cases, with particles of unit density and with an extreme case of iron particles with a density of about 7.9 g/cm³.

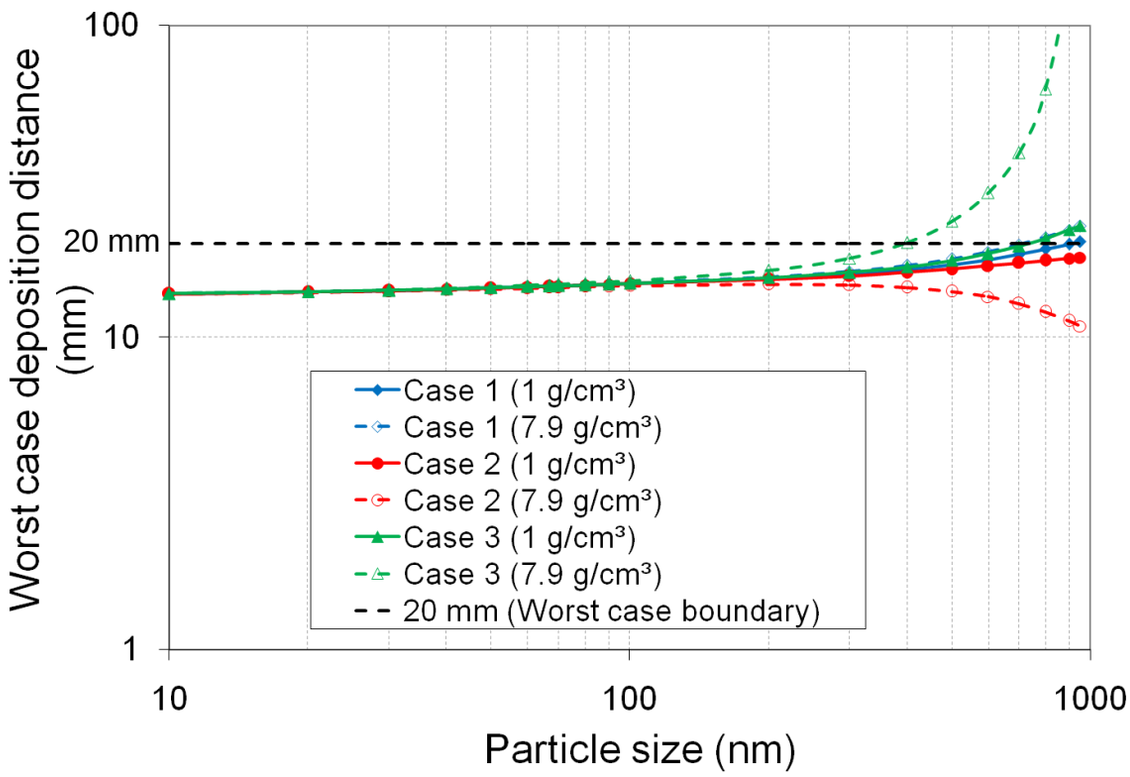

Fig. 4.7 Deposition distances for particles with unit density (1 g/cm³) and iron particles with a density of 7.9 g/cm³ for three TP orientation cases, for a temperature gradient of 15 K/mm and a plug flow velocity of 5.5 mm/s

It can be seen from Fig. 4.7 that there are significant differences between the deposition distances particularly for larger particles (D_p > 300 nm). The worst case deposition distance for a 300 nm particle considering the extreme case of iron particles (ρ = 7.9 g/cm³) is 17.9 mm. From the above analytical calculations, it can therefore be expected that all particle sizes up to 300 nm shall be completely deposited on a 20 mm long substrate for a gap distance of 1 mm, an average flow velocity 5.5 mm/s, and a temperature gradient of 15 K/mm, irrespective of the particle density or orientation of the TP2 during sampling. The evaluation of the deposition for particle sizes up to 300 nm can thus be carried out with sufficient accuracy without prior knowledge of the TP2 orientation or the material type of the sampled particles.

Above this size range, knowledge of the TP2 orientation and particle material is required for an accurate evaluation of the deposit. These preliminary considerations showed that use of rectangular substrates with a length of 20 mm is feasible with a temperature gradient of 15 K/mm, a gap distance of 1 mm between the plates and a flow velocity of 5.5 mm/s. With a cross-section area of flow channel of 1 x 6 mm², the flow velocity of 5.5 mm/s corresponds to a volumetric flow rate of 2 ml/min.

The temperature difference of 15 K for a gap distance of 1 mm corresponds to a Grashof number of ~ 1.81. In fluid dynamics and heat transfer, the Grashof number represents the ratio of buoyant forces (in this case as a result of a temperature gradient) to viscous forces acting on a fluid. It is a dimensionless number which is commonly used to describe the transition from laminar to turbulent flows as a result of convection. The range of 10^8 to 10^9 is given as the margin where this transition occurs for natural convection from flat vertical plates. The Grashof number of 1.81 is therefore far below the transition range and shows that for the operating conditions of the TP2, no turbulence as a result of convection is expected.

The inlet tunnel which leads from the entrance slit up to the deposition region of the TP1 is 8 mm long. Numerical modelling results showed that many especially smaller particles are deposited in this region due to Brownian diffusion. Diffusional deposition in this region is enhanced because of the low flow velocity resulting in a long residence time. In the model for the TP2, the entrance tunnel was shortened from 8 mm as in the TP1 to 2 mm in order to minimise the particle losses due to Brownian diffusion By reducing the length of this section by a factor of four, the time needed for particles to go through this section is reduced by about the same factor. Due to the square root relationship between the Brownian particle displacement and time, the average particle loss in the inlet tunnel is about halved. A sketch of the optimised geometry is shown in Fig. 4.8.

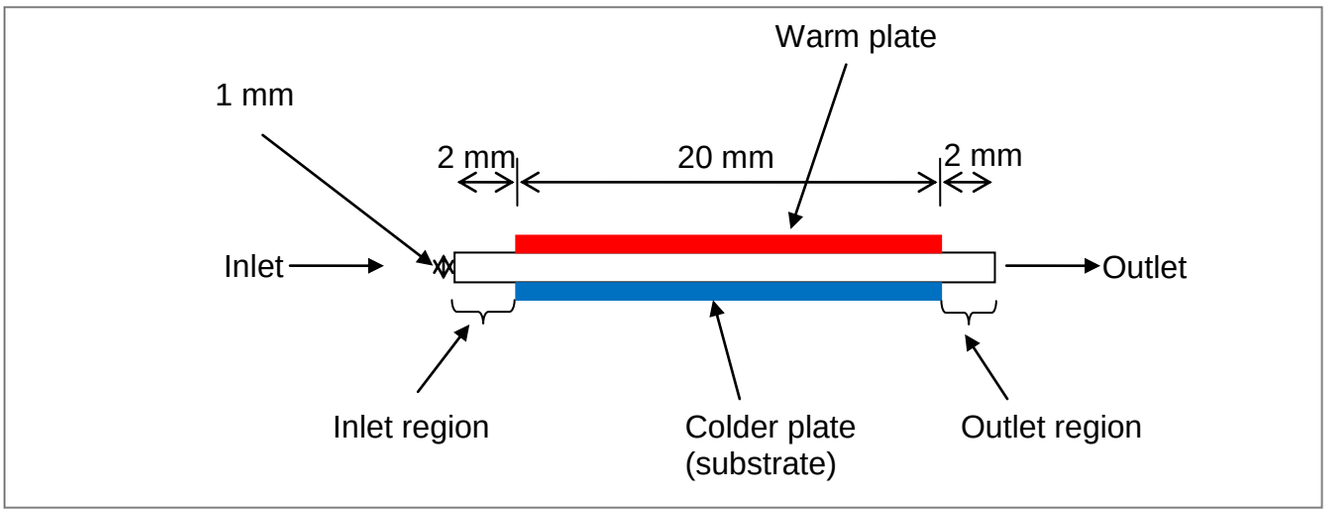

Fig. 4.8 Two-dimensional cross-section sketch of the TP2

4.2 Numerical modelling of the TP2

The analytical pre-calculations were done under simplified conditions with many assumptions. A plug flow was assumed for the flow profile in the TP2 and the effect of Brownian diffusion was neglected. These analytical pre-calculations however provided the basis to create a model grid which was used to do more complex numerical simulations. Numerical modelling takes into account the effect of a realistic laminar flow profile (Reynolds number ~ 0.62), particle losses due to Brownian diffusion, as well as non-uniformities of the temperature field around the edges of the plates.

A model grid was developed, representative of the proposed geometry for the TP2. A three dimensional grid as shown in Fig. 4.9 was first developed for the simulations having dimensions of 1 mm x 3 mm x 24 mm, representative of half the sampling section of the TP2 (including 2 mm each of inlet and outlet regions). Only one half of the TP2 was simulated because of the symmetry of the TP2 along the width. The middle plane in the grid (along the length) was therefore defined as a symmetry plane. The 3-D grid was developed with a resolution of 240 finite elements along the length of the TP2, 30 elements between the plates and 30 elements wide, i.e. a total of 216,000 rectangular finite grid elements. There was an increment ratio in element size of 1.05 in the direction of the warmer plate. The elements on the colder side of the TP2 are of particular interest since this is the side which is to be eventually evaluated. More precise calculations were therefore desired on this side and hence the smaller-sized elements. The time needed for one simulation with this three dimensional grid was found to be very long (approx. 48 hours).

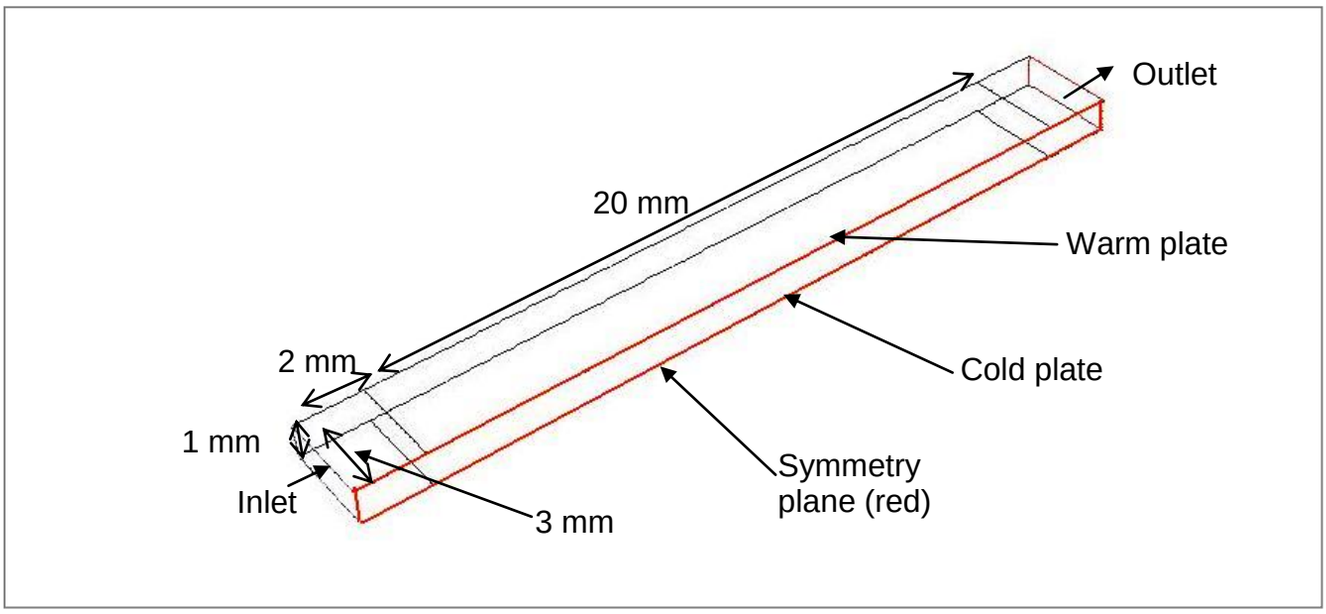

Fig. 4.9 Three dimensional TP2 grid for numerical simulations. Grid represents one half of the TP2 sampling region with a symmetry plane (red) along the middle. The grid is made up of 216,000 rectangular cells with a cell size increment ratio of 1.05 towards the warm plate

A two dimensional grid which represents the middle section of the TP2 along the flow axis, was consequently developed in order to reduce the simulation time. The 2-D grid was developed with a resolution of 240 finite elements along the length of the TP2 and 40 elements between the plates, a total of 9600 rectangular finite grid elements, with an increment ratio in element size of 1.05 (Fig. 4.10) in the direction of the warmer plate. The simulation time was consequently reduced from about 48 hours for the 3-D grid to about 2 hours for the 2-D grid. Boundary effects at the sides are not covered by such an approach; these however play a very minute role as the section which will be evaluated is exactly the section in the middle covered by this two dimensional grid. All following results were achieved from simulations with this grid.

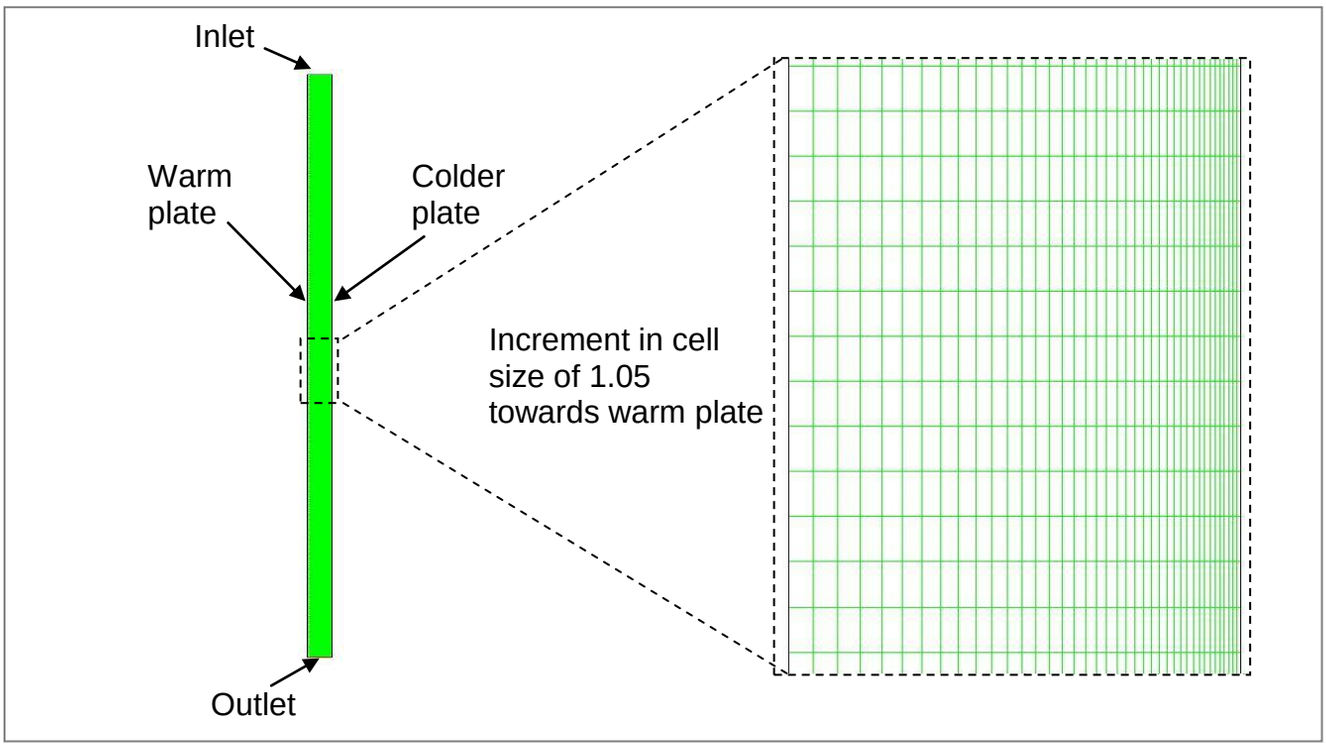

Fig. 4.10 Two dimensional TP2 grid for numerical simulations. Smaller grid cells towards the colder plate for more precise calculations in this section. The grid is made up of 9600 rectangular cells with a cell size increment ratio of 1.05 towards the warm plate

For the simulations, a flow velocity of 5.5 mm/s was set at the inlet. The temperature gradients were varied with simulations being carried out with temperature gradients of 12 K/mm, 15 K/mm and 18 K/mm for all orientation cases. Water liquid particles with unit density were used for the simulation as well as the extreme case of iron particles with an approximate density of about 7.9 g/cm³. Particle behaviour in the TP2 was investigated under the set conditions by evaluating the particle number concentrations at several points in the TP2. Monodisperse particles of sizes 20 nm, 30 nm, 40 nm, 50 nm, 75 nm, 100 nm, 300 nm, 500 nm and 1000 nm each with a total concentration of 10.000 1/cm³ (=10^{10} 1/m³) at the inlet, were considered. Unlike with the Discrete Phase Model (DPM) of FLUENT, which uses a Langrangian approach to track single particles and plot their trajectories, the Fine Particle Model (FPM) uses an Eulerian approach to simulate the dynamics of a population of particles with a given size distribution. With the DPM, In order to achieve better statistics it would be necessary to simulate the trajectories of many thousand particles. This usually is computationally very demanding. The DPM also does not include the effect of the interaction between particles as it simulates the dynamics of only discrete particles. The FPM includes the effect of flow, temperature, dilution etc. on the particle number concentration and size distribution. Eulerian simulations however have to deal with the problem of numerical diffusion

which is a difficulty that occurs with computational simulations of continuous systems by the discretisation of the continuous differential equations of motion into finite-differential equations. Due to the fact that the flow rate at the wall is zero, and assuming the shortcoming caused by numerical diffusion that a transition from a non-zero concentration to a zero concentration cannot be displayed within a single cell, the concentration at the walls of the grid is set in FLUENT to zero (Engelke *et al*, 2007).

4.2.1 Results of the numerical modelling

A parabolic laminar flow profile develops in the TP2 for a set inlet velocity of 5.5 mm/s, with flow velocities of 0 mm/s at the plates and up to about 8.4 mm/s in the middle as illustrated in Fig. 4.11. Velocity increase in the image shown in Fig. 4.11 is denoted with the colour scale starting with blue for the lowest velocity and red for the highest velocity. Values of the velocity shown in the plot are taken from the cross-section in the middle of the TP2 (circled in the image of the flow profile).

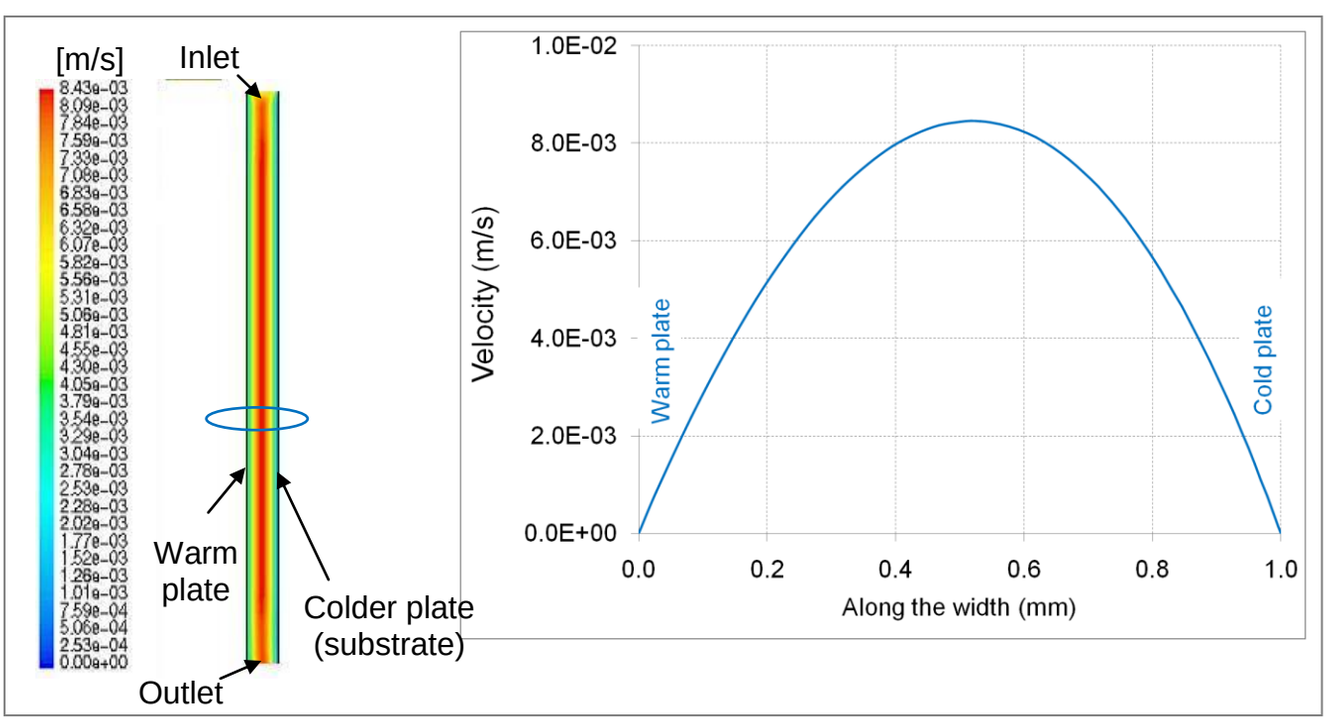

Fig. 4.11 Flow profile in the TP2

A temperature profile in the TP2 for a temperature gradient of 15 K/mm is shown in Fig. 4.12. The increase in temperature from the cold to the warm plates is denoted in the colour scale with blue representing the lowest temperature considered; in this case, 293 K for the cold plate and red for the highest temperature which is 308 K for the warm plate. This two dimensional view of the temperature profile shows more clearly the uniformity of the

temperature gradient with an unavoidable but very short non-uniformity at the start and end of the plates. The temperature of the walls of the inlet and outlet regions of the TP2 was set to the assumed ambient temperature of 293 K. Fig. 4.12 also illustrates the profile of these sections.

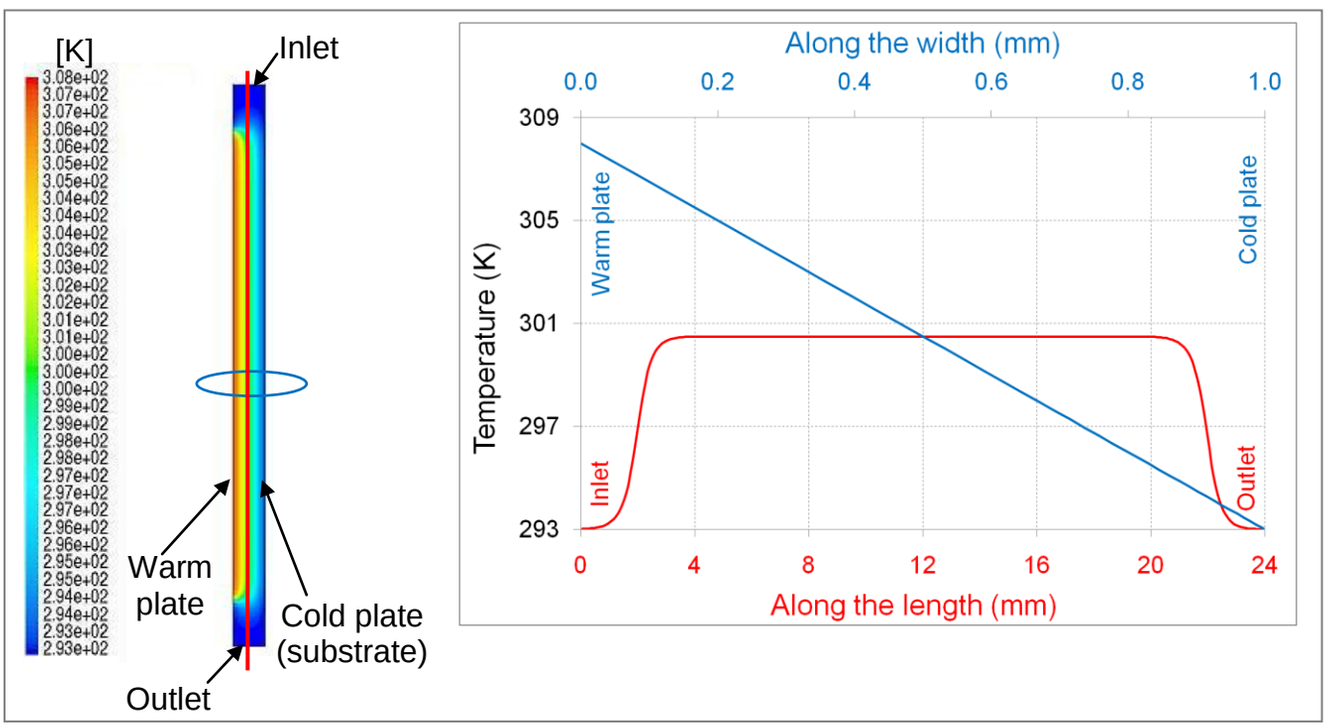

Fig. 4.12 Temperature profile along the length and width (in the middle) of the TP2 with the temperature of the warm plate set at 308 K and the temperature at the cold plate as well as the ambient temperature set at 293 K

An exemplary particle number concentration profile for 100 nm particles with an inlet particle number concentration of 10^{10} 1/m³ is shown in Fig. 4.13. This simulation was performed for a temperature gradient of 15 K/mm and a flow velocity of 5.5 mm/s. The increase in concentration is denoted by the change in colouration from blue to red. At the inlet of the TP2, there exists a constant concentration along the width. Thermophoresis causes the particles to drift in the direction of the cold plate (substrate) and hence an increase in the concentration in that direction. Due to the deposition of particles on the cold plate, the concentration of particles in the flow drops and eventually tends to zero towards the end of the plate. It should be noted that the concentration curve shown in Fig. 3.19 (right) is plotted from values taken just above the cold plate of the TP2. The trend of this concentration curve shall be explained in detail later.

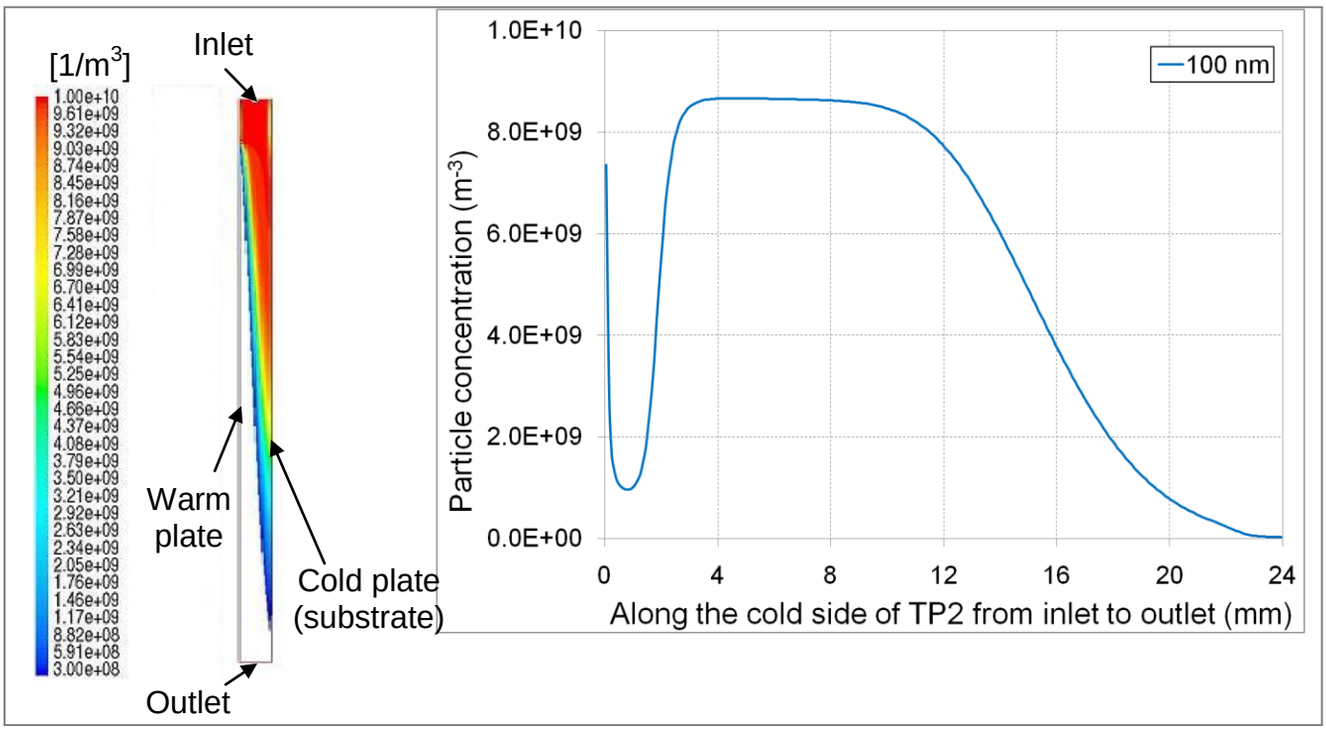

Fig. 4.13 Particle number concentration profile in the TP2 illustrated exemplarily for 100 nm particles

The particle deposition in the TP2 was investigated by examining the particle number concentration of particles along the side of the TP2 which contains the substrate. Consequently, the 2 mm entrance tunnel was also examined to assess the particle losses which occur in this region. It should be noted that, due to the fact that the concentration at the walls is set to zero, the last but one layer of cells was considered for the above examination of particle number concentrations along the wall as described by Engelke *et al.* (2007). The last layer of cells has a height of about 8 µm. A 10 nm Particle in the last but one cell with a thermophoretic velocity of about $4*10^{-4}$ m/s for a temperature gradient of 15 K/mm, is deposited after only 0.02 seconds. The values of particle number concentration in these last but one cells can be assumed to be representative for the deposition on the walls. Fig. 4.14 illustrates the concentration profile along the cold side of the TP2 for all particles sizes examined.

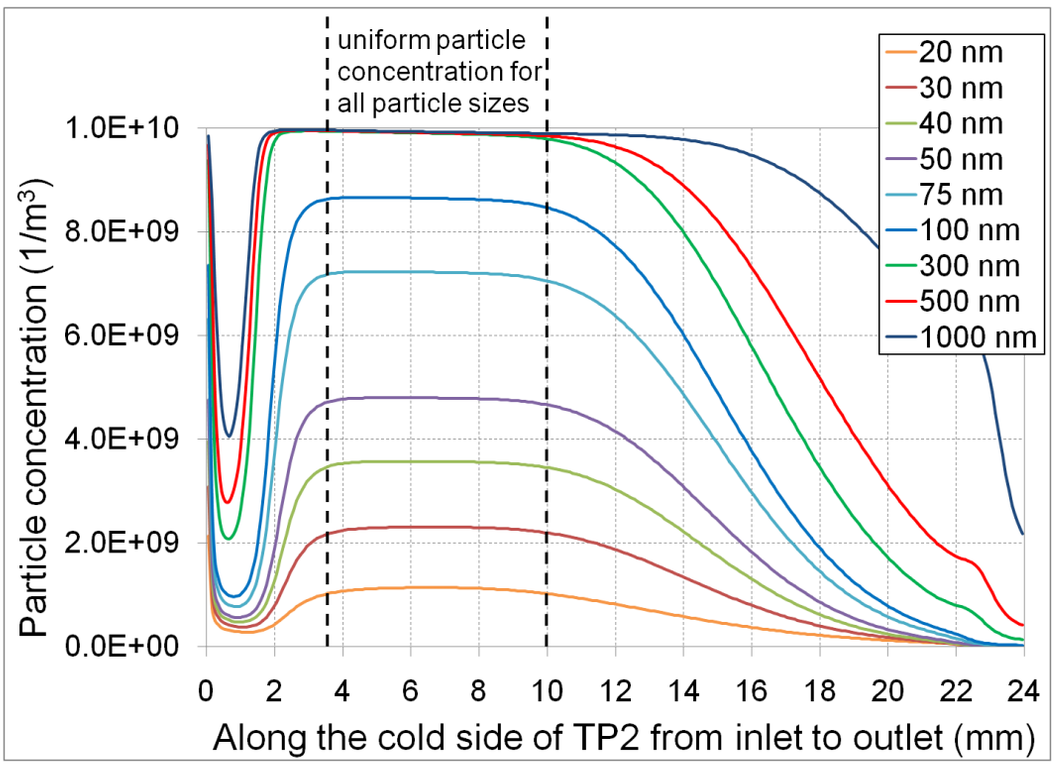

Fig. 4.14 Concentration profile along the cold side of the TP2 for nine different particle sizes from 20 nm to 1000 nm. The section of the plates is between 2 mm and 22 mm, with 2 mm of inlet and outlet regions each.

A particle number concentration of 10^{10} 1/m^3 was set at the inlet (0 mm). Due to the parabolic nature of the flow profile, the particles are drawn towards the region of highest velocity which is in the middle of the TP2. At the beginning of the plates (2 mm), thermophoresis causes the particles to be diverted towards the cold plate. The concentration therefore increases accordingly. Because of particle deposition, the number of particles in the flow constantly reduces and thus the concentration sinks towards zero.

The absolute values of particle number concentration observed close to the cold plate, increase with increasing particle size. This is partly due to the effect of numerical diffusion, whereby the particle number concentration at the walls has to be set to zero. Due to the concentration gradient at this section in combination with the higher thermophoretic velocity, especially the smaller particles are quickly deposited on the cold plate. The value in the last but one cell is therefore smaller for smaller particles because these particles are deposited faster. This effect is further illustrated in Fig. 4.15. By displaying the particle number concentration from the warm to the cold plate, 5 mm from the start of the plates, It is observed that the particle number concentration is zero at the warm plate, rises to set the inlet concentration in the middle and drops towards zero at the surface of the cold plate, with a more rapid drop observed for smaller particle sizes.

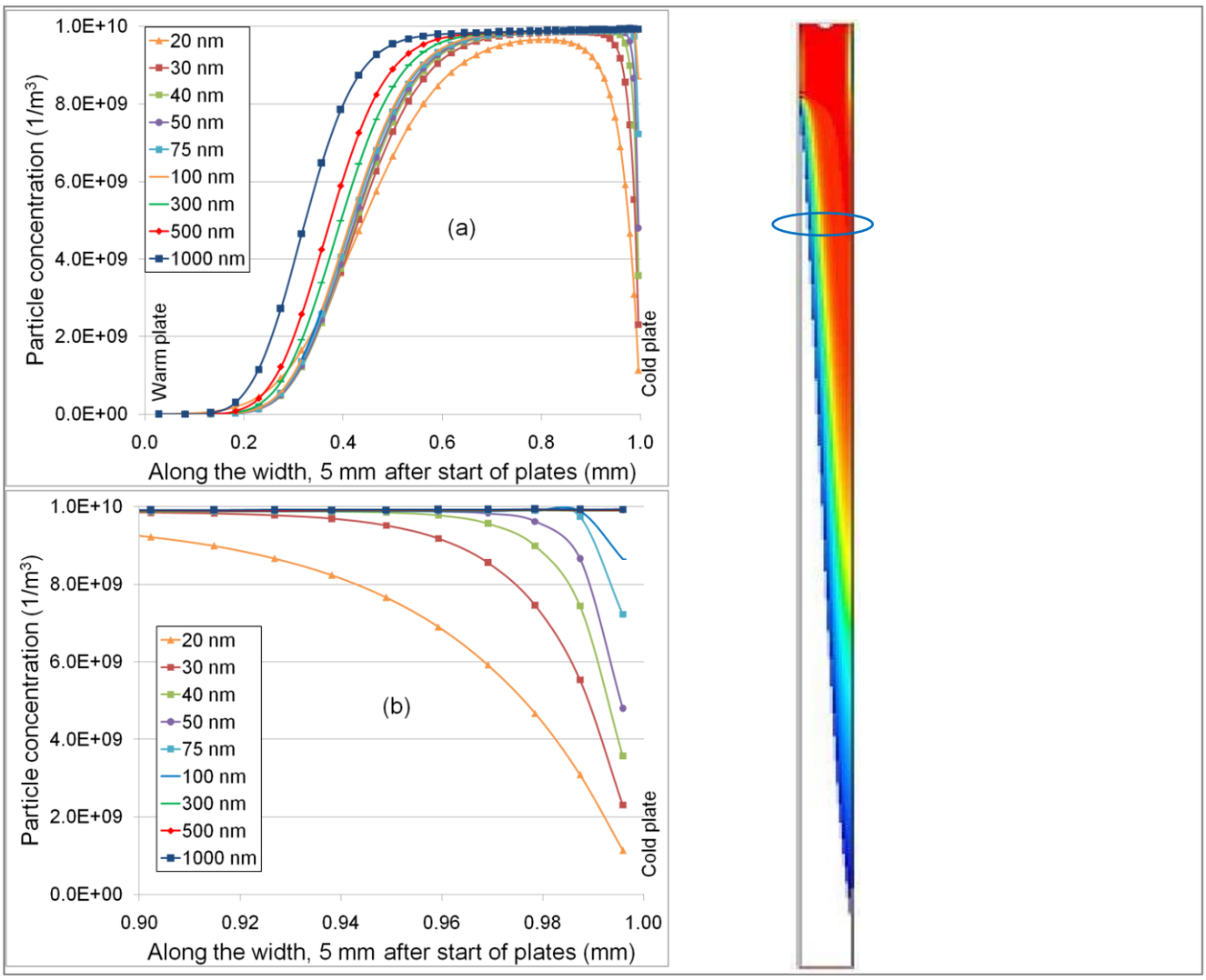

Fig. 4.15 (a) Concentration profile for particle sizes from 20 nm to 1000 nm, from warm to cold plate in the TP2, at a position 5 mm (circled in blue) from the start of the plates. (b): more detailed look close to the cold plate

For all particle sizes however, as shown in Fig. 4.14, a section of uniform particle number concentration was observed, starting from about 3.5 mm from the inlet (1.5 mm after the start of the plate) to about 10 mm from the inlet (8 mm into the plate), a total length of 6.5 mm. This length of uniform particle number concentration is valid for the case where the temperature gradient is 15 K/mm and the orientation of the TP2 is vertical (Case1). The uniform particle number concentration for all particle sizes together with a uniform temperature gradient and flow velocity in this section should lead to a homogeneous deposition of particles in this section. This section should therefore be the most suitable for subsequent analysis of the deposit.

In order to evaluate the deposition of particles, the TP2 was divided into five sections considering the inlet and outlet regions as well as concentration changes along the length of

the plate. Section R1 and R5 in Fig. 4.16 represent the inlet and outlet regions respectively. The region of the plates was divided into three different sections. At the beginning of the plates, there is a rise of the concentration level towards the cold plate the concentration levels only become constant after about 1.5 mm from the start of the plates. This 1.5 mm section (R2) as well as the section where homogeneous particle deposition is expected (R3) and the rest of the plate (R4) was evaluated for the uniformity of the deposition.

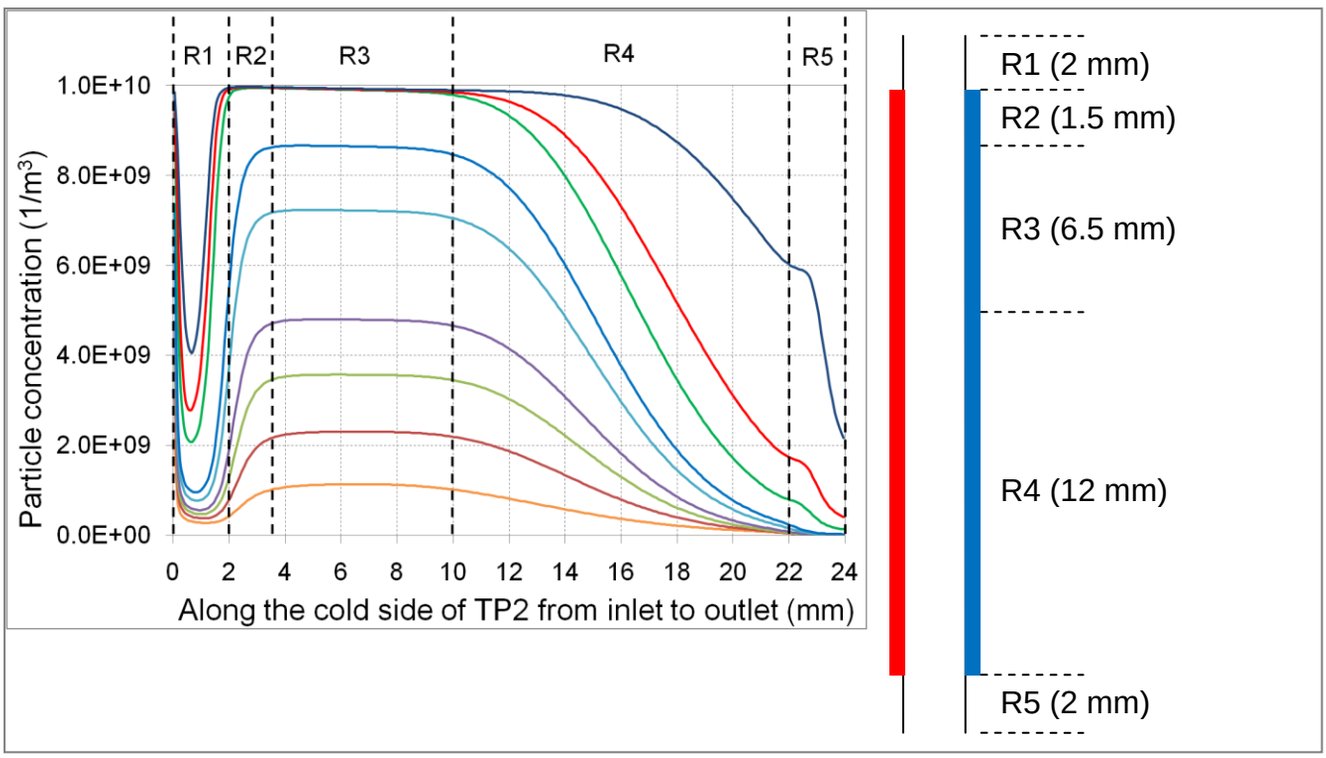

Fig. 4.16 Division of the TP2 into different sections with respect to changing concentration values along the cold plate as well as for the investigation of the deposition in the inlet and outlet regions

4.2.2 Effect of particle size on the deposition

In the numerical model used, it was not possible to directly investigate the number of deposited particles, since the concentration at the plate was set to zero. It was however possible to calculate the number of particles in the flow at any point in the TP2. By calculating the number of particles that flow into the TP2 inlet and the number of particles that flow across the boundary of R1 and R2, it was assumed that the difference represents the number of particles deposited in R1. Using the same method for the rest of the TP2, the deposition in each section was obtained. Fig. 4.17 illustrates the particle deposition per millimeter, for each of the chosen regions (R1 – R5). This simulation was performed with a temperature gradient of 15 K/mm and for the default vertical orientation (case 1) of the TP2.

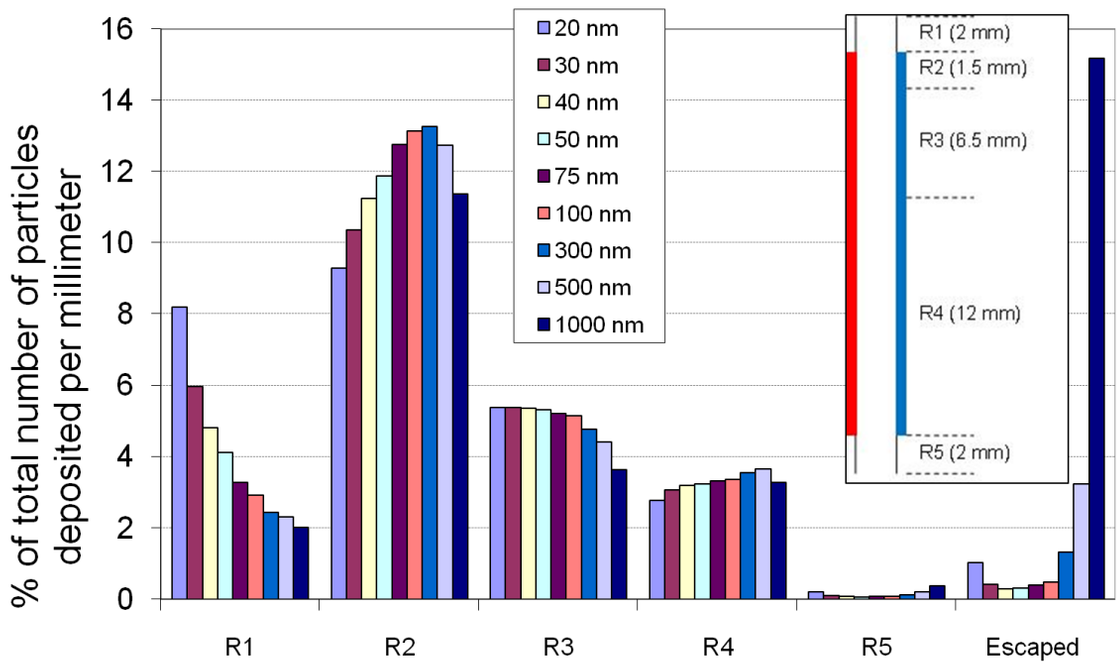

Fig. 4.17 Deposited particles per millimeter in the different regions of the TP2. Escaped particles displayed as an absolute percentage (i.e. not per millimeter).

Some particle deposition can be observed in the inlet tunnel (R1), especially the smaller particles which are most affected by Brownian diffusion. At the beginning of the plates (R2), thermophoresis causes a rise in the deposition rate. This deposition is however non-uniform, representative of the non-uniform temperature gradient which exists at the edges of the plates. Furthermore, due to the reduced concentration of smaller particles which were deposited in the R1, the number of smaller particles deposited in R2 is smaller. For the larger particles, which were not affected much by diffusion, the lower thermophoretic velocity for 1000 nm in comparison to 300 nm particles for example, causes the 1000 nm particles to be deposited less in this section in comparison to 300 nm particles. In the 6.5 mm section (R3) of uniform particle number concentration, where a uniform deposition is expected, about 5 % of all particles which enter the TP2 are deposited per millimeter. This shows that about 33 % of all particles which are sucked into the TP2 are deposited on this 6.5 mm section. Also in this section a nearly size independent deposition can be seen for particle sizes up to about 300 nm. The fact that all particle sizes are deposited with very similar deposition rates shows that the deposited particle size distribution can be assumed to be representative of the airborne size distribution. The small differences in deposition rates, however, can be accounted for during the evaluation of the deposit. Particles are non-uniformly deposited on the rest of the plate (R4). In the outlet tunnel (R5), a low rate of particle deposition is observed, firstly because of the absence of a temperature gradient in this region and secondly

because of the low particle number concentration at this point. The rest of the particles, mostly the larger particles with a smaller thermophoretic velocity, are carried away with the flow. These escaped particles are displayed as the absolute percentage and not per millimeter in Fig. 4.17. Section R3 is further illustrated in detail (per millimeter) in Fig. 4.18. A size dependent uniform deposition of particles as expected is clearly demonstrated. For all particle sizes ≤ 300 nm there is an acceptable maximum deviation in the deposition of about 11% is found. The deposition can therefore be considered as size-independently homogeneous for this uncertainty.

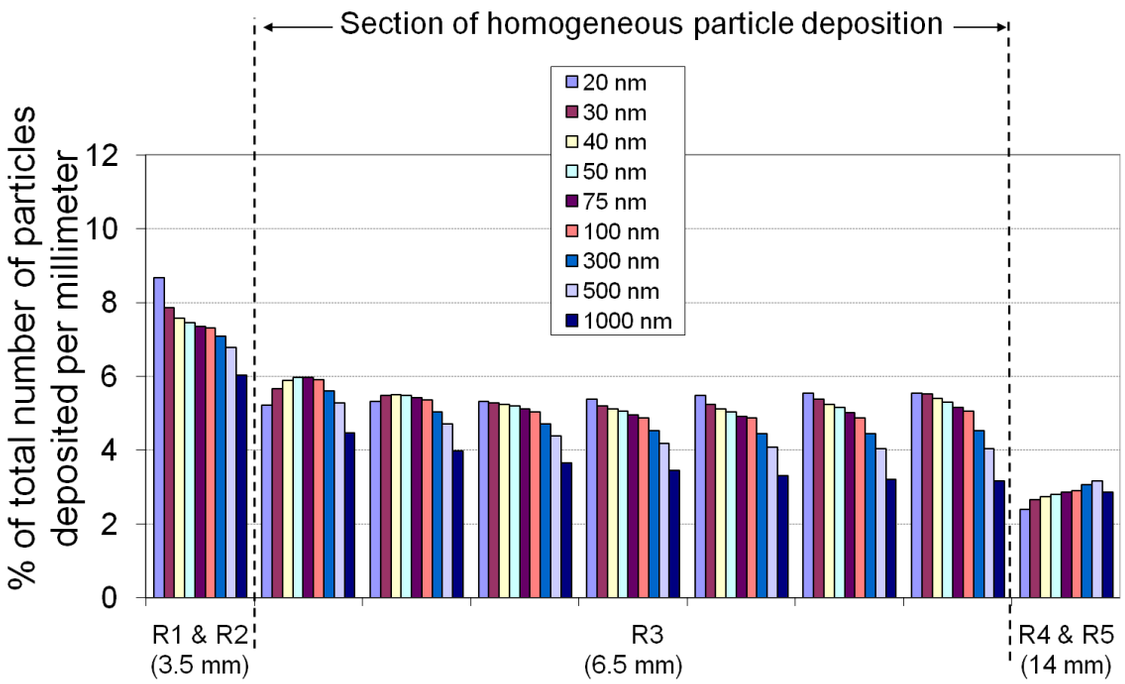

Fig. 4.18 Detailed deposition in the region where uniform deposition is expected. The deposition in every millimeter as well as the last 0.5 mm of section R3 is illustrated per millimeter.

The average deposition rates in R3 are shown in Fig. 4.19 as a function of particle size. Smaller particles with a higher thermophoretic velocity are deposited faster than larger particles with a lower thermophoretic velocity.

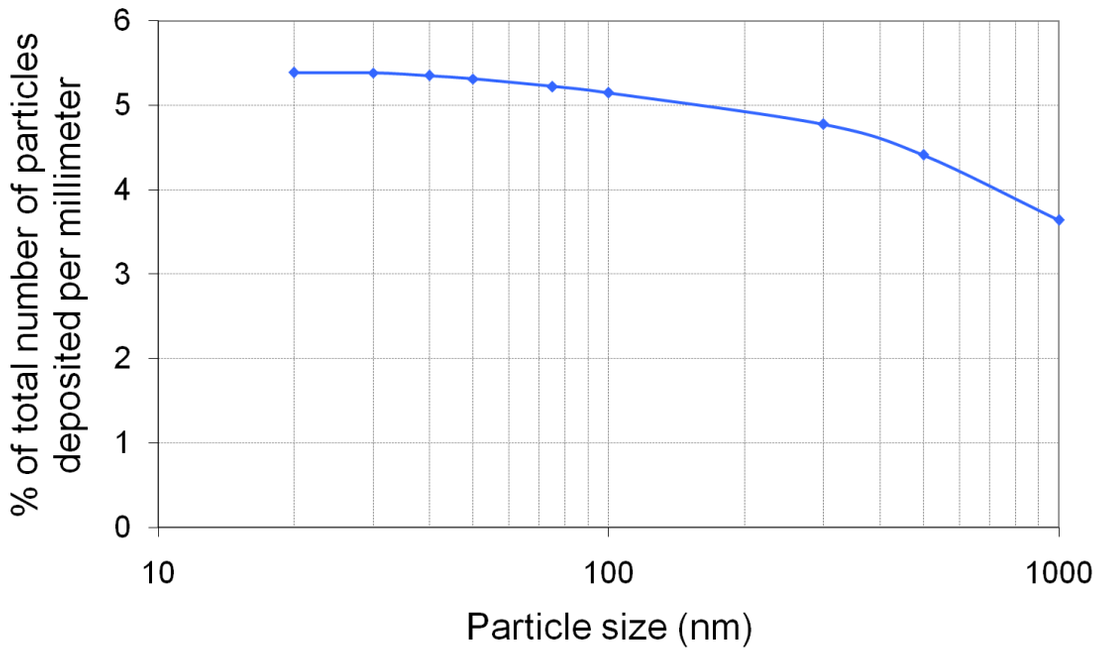

Fig. 4.19 Particle deposition with respect to particle size in section R3 of the TP2

4.2.3 Effect of temperature gradient on deposition

Results from simulations with different temperature gradients showed that, as expected, the particle number concentration close to the substrate, and consequently the deposition rate increases with increasing temperature gradient (Fig. 4.20). The length of constant particle number concentration however decreases.

For a temperature gradient of 18 K/mm, the length reduces to about 4.5 mm and for a temperature gradient of 12 K/mm, the length increases to about 8.5 mm. For a higher temperature gradient of 18 K/mm, particles are deposited faster on the cold plate and therefore the concentration of particles in the flow also drops accordingly. The reverse is true for a lower temperature gradient of 12 K/mm. It should however be noted that for a temperature gradient of 12 K/mm, the particle number concentration at the walls also drops due to the lower rate of deposition and for this particular geometry, many particles are carried out with the flow. This therefore means that by getting a longer evaluation distance, which may be desirable, one would eventually get an undesirable reduction in the deposition rate. In case of an aerosol with low concentration, sampling time may increase in order for enough particles to be deposited on the substrate. One therefore has to find a compromise between the sampling time and distance of uniform deposition.

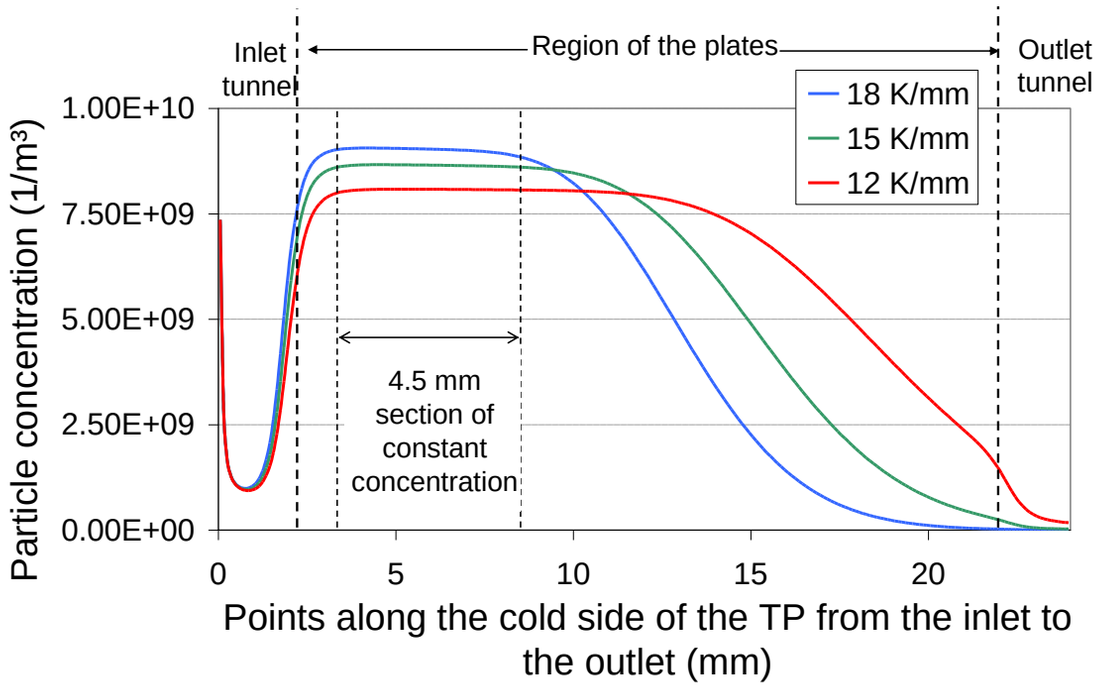

Fig. 4.20 Exemplary particle number concentration along the cold side of the TP2 for a particle size of 100 nm with an inlet particle number concentration of 10^{10} 1/m^3 and for three different temperature gradients.

Fig. 4.21 shows the deposition per millimeter for a 4.5 mm section (see Fig. 4.20) where for all temperature gradients, the particle number concentration on the cold plate is seen to be constant.

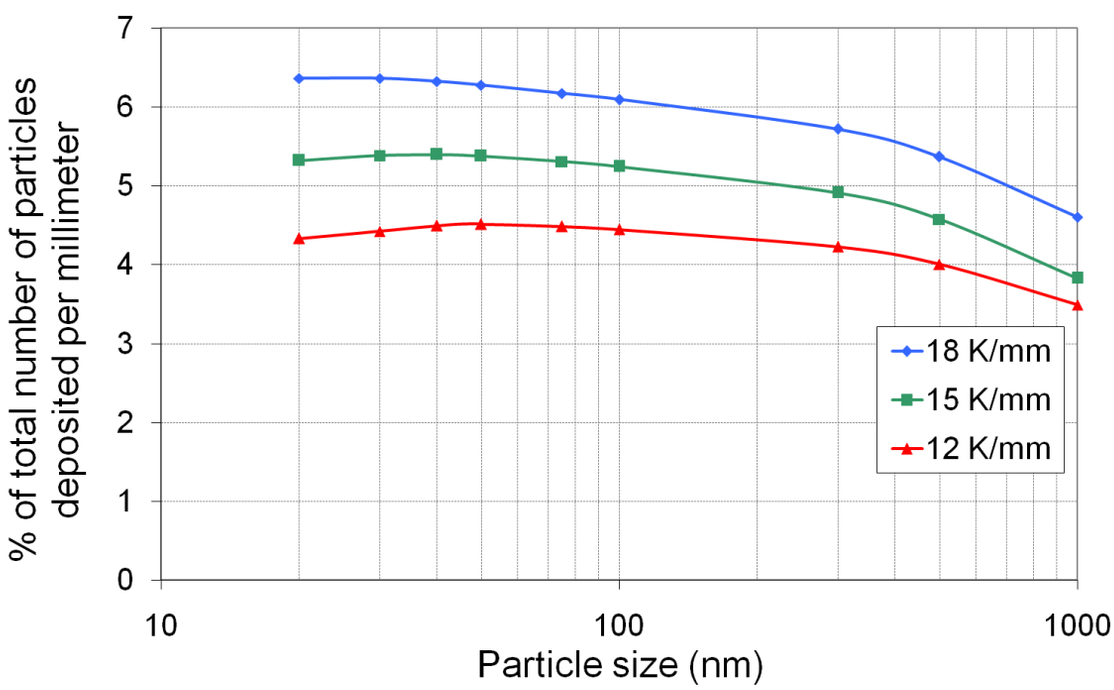

Fig. 4.21 Particle deposition in a 4.5 mm section of homogeneous deposition for three different temperature gradients.

4.2.4 Effect of device orientation on deposition

Results of numerical modelling for orientation cases 2 and 3 with a temperature gradient of 15 K/mm, showed a similar length of constant particle number concentration as with case 1. There was however a slight difference in the level of particle number concentration for cases 2 and 3 than those obtained for case 1 for the considered case of 100 nm particles. Fig. 4.22 illustrates this difference. This difference is more pronounced for particle sizes larger than about 300 nm. For case 2, the additional effect of gravity on the deposition should case an increase in the concentration close to the wall. However since the thermophoresis already causes almost all particles of the considered size to be deposited, gravity in the direction of thermophoresis does not produce an additional effect. For case 3 on the contrary whereby gravity counteracts thermophoresis, the concentration close to the walls drop as a result.

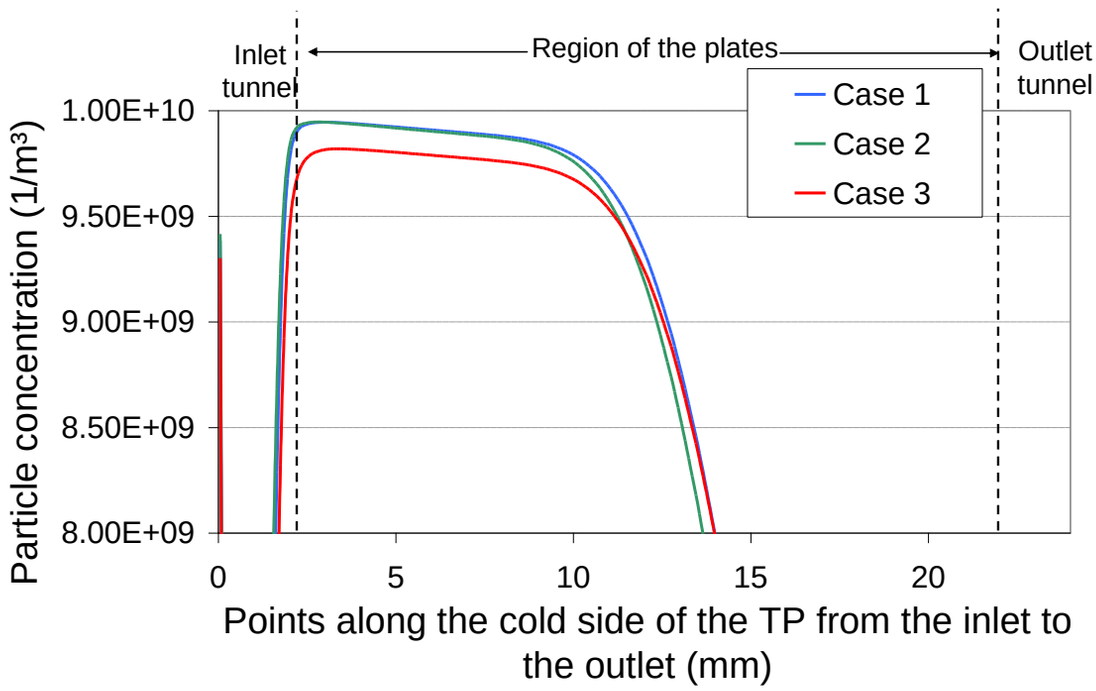

Fig. 4.22 Particle number concentration profile along the cold side of the TP2 for a particle size of 100 nm with an inlet particle number concentration of 10^{10} 1/m^3 and for the different orientation states.

Examining the particle deposition in section R3 as given by the model for different orientation cases, it is shown (Fig. 4.23) that especially for larger particles, more particles are deposited for case 2 than for case 1 with case 3 showing the lowest deposition of particles for these large particles. For particle sizes up to 300 nm, the deviation from case 1 for the number of deposited particles is in the acceptable range of ± 1.6 % (cases 2 and 3). It can therefore be assumed that the deposition and eventual evaluation of all particles smaller than 300 nm can be done irrespective of the orientation of the TP during sampling.

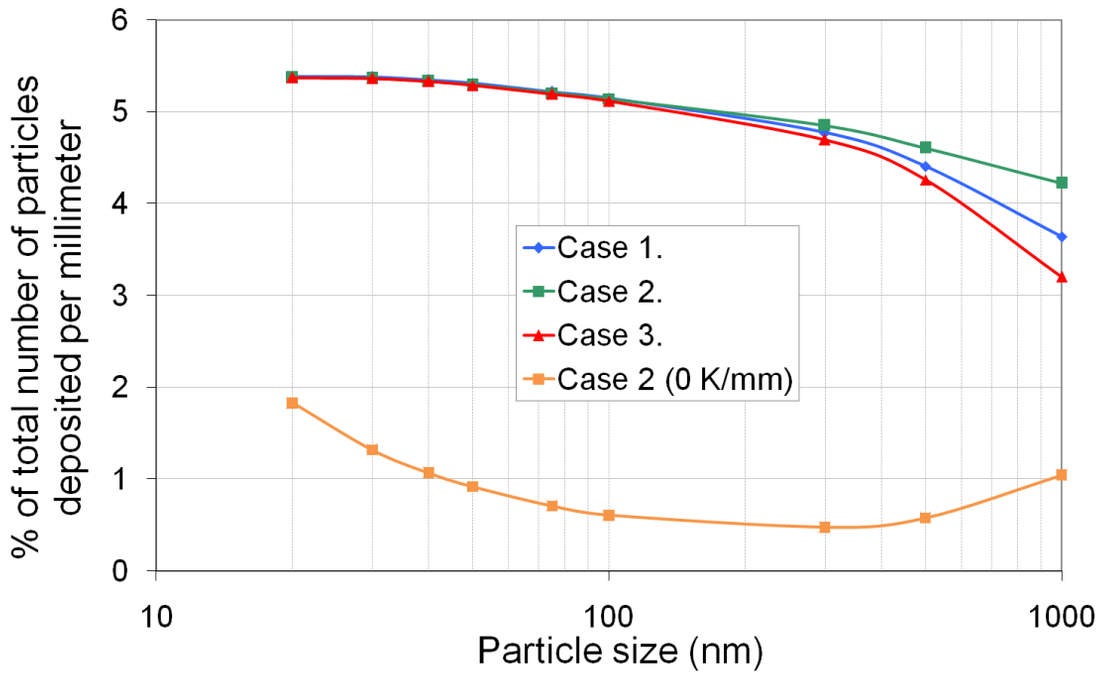

Fig. 4.23 Percentage deposition of particles on a 6.5 mm section of the substrate, for a temperature gradient of 15 K/mm. Effect of Brownian diffusion and gravity shown for a case where no temperature gradient exists.

4.2.5 Effect of Brownian diffusion on deposition

The effect of Brownian diffusion on the deposition especially for the smaller particles as well as the effect of gravity on the deposition particularly for the larger particles in the worst case (case 2: gravity working in the same direction as thermophoresis) is illustrated in Fig. 4.23. For 20 nm particles for example about 11.9% of all inflowing particles of this size would be deposited in section R3 by Brownian diffusion without the presence of thermophoresis. This amounts to 34% of all particles of this size deposited in this section with the influence of thermophoresis. Since thermophoresis is however directed diffusion, its effect in the TP2 for the operating conditions, overwhelms the Brownian random diffusion. Brownian diffusion therefore only plays a role in the inlet region. Considering that up to 16% of all inflowing 20 nm particles were deposited in the inlet region, the decision to shorten the inlet tunnel to 2 mm was justified. Up to 32% of all inflowing 20 nm particles would be deposited in the inlet region on a stretch of 8 mm (as in the TP1). The difference between the three deposition curves for the three different orientations of the TP2, and the curve for the case with 0 K/mm clearly shows the efficiency of thermophoresis.

4.2.6 Effect of particle material type (density) on deposition

Simulations with particles of different densities also confirmed the analytical calculations. The particle deposition curves for the different orientation cases are illustrated in Fig. 4.24 for particles with unit density (1 g/cm³) and iron particles (7.9 g/cm³).

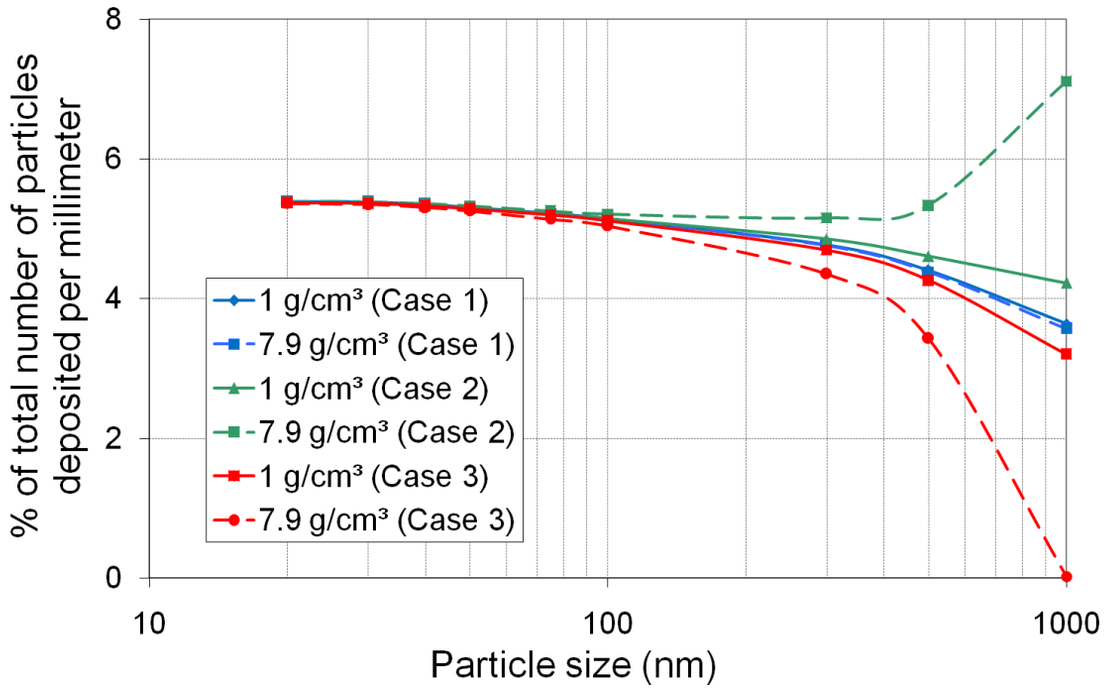

Fig. 4.24 Percentage deposition for particle with different densities and for the three orientation cases.

For smaller particles, there is no observable deviation in the percentage deposition of cases 2 and 3 from case 1, in the region of uniform deposition. For 300 nm particles with unit density, a deviation of about ± 1.6 % was observed. For 300 nm iron particles (ρ = 7.9 g/cm³), there is a deviation of about ± 8.4 %. For the default orientation (Case 1) however, there is a minor difference between the deposition patterns of particles of unit density and iron particles which is only noticeable for very large particles (~1000 nm). This minor difference is caused by the higher thermal conductivity of the iron particles which leads to a smaller thermophoretic velocity. Generally one can conclude from Fig. 3.30 that for the default orientation, the deposition of particles sizes up to 1000 nm is only slightly dependent of particle material type (density and thermal conductivity) and for the case of iron particles and water liquid, there is an acceptable deviation of 2% in the deposition rate. If the TP2 is not carried in the default orientation, i.e. cases 2 and 3, particle sizes up to 300 nm can be evaluated without prior knowledge of the orientation with a ± 8.4 % uncertainty. For larger particles up to 1000 nm, the use of calibration factors may be feasible if the main orientation is known. For Case 3 for example, large particles with higher densities will not be deposited on the substrate. Such an

orientation may be used to separate larger high density particles from smaller particles (which may be of interest).

4.3 Uncertainties

In the numerical modelling of the TP2, some assumptions are made and boundary conditions are simplified in order to save simulation time as well as facilitate the convergence of the solution. As a result of the assumptions, uncertainties may arise in the final result of the numerical model. Uncertainty is defined in this context as the margin of error than can be made when comparing the results of a numerical model with the results one would expect in the reality given the changes in physical conditions that occur in reality.

As has been described before, numerical modelling was carried out using a two dimensional grid in order to reduce the simulation time from about 48 hours to about 2 hours. In the 2D model, it was assumed that the flow tunnel is infinitely wide. The effect of the side walls in this case is therefore neglected. Considering the fact that the flow tunnel should have a width of 6 mm compared to a height of 1 mm, the effect of the side walls on the flow and temperature profile is expected to be very small. By taking a look at the 3D grid one can examine the flow and temperature profiles in the TP2 along both the length and the width. Fig. 4.25 shows the flow and temperature profiles along the width (in the middle) of the TP2. No notable differences were found between the temperature gradients and flow profile in the middle of the 3D Model and the representative 2D Model. The effect of the side walls on these profiles in the middle of the TP2 was therefore not noticeable There is a similar profile about 0.5 mm from the wall as the middle which is represented by the 2D. The assumption of infinitely wide plates in the 2D-model is therefore a fair assumption.

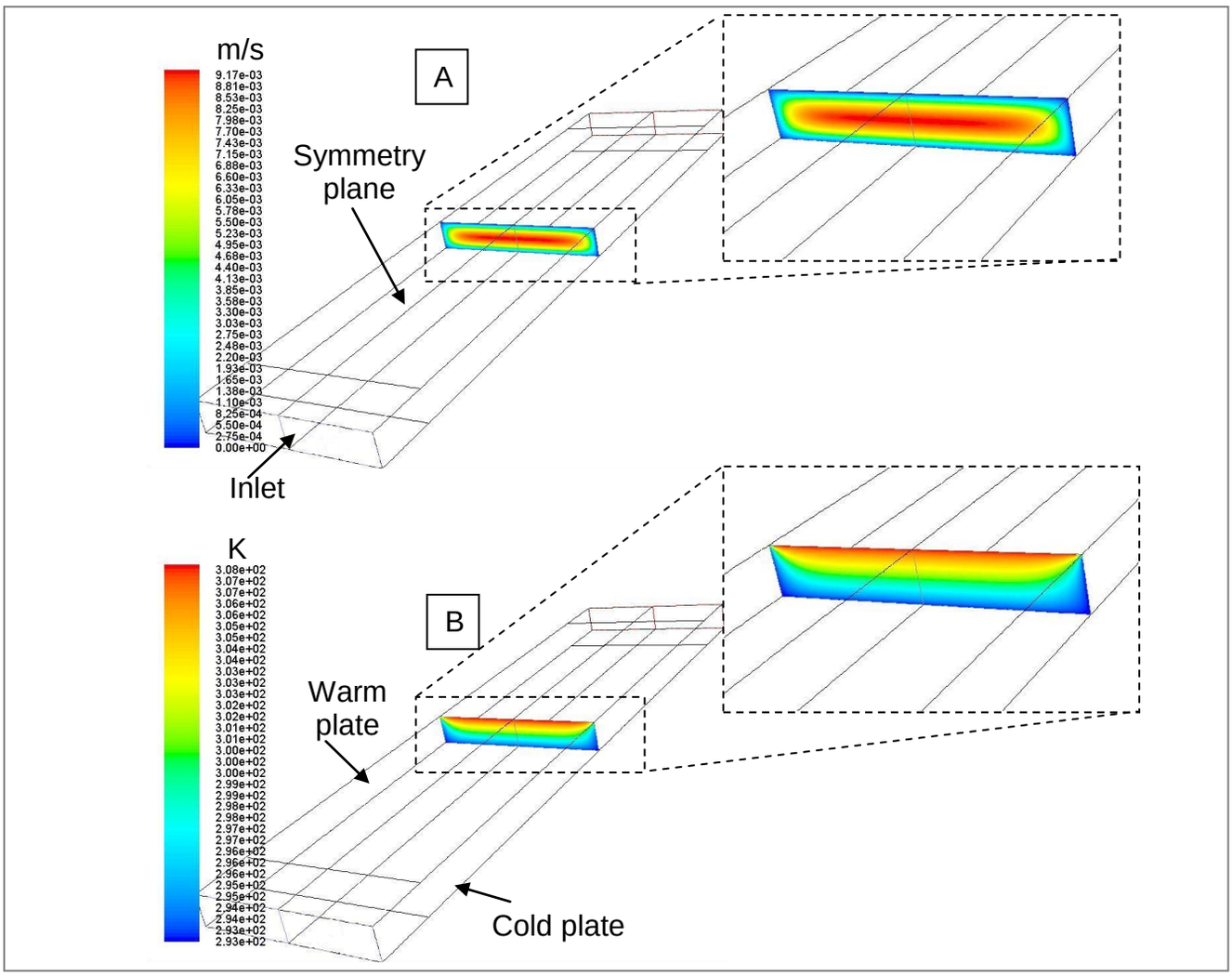

Fig. 4.25 Flow profile (A) and temperature profile (B) in the middle of the TP.

In the numerical model, the boundaries were all assigned specific values of temperature. This is in order to keep the model as simplistic as possible and ensure that the solution can easily converge. A temperature gradient is created in the gas with respect to these assigned values at the boundaries. There however exist no temperature gradients in the walls. The temperatures of the inlet and outlet regions of the TP2 were always set to the temperature of the cold plate at 293 K which was set to be the operating temperature of the TP2. In this case, particles which flow into the TP2 only experience a temperature gradient when they reach the region of the plates. The inhomogeneous temperature gradient which builds up in this region between the warm plate and the cold plate as well as between the warm plate and the inlet region causes particles to deposit inhomogeneously at the start of the plates. In reality, due to heat transfer, the temperature of particularly the upper wall (warmer side) of the inlet tunnel shall increase due to contact with the warm plate. This increase in temperature shall lead to the development of a temperature gradient in the inlet region of the TP2. Particles that flow

into the TP2 shall therefore experience a temperature gradient before they reach the region of the plates. The temperature gradient in this section is expected to be relatively low so that the amount of particles deposited thermophoretically in this section should be just only a very small fraction of the total number of particles which flow into the TP2. The presence of a temperature gradient in this section may however cause particles to be deposited on the plate, earlier than predicted by the numerical model.

When calculating the number of deposited particles, FLUENT-FPM does not provide a direct tool to investigate the number of particles deposited at each position on the walls. The flow rates and mass flow rates in the flow at various positions in the model were used to calculate the number of particles which are in the flow at that position. The difference between the numbers of particles in the flow at two consecutive positions represents the number of particles deposited.

In the inlet region of the TP2, where particles are deposited mainly by Brownian diffusion, one cannot tell if these particles are deposited on the upper or lower wall of the inlet region. This section of the TP2 is however not meant for subsequent examination; therefore a quantitative value of the deposition is sufficient information from the model. At the start of the plates however, the existence of a sudden temperature gradient in this region causes an inhomogeneous deposition in this area. Even though the particles are deposited primarily by thermophoresis in this region, it is not clear if all the particles are deposited on the cold plate. This section is however also not suited for subsequent analysis due to the inhomogeneous deposition in this section. In the middle of the TP2, where the thermophoretic force is the overwhelming force especially for orientation cases 1 (vertical default position) and 2 (horizontal with cold plate at the bottom), calculation of particle deposition using this method can be assumed to be accurate. For case 3 (horizontal with cold plate at the top), gravity may cause some larger particles to be deposited on the warm plate. For particle sizes up to 300 nm, modelling results show that thermophoresis is still the overwhelming force for this orientation and therefore the assumption that the particles are deposited on the cold plate is also reasonable for this case.

The FPM model can simulate particle growth and transportation with respect to physical conditions such as flow, temperature etc. One assumption that is made with the FPM is that the particles are spherical in shape. Since the diffusion equivalent diameter of particles is the important property for thermophoresis, the shape of the particle is of particular importance. Zheng (2002) compared available theories of thermophoresis of spherical and non-spherical particles and conclude that meanwhile there are a few studies for thermophoresis of non-

spherical particles in the near-continuum and free molecular regime, knowledge of thermophoresis of non-spherical particles is still very limited.

4.4 Summary of analytical and numerical models

Development of the TP2 was performed by analytical and numerical modelling. The developed analytical model was a simplistic model neglecting some physical effects, e.g. Brownian diffusion, buoyancy, parabolic flow profile in the TP2 as well as temperature effects at boundaries. Analytical modelling provided initial estimates for the design of a grid and also estimates of some boundary conditions which were put into a numerical model. For a plug flow velocity of 5.5 mm/s and a gap distance of 1 mm between the plates, a temperature gradient of 15 K/mm was calculated by the analytical model which ensures a complete deposition of sub-micron particles along the entire length of a 20 mm long substrate. Because of a homogeneous temperature gradient created between the warm and cold parallel plates of the TP2, a homogeneous deposition was expected along the entire length of the plate.
Numerical modelling was performed with FLUENT using the analytically obtained parameters as boundary conditions. The numerical model takes into consideration, a more realistic parabolic flow profile between the plates, temperature irregularities at the boundaries of the plates, buoyancy effects, Brownian diffusion and the effect of gravity on the deposition. Results from the numerical model show that the estimate of a temperature gradient of 15 K/mm for a gap distance of 1 mm was a very good. For these conditions, a representative homogeneous deposition of all particles < 300 nm was realized on a 6.5 mm length of the substrates with an acceptable maximum deviation (particle size and TP2 orientation dependent) of 11%. This 6.5 mm length of homogeneous particle deposition provides a sufficient area for eventually SEM analysis. Results from the numerical model also show that, for larger particles up to the examined size of 1000 nm, the deposition in the 6.5 mm section be examined and the airborne particle number concentration can only be calculated if the TP2 orientation during sampling in known. These results from the numerical modelling provided the basis for the design and construction of the TP2.

5 Design and Construction of the TP2

As a personal sampler which should be carried by a worker for an entire shift, the TP2 had to be light weight and small to be easily carried. The TP2 should also be battery operated and therefore the power consumption should be low so that it can be operated continuously for at least 8 hours. The above conditions were considered when choosing components for the TP2. Two determining factors in the design of the TP2 were the creation of a stable and constant temperature gradient and the reliable provision of an appropriate volumetric flow rate.

5.1 Creating a stable and constant temperature gradient

Peltier elements were utilised to realise a constant temperature gradient. A Peltier element is a thermo-electrical diode which creates a heat flux when a current is applied. Connecting a Peltier element to a DC source causes one side to become colder, while the other side becomes warmer. The temperature difference between the two sides is a function of the applied current. By using two Peltier elements in parallel (see Fig. 5.1), with one Peltier element used to heat up the warm plate and the other used to cool the substrate, a temperature gradient is created between the plates.

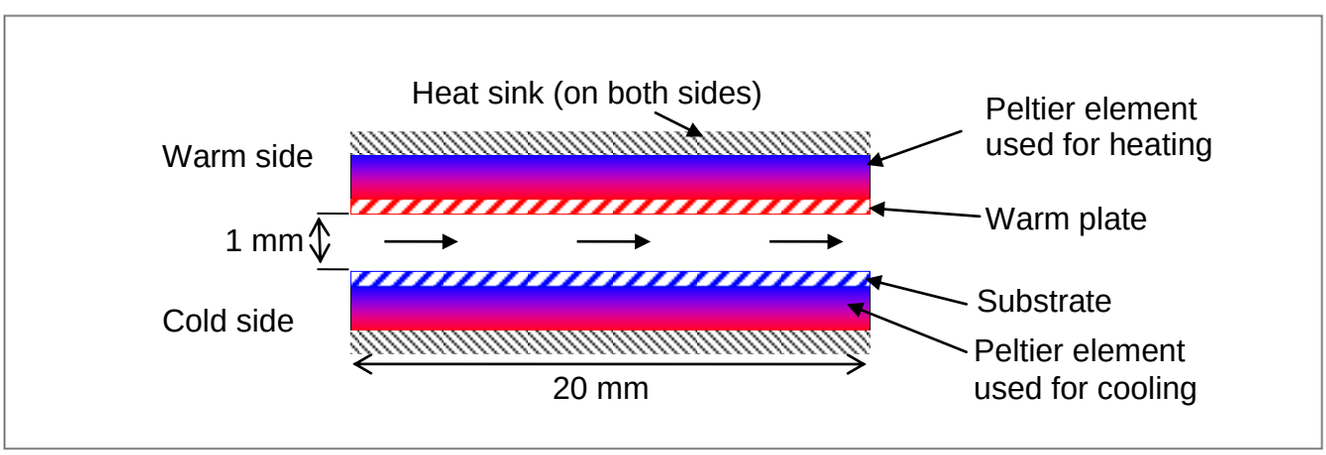

Fig. 5.1 The functioning principle of the TP2. The change in colouration from blue to red in the Peltier elements, indicates an increase in temperature.

To check the feasibility of Peltier elements for this application, laboratory tests were conducted with commercial Peltier elements (TEC1-3105) with dimensions of 20 mm x 20 mm x 3.9 mm. A 0.5 mm thick copper plate was placed on the warm side to simulate the warm plate and a 0.625 mm thick silicon substrate was placed on the cold side. The warm and cold sides were held apart by a 1 mm thick custom made spacer made from

heat insulating polycarbonate. Accurately measuring the temperatures of the inner surfaces of the plates, hence the temperature difference between the plates was rather difficult with the plates held only 1 mm apart. The smallest available thermocouples were about 0.5 mm in diameter. It was not possible to place and hold two of such thermocouples in place in the 1 mm gap without influencing the temperatures. Furthermore since the temperatures of the plates have to be continuously measured and regulated during sampling in order to guarantee a constant temperature gradient during the entire sampling period, measuring the temperatures on the inner surfaces of the plates will interfere with the flow in the TP2. For these reasons, the temperatures were measured between the Peltier elements and the plates. Laboratory tests showed that there is about a 0.5 K temperature loss across the plates. This means that to achieve a temperature difference of 15 K between the plates, a temperature difference of 16 K had to be achieved between the locations where the thermocouples were placed. The required temperature difference of 16 K (15 K between the inner surfaces of the plates) was achieved and held constant by additionally applying heat sinks to both Peltier elements and by cooling the cold side with a small fan. The total power consumption was in the order of 1 W, which can be provided for several hours by modern batteries. These preliminary experiments showed that the use of Peltier elements is feasible to operate the TP2.

5.2 Creating a stable and constant flow rate

The dimensions of the inlet slit as well as the flow tunnel is 1 mm x 6 mm. A flow velocity of 5.5 mm/s in the TP2 corresponds to a volumetric flow rate of 2 ml/min. Due to the difficulty of creating and measuring this small flow rate, a custom made setup was built for this purpose as shown in Fig. 5.2.

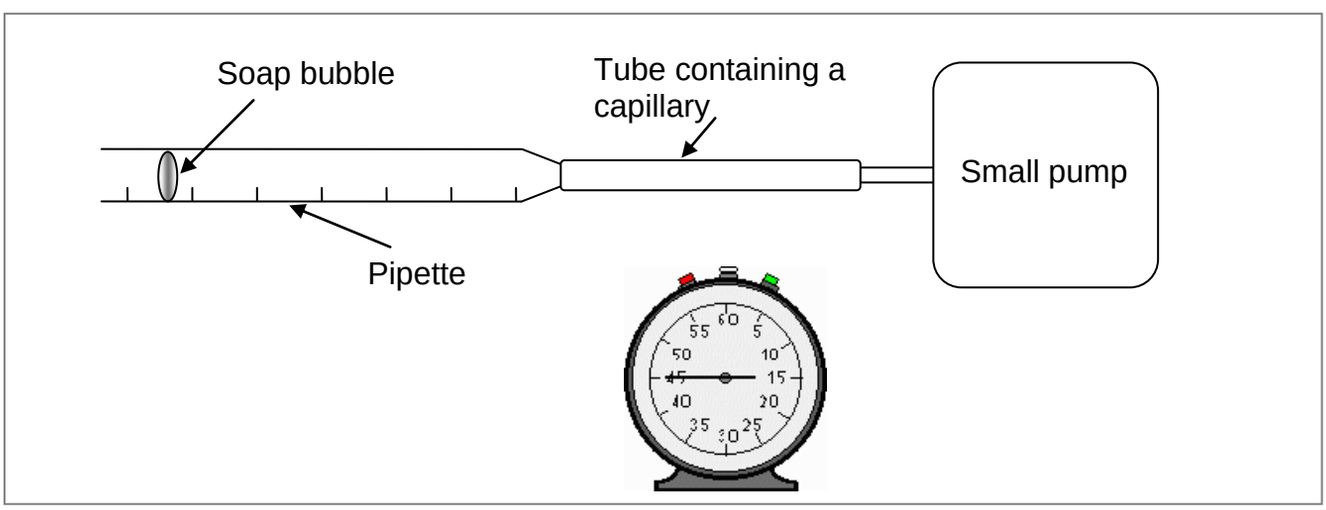

Fig. 5.2 Experimental setup used to calibrate the flow rate of the TP2

A soap bubble was created and sucked into a pipette. A small ventilator pump was used in connection with a capillary, using the pressure drop over the capillary to create a small flow rate which moves the bubble across the pipette. The time taken for a bubble to cover a volume of 2 ml in the pipette is measured. The rotational speed of the pump was adjusted for capillaries of different diameters and lengths in order to achieve a time of exactly 1 min, thereby achieving a flow rate of 2 ml/min. The procedure was repeated for several adjustments of the pump rotational speed and for different capillary sizes until an optimal combination was found. A volumetric flow rate of 2 ml/min was created and measured for a rotational speed of 5820 revolutions per minute and for a capillary with a diameter of 0.55 mm and 25 mm long

5.3 Graphical design of the TP2

Under consideration of the dimensions of the Peltier elements, heat sinks and plates that have to be built into the TP2, a graphical design was created. The graphical design was done with the CAD software Cocreate Modeling from PTC® (*http://www.ptc.com*).

5.3.1 First prototype of the TP2

Fig. 5.3 shows an explosive drawing of the first design of the TP2. In the design of this first version of the TP2, various considerations were taken. All the components had to be designed to fit optimally in an appropriate casing. The sizes of the heat sinks for example were therefore designed to match the sizes of the Peltier elements and the ventilator. Due to the unsuitability of measuring the temperatures directly on the inner surfaces of the plates during sampling, thermocouples were placed in between the Peltier elements and the plates and the temperatures at these points were measured. The ventilator which cools the heat sink pulls air from the opening in the lid. The ventilator cap ensures that the air intake is directed away from the inlet slit of the TP2 so as not to affect the intake of aerosol during sampling.

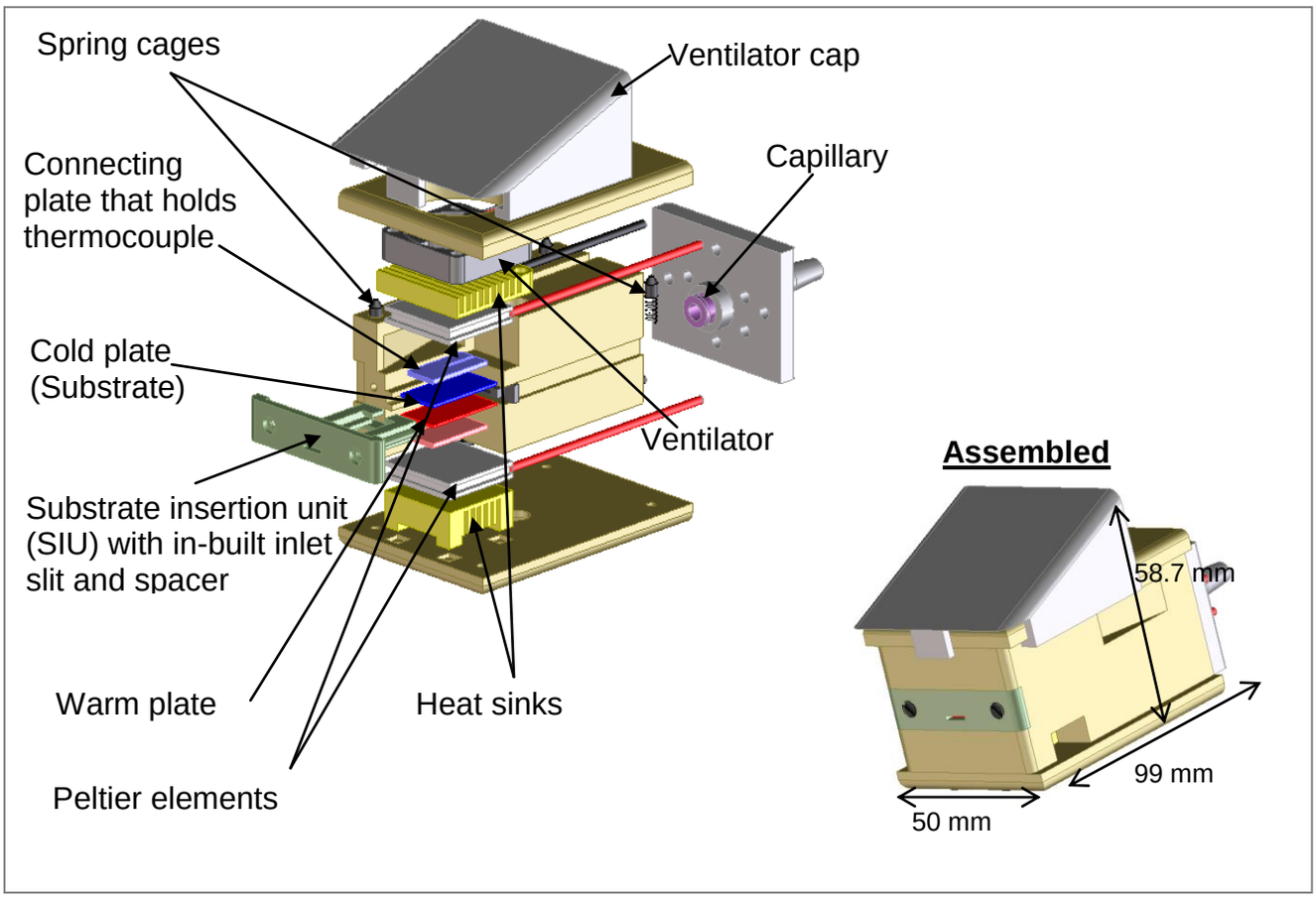

Fig. 5.3 Graphical design of the first version of the TP2 as an exploded view drawing and as an assembled unit with dimensions of 50 mm x 58.7 mm x 99 mm

One new concept in the design of the TP2 is the substrate insertion unit (SIU). This is a major improvement in the handling of the substrate over the TP1. The SIU ensures that the TP2 does not need to be dismantled in order to retrieve the substrate. This saves time and ensures that the substrate can be retrieved in the field and not necessarily in a laboratory before analysis. In a case where the particle number concentration at a workplace is very high, multiple samples can therefore be taken.

The substrate and the warmer plate are placed into the SIU which has an inbuilt inlet slit and a 1 mm spacer which keeps the plates at the required gap distance. The SIU is then introduced into the TP2. On one side of the TP2, the lid is connected to the heat sink which is glued with special thermally conductive glue to the corresponding Peltier element and the connecting plate. Thermocouples are placed between the Peltier elements and the connecting plates before these components are glued together. On the other side of the TP2, the other lid is connected to the other heat sink and the ventilator. This is then glued with the special glue to the other Peltier element and the other connecting plate. These connecting plates containing the thermocouples, serve as a medium to transmit heat to the plates as well

as measure the temperature of the substrate and the warmer plate. Both sides of the TP2 are placed on spring cages, four on each side, which hold the sides apart. The function of the spring cages is to push the lids a few millimeters away from the body in order to provide room for inserting or retrieving the substrate insertion unit. After insertion of the SIU the sides are pressed together to ensure contact with the plates and are then held in place by screws. Fig. 5.3 also shows the assembled TP2 having dimensions of 50 mm x 58.7 mm x 99 mm with the first prototype weighing 185 g.

5.3.2 Improvement on the first prototype of the TP2

The first version was built at the University of Duisburg-Essen and first tests were carried out. These tests provided various indications where the design of the TP2 could be improved on. One major finding from the tests was the redundancy of the ventilator. The ventilator was desired for cooling the warmer side of the Peltier element (used for cooling the substrate) so that the temperature of the substrate would not rise infinitely. It was found that the temperature of the substrate was never more than 3 K above ambient temperature without the use of the ventilator. The temperature gradient however always stayed constant since both Peltier elements are set up such that the same current runs through them and thereby causing the temperatures to change simultaneously. The ventilator was therefore found to be unnecessary. In a second version of the TP2, the ventilator was taken out along with the ventilator cap and the width and height of the TP2 consequently reduced. Improvements were also made to the SIU for easier handling. The spacer which was previously built into the SIU was designed as a separate component. This made it easier to place and retrieve the plates from the SIU. An explosive view of the improved second version of the TP2 is shown in Fig. 5.4 together with the assembled version. The dimensions of the improved version are 45 mm x 32 mm x 97 mm and which is 5 mm x 26.7 mm x 2 mm smaller in dimensions than the first design. The Improved TP2 now weighs only about 140 grams which is 45 grams lighter the first design due to the elimination of the ventilator, ventilator cap and some body material.

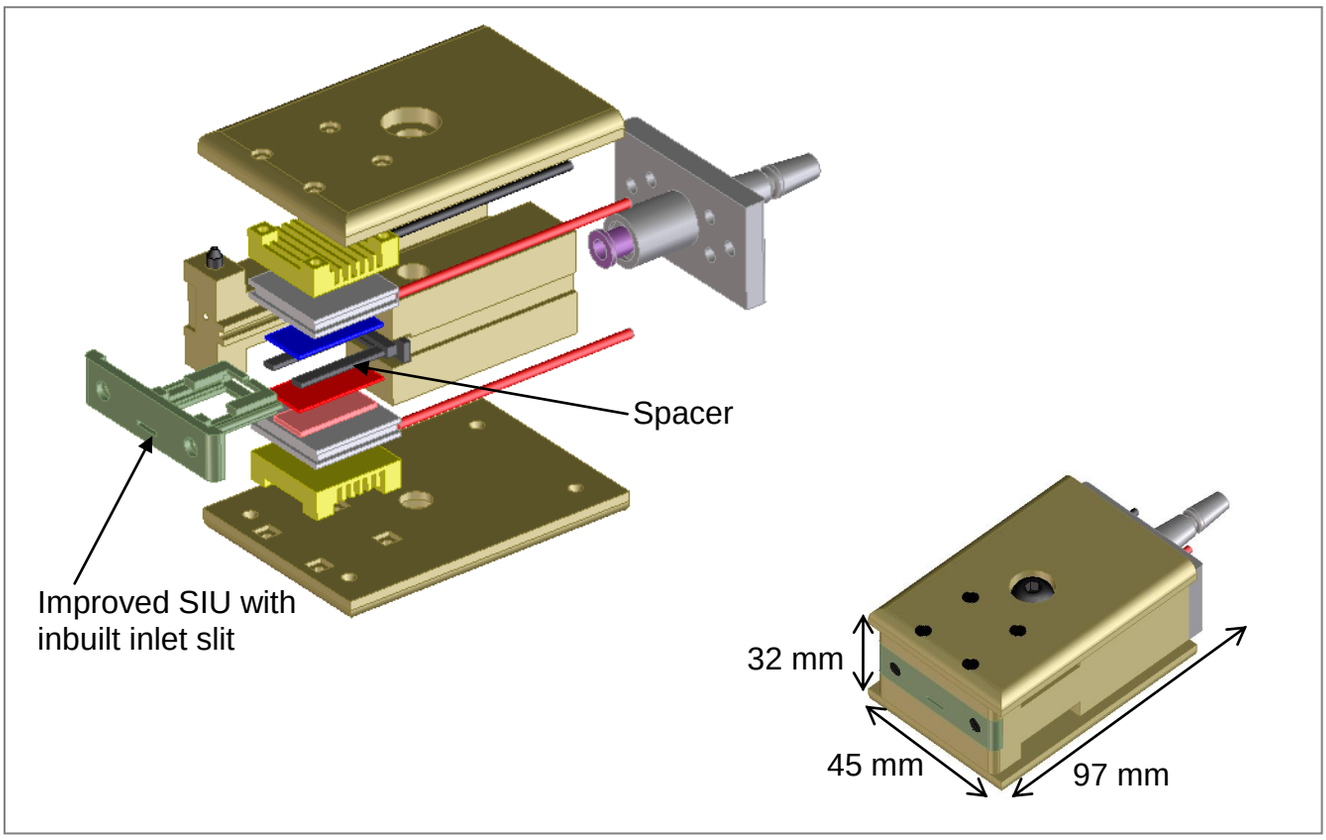

Fig. 5.4 Improved second version of the TP2 with dimensions of 32 mm x 45 mm x 97 mm.

5.4 Choice of materials for construction of the TP2

A key step in the construction of the TP2 is the choice of materials whose properties are suitable for such an application. The major points which were considered for the choice of materials for the housing of the TP2 are the following:

- It had to be lightweight so that the TP2 can be easily carried by a worker.
- It should have a low thermal conductivity so that the heat is conserved and thereby enable the process of keeping the temperature gradient constant.
- It should not be vulnerable to permanent static charges. This is to prevent the charged fraction of the particles to be electrostatically deposited in an undefined manner.

Considering the above points, Polyoxymethylene, also known as Delrin®, was chosen. Anodised Aluminium was used to build the heat sinks and the rear parts. Anodised Aluminium is more resistant to corrosion and wear and has a better adhesion to glues than bare Aluminium, while maintaining its thermal properties. These properties make it ideal for this application.

The connecting plates which hold the thermocouples for temperature measurements also serve as a medium to transmit heat to the substrate and warm plate. A highly thermal conductive material is therefore used as a connecting plate in order to minimise heat losses.

Copper was used for the construction of these connecting plates. Fig. 5.5 shows images of the first version (left) and the improved version (right) of the TP2.

Fig. 5.5 Image of the first and second version of the TP2

6 Experimental evaluation of the TP2

The TP2 was built to sample particles in the size range of a few nanometers up to about 300 nm independent of the orientation of the device during sampling. For the experimental evaluation of the TP2, monodisperse Polystyrene Latex (PSL) particles were envisaged as test particles because of their almost perfectly spherical shape. Spherical particles are assumed in the description of the theory of thermophoresis hence the expressions describing thermophoresis also used in the model. PSL spherical particles which also have a density of 1.05 (~ unit density used in the model) are therefore ideal evaluating the predicted homogeneous deposition characteristic of the TP2. Moreover, comparative particle number concentration measurements are made under the assumption of spherical particles which further supports the use of such particles for the experiments.

6.1 Experimental setup

The experimental setup for evaluating and validating the TP2 is shown in Fig. 6.1. Two different methods were used to disperse particles of different size ranges. The dispersion of PSL particles above a particle size of about 90 nm could be easily achieved using an Atomizer. Dispersion of PSL particles of sizes smaller than 90 nm was difficult. By using an Atomizer to disperse these particles, there is a high background concentration of small particles present in the solution (usually distilled water) in which the particles are suspended. This high concentration of small particles sometimes overwhelms the real particle signal. When dispersing these particles using an electrospray, which is known to effectively disperse smaller particles, particles could be generated constantly for only a few minutes because a small capillary used in the device gets blocked after a short while. It is usually necessary to sample particles for at least a few hours in order to have a high enough deposition density of particles for meaningful quantitative analysis. Experimental validation of the TP2 was therefore performed using soot agglomerates in the size range of 14 nm to 98 nm generated by a graphite aerosol generator (GFG-1000, PALAS GmbH).

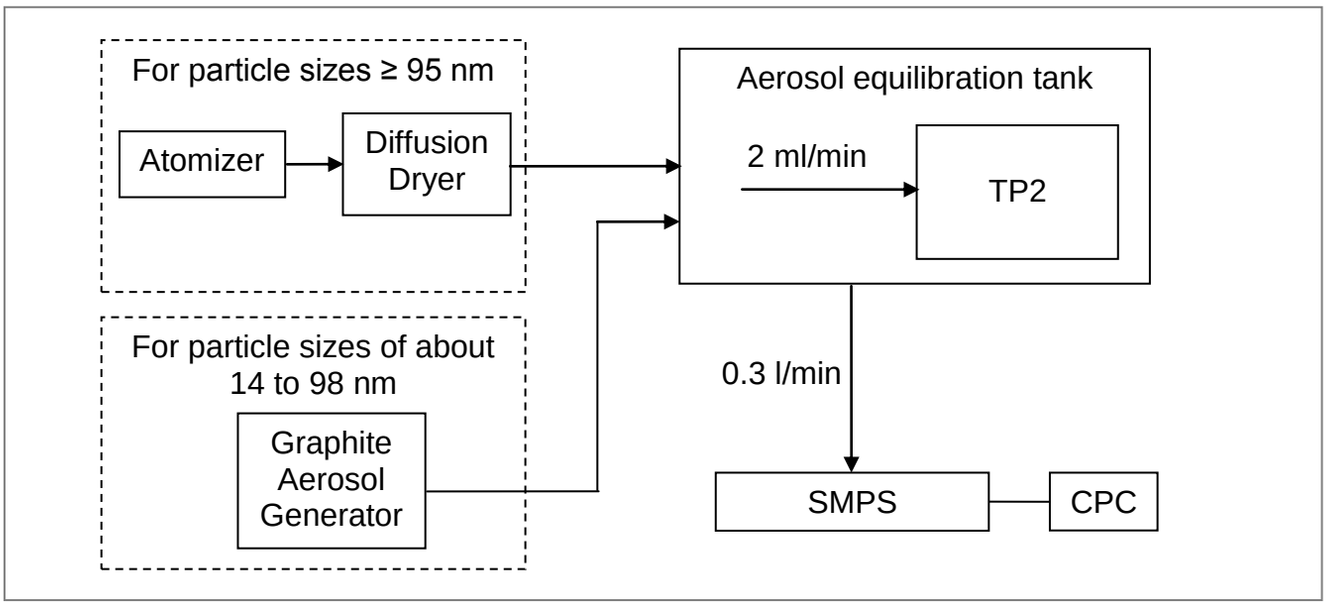

Fig. 6.1 Experimental setup for evaluating the TP2.

6.1.1 Description of deployed equipment

For the evaluation of the TP2, an Atomizer (TSI Model 3076) was used to generate test particles for particle sizes larger than about 95 nm. A graphite aerosol generator (PALAS GFG-1000) was used to generate soot agglomerates in the electrical mobility size range of 14 nm to 98 nm. Parallel comparative measurements were carried out with a Scanning Mobility Particle Sizer (SMPS, TSI Model 3936) using a Differential Mobility Analyzer (DMA, TSI Model 3081) in connection with a Condensation Particle Counter (CPC, TSI Model 3776). The equipment used is described in detail in the following sub-chapters.

6.1.1.1 Atomizer (TSI Model 3076)

Fig. 6.2 shows a schematic of an assembly block of an Atomizer. An Atomizer generates particles by creating a fine spray of suspension droplets containing the particles. Compressed air is connected directly to the input of the Atomizer. The air is then expanded through the atomizer nozzle, producing a high-velocity jet. As a result of the Bernoulli effect, liquid is drawn into the atomizing section through a vertical passage and is then atomized by the jet. Large droplets are removed by impaction on the wall opposite the jet and excess liquid is drained at the bottom of the Atomizer vessel. Fine spray leaves the Atomizer through a fitting at the top.

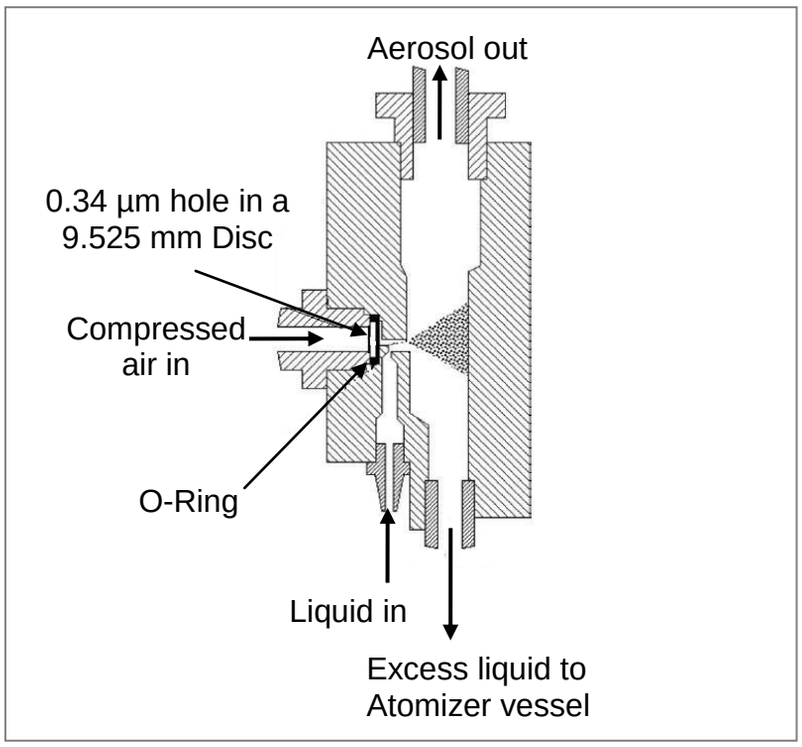

Fig. 6.2 Schematic of Atomizer (TSI Model 3076) assembly block

6.1.1.2 Diffusion Dryer (TSI Model 3062)

A diffusion dryer removes moisture from a gas. A diffusion dryer is commonly used with aerosol generators like an Atomizer where the particles are suspended before dispersion. The aerosol inlet of the dryer used for these experiments incorporates a water trap that collects coarse water droplets. Two concentric cylinders formed by an inner wire screen cylinder and an acrylic outer cylinder contain an annular volume of silica gel. As wet aerosol flows through the inner cylinder, water vapour diffuses through the wire screen and is absorbed by the silica gel. Particle loss is minimized because the particles do not come into contact with the silica gel. Upon saturation, the silica gel is easily regenerated in an oven at 120°C. A sketch as of the TSI Model 3062 diffusion dryer is shown in Fig. 6.3. The drying section of the tube is shown in Fig. 6.4.

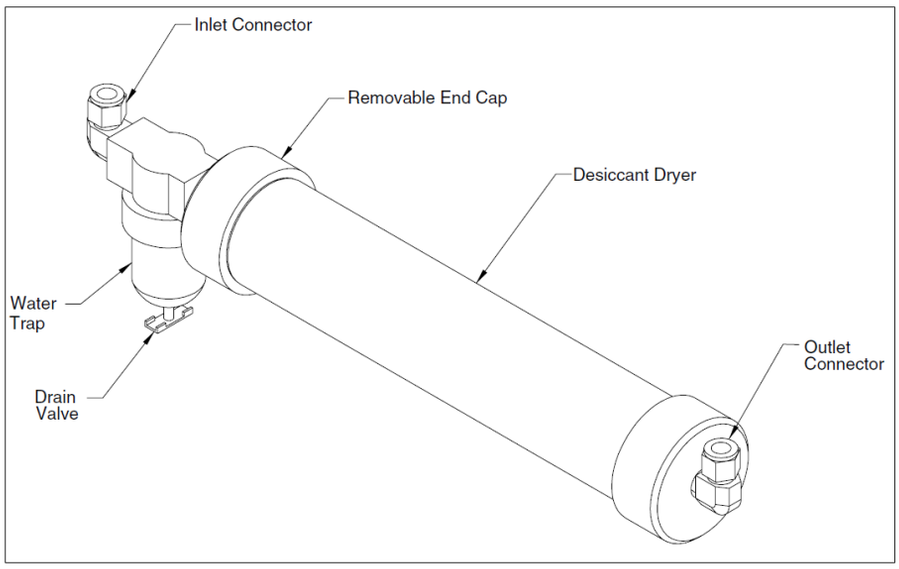

Fig. 6.3 TSI Model 3062 Diffusion Dryer

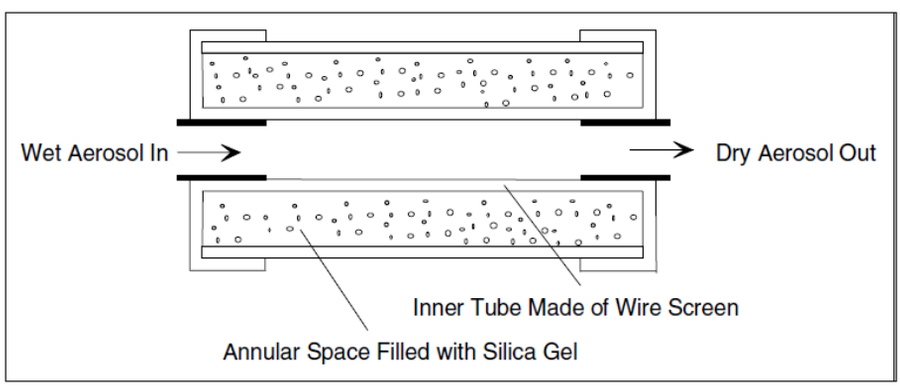

Fig. 6.4 Schematic of a desiccant dryer tube

6.1.1.3 Graphite Aerosol Generator (PALAS GFG-1000)

The GFG-1000 generates very small soot particles through high voltage sparks between two graphite electrodes. In order to avoid oxidation of the particles, the area between the electrodes is washed with Argon. The carbon which is vapourised in the spark gap is transported out of the area between the electrodes and condensed to form very small primary particles, which then form larger agglomerates. The degree of agglomeration is dependent on the concentration of the primary particles. By changing the frequency of the sparks or the flow rates, the particle mass current can be can be varied. One can also reduce the degree of agglomeration by diluting the aerosol immediately after formation. A schematic of the PALAS graphite aerosol generator is shown in Fig. 6.5. In the setup to evaluate the TP2 with the GFG-1000, other parameters such as temperature can be regulated so that the particles can be introduced into the compensation tank at room temperature.

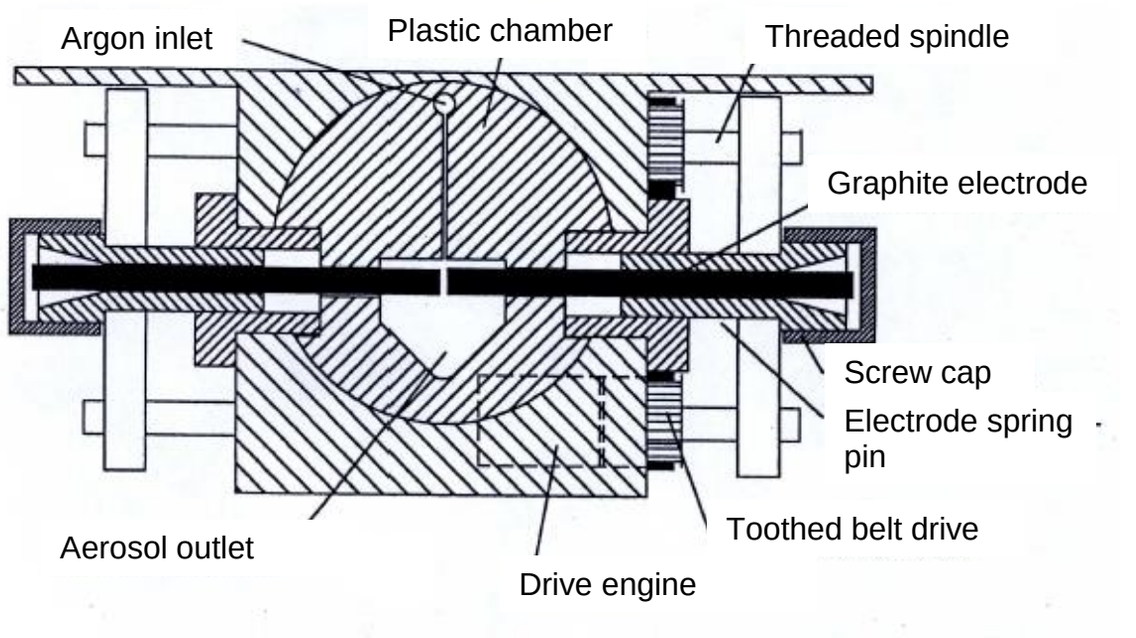

Fig. 6.5 Schematic of a graphite aerosol generator (PALAS GFG-1000)

6.1.1.4 Scanning Mobility Particle Sizer (SMPS – TSI Model 3936)

In an SMPS (Wang and Flagan, 1990), charged particles are classified based on their electrical mobility. With the SMPS (Model 3936 with electrostatic classifier Model 3080, Differential Mobility Analyzer (DMA) Model 3081, Neutralizer Model 3077 and CPC Model 3776, TSI Inc.), the number size distribution of submicron particles can be determined under the assumption that the particles are spherical in shape. The electrical mobility of an aerosol particle is defined as a measure of its ability to move in an electric field. An aerosol particle in an electric field, E, carrying n electric charges experiences an electrical force, causing it to move through the gas in which it is suspended. It very quickly reaches its terminal velocity, v. The resulting drag force on the particle is given by Stokes law and can be equated to the electrical force to determine the electrical mobility of a particle. The electrical mobility Z_P, is given by equation 6.1 as follows:

$$Z_P = \frac{neC_c}{3\pi\eta D_p} \qquad (6.1)$$

Where

n = number of elementary charges on particle

e = elementary charge (1.6 x 10^{-19} Coulomb)

C_c = Cunningham slip correction factor (equation 3.7)

η = gas viscosity (kg/ms)

D_p = Particle diameter (m)

All singly charged particles that have the same value of electrical mobility also have the same electrical mobility diameter. For spherical particles, the electrical mobility diameter is identical with diffusion equivalent diameter of the particles. For non-spherical particles the measurement is based on the mobility equivalent particle size.

When entering the SMPS, particles are neutralized using a radioactive source such that they have a Fuchs equilibrium charge distribution (Fuchs, 1963). The particles are then fractionised with respect to their electrical mobility by a Differential Mobility Analyser (DMA), with only particles of a narrow range of mobility exiting through the outlet slit. By continuously changing the voltage in the DMA (0 to - 10,000V), an electrical mobility diameter range of 2.5 nm to 1000 nm can be covered, depending on the applied DMA as well as the employed flow rates. The monodisperse aerosol fraction is subsequently counted using a Condensation Particle Counter (CPC), described in the next sub-chapter. By fractionising the particles, the size distribution of the aerosol can be determined using the known and defined charge distribution of the particles as well as their mechanical mobility. Electrical mobility analysis has been well known for decades and is considered as the standard method for determining the number size distribution of submicron particles. The SMPS used, has a size resolution of up to 64 channels per decade. The LongDMA (LDMA) was used with an aerosol flow rate of 0.3 l/min and a sheath flow rate of 3.0 l/min. For a scanning time of 240 s, a particle size range of 13.8 – 750 nm is be covered. A schematic flow diagram of the SMPS system used is shown in Fig. 6.6.

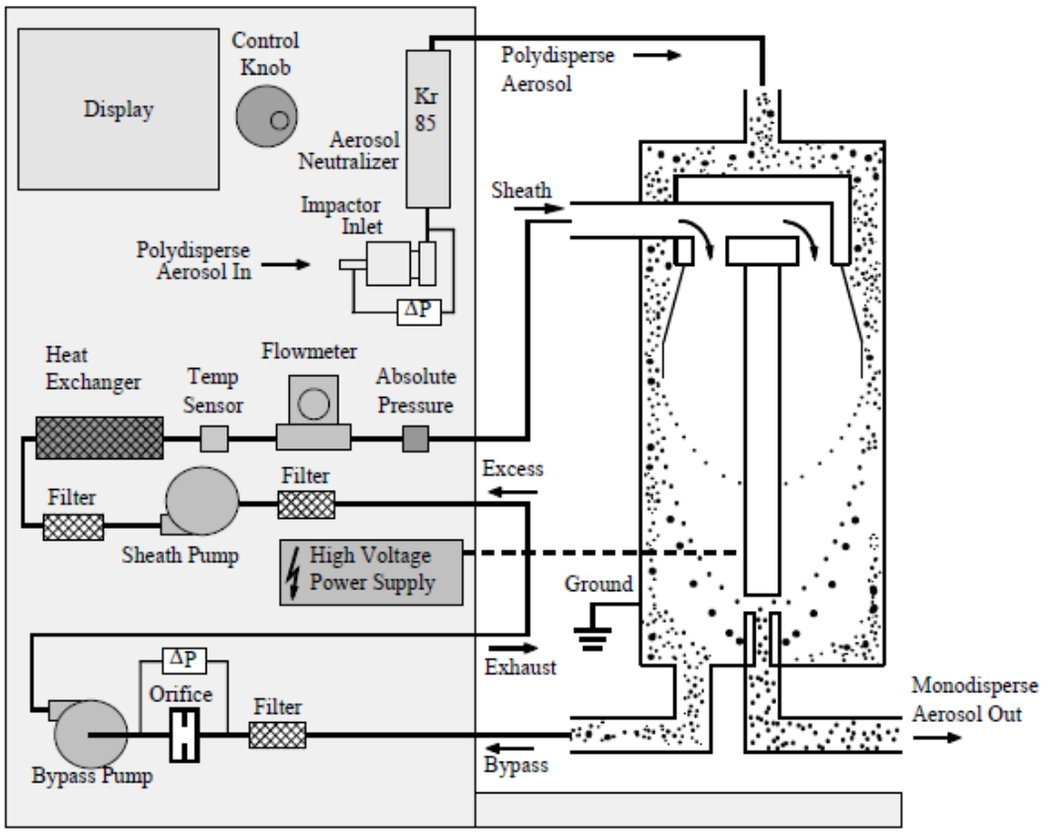

Fig. 6.6 Schematic flow diagram of an SMPS with LDMA

6.1.1.5 Condensation particle counter (CPC – TSI Model 3776)

In a CPC, an aerosol sample is drawn continuously usually at a flow rate of 0.3 l/min, through a heated saturator where alcohol is vapourised and diffuses into the aerosol sample stream. The aerosol sample and alcohol vapour together pass into a cooled condenser where the vapour becomes supersaturated and ready to condense. Particles present in the sample stream serve as condensation nuclei. Once condensation begins, particles that are larger than a threshold diameter quickly grow into larger droplets and pass through an optical detector where they are counted easily. At low concentrations, the optical detector counts individual pulses produced as each particle (droplet) passes through the sensing zone. For very high particle number concentrations, the Model 3776 transitions from the single count mode to a photometric mode where the total light scattered from the particles is used to determine the concentration based on calibration. A schematic flow diagram of the CPC used is shown in Fig. 6.7.

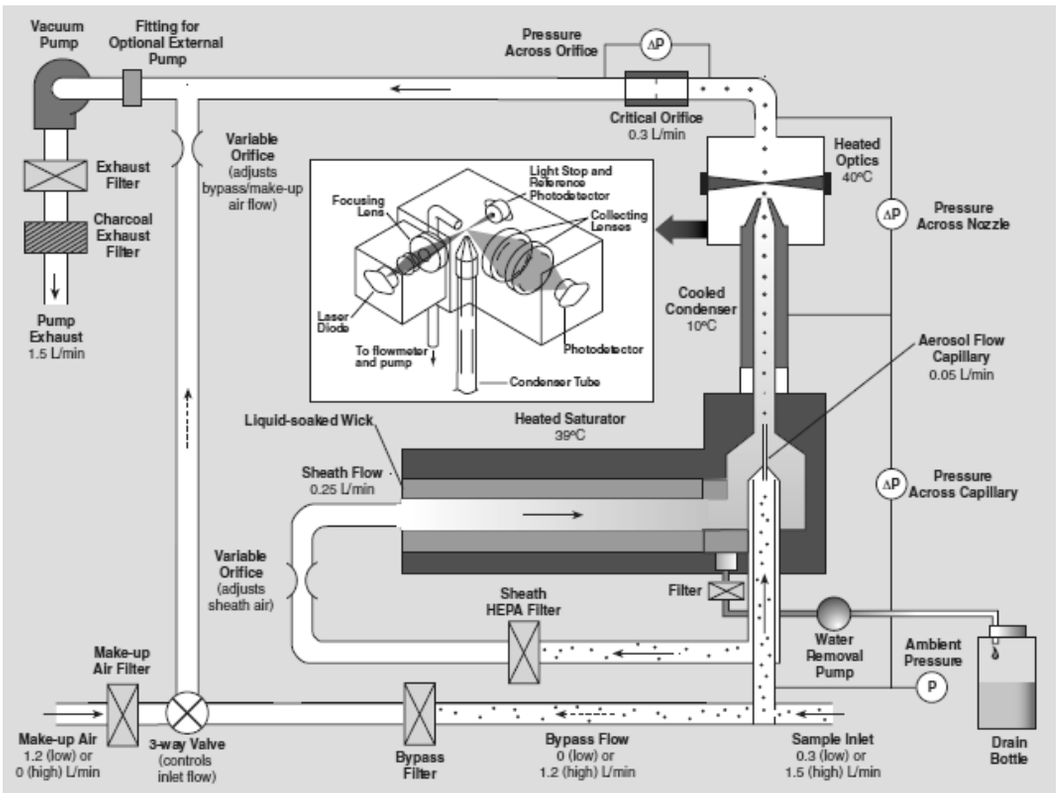

Fig. 6.7 Schematic flow diagram of a TSI Model 3776 Condensation Particle Counter (CPC)

6.2 Experimental process

The TP2 was evaluated for a size range from 14 nm up to about 300 nm, which is the upper size limit for which device-orientation-independent sampling efficiency is expected according to modelling results. For a particle diameter larger than about 95 nm, monodisperse PSL particles were used to evaluate the performance of the TP2. PSL particles have a density of 1.05 g/cm³ and are spherical in shape. In this case the diffusion equivalent diameter of the particles, which is the determining size in thermophoretic deposition, is equivalent to the electrical mobility diameter of the particles as they are classified by the DMA. A direct comparison and thus validation can therefore be made.

Due to the difficulty in dispersing monodisperse PSL particles below the particle size of about 90 nm using an Atomizer or an Electrospray, a graphite aerosol generator was used to generate soot particles within the size rage of about 14 nm to 98 nm with a mode of about 35 nm. Due to the polydisperse nature of the aerosol and the non-spherical shape of the particles, a direct comparison cannot be made between the diffusion equivalent and the electrical mobility diameter of the single particles. Since the homogeneity of the entire size range (ca. 20 nm to 300 nm) which is shown by the model is to be evaluated, the mobility size range of 14 to 98 nm was therefore evaluated as one size class. Soot has a density of about 2.1 g/cm³ which is higher than the density of PSL particles. Density however plays a negligible

role in this size range. An advantage in this method of dispersing particles is that the aerosol contains little or no impurity as the aerosol is not suspended prior to dispersion.

Before sampling particles with the TP2, a cleaned 10 mm x 20 mm substrate was placed into the substrate insertion unit and introduced into the TP2. The TP2 was then placed into the aerosol equilibration tank and then powered up by a laboratory power adaptor. By applying a current of about 1.4 A unto the Peltier Elements, a temperature difference of 15 K is created between the plates. This temperature difference was continuously monitored with a thermometer using thermocouples as sensors inside to the TP2. The current necessary to create the temperature gradient of 15 K/mm may vary minimally as a result of heat losses caused by outside factors e.g. ambient temperature. Aerosol was then introduced into the equilibration tank. The pump of the TP2 was kept off until a stable temperature gradient was reached in order to keep the substrate clean. After about 10 to 15 minutes, when the aerosol equilibration tank is saturated and a stable temperature gradient achieved, the pump was turned on and parallel SMPS measurements started. Due to the low flow rate in the TP2, no influence of the flow on the temperature gradient was detected. Parallel SMPS measurements were used to calculate the particle number concentration in the equilibration tank, which was assumed to be the particle number concentration at the inlet of the TP2. This value of particle number concentration can therefore be used to evaluate the uniformity of the deposition as well as for comparison with the model. The SMPS was set to repeat measurements of the particle size distribution every five minutes while the temperature gradient between the plates of the TP2 was also measured and recorded by a thermometer. Sampling was done for a few hours after which the substrate was retrieved and stored in a particle free casing for eventual SEM analysis.

6.2.1 Experiments with particle sizes ≥ 95 nm

Experimental evaluation of the TP2 was performed with two monodisperse PSL particles sizes of 95.6 ± 1.2 nm and 305 ± 8 nm. A suspension of each particle size was generated in distilled water and placed in an ultrasonic bath for about 30 minutes. This suspension was then dispersed with an Atomizer at a flow rate of about 3.5 l/min. The aerosol was conditioned using a diffusion dryer to a relative humidity of about 20 % and introduced into a 30 litre aerosol equilibration tank where the TP2 was placed. These particles were sampled for several hours while parallel SMPS measurements were made. An example of a size distribution for experiments with 305 ± 8 nm is shown in Fig. 6.8.

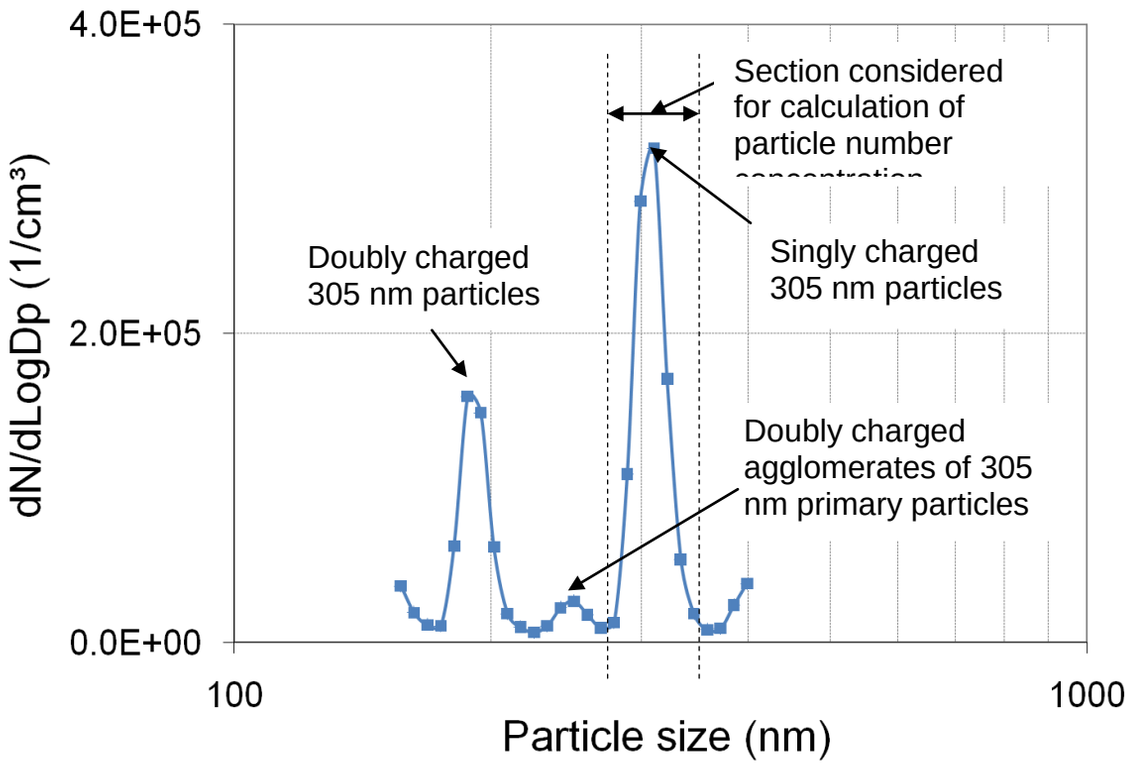

Fig. 6.8 SMPS results (mean values of several measurements) for a validation experiment with monodisperse PSL particles with a size of 305 ± 8 nm.

6.2.2 Experiments with particle sizes from 14 – 98 nm

A custom made experimental setup was used to disperse and sample soot agglomerates in the size range of about 14 – 98 nm.

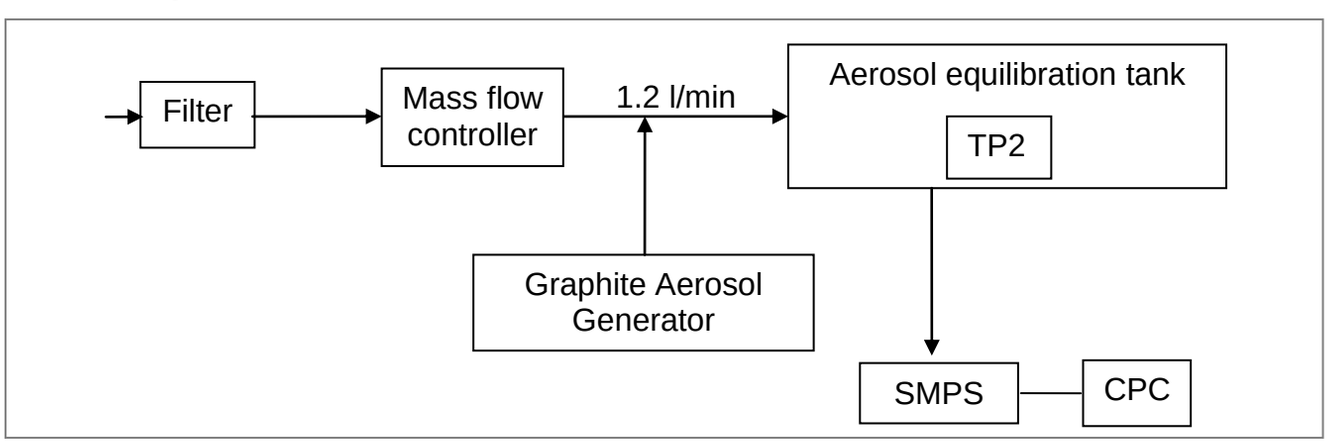

Fig. 6.9 Experimental setup for dispersing soot agglomerates in the size range of 14 – 98 nm

For the dispersion of particles with the setup shown in Fig. 6.9, filtered air was passed through an extra fine-pored filter to take out any impurities. The air flow was then regulated by a mass flow controller and introduced into a pipe at a constant flow rate of 36.7 l/min. In the Graphite aerosol generator, soot agglomerates produced through high voltage sparks between two

graphite electrodes, were carried out of the region of the electrodes by argon and diluted with filtered air in order to minimise the degree of agglomeration. The aerosol was then introduced into the flow pipe about 20 cm after the point of air input, with a flow rate of 18.3 l/min creating a combined flow rate of 55 l/min (*Re* 3043). The aerosol was sampled at a flow rate of about 1.2 l/min at a point, 5.4 m from the start of the pipe. The aerosol was then introduced into the equilibration tank and sampled with the TP2. An example of a size distribution for experiments with polydisperse soot agglomerates in the size range of 14 – 98 nm is shown in Fig. 6.10.

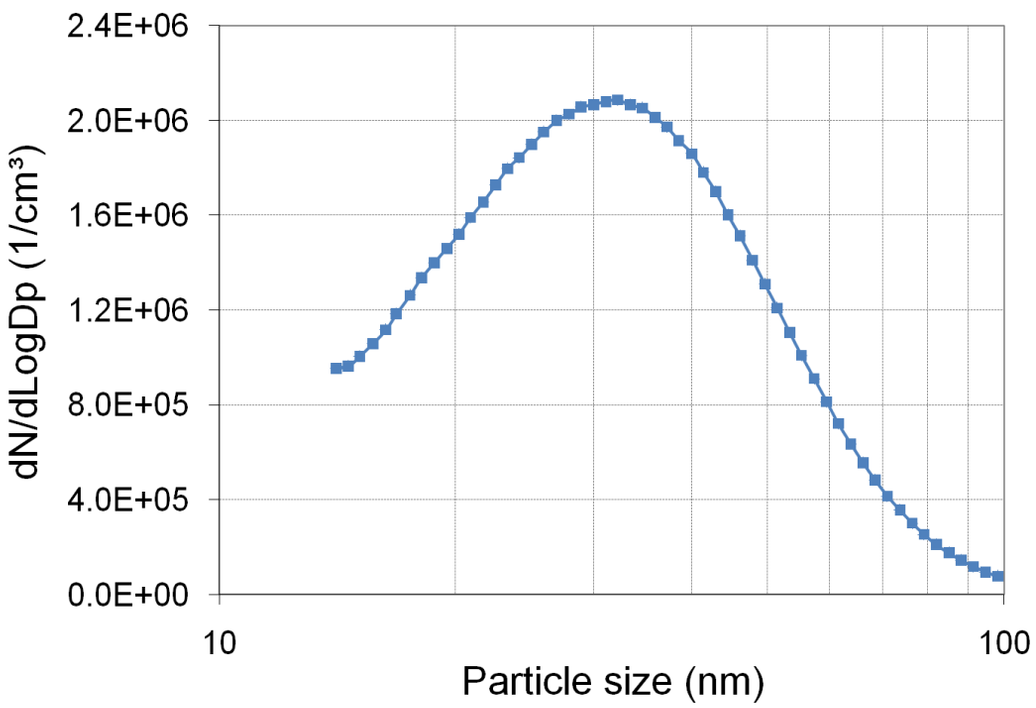

Fig. 6.10 SMPS results (mean values of several measurements) for a validation experiment with soot agglomerate particles with an electrical mobility size range of 14 – 98 nm.

6.3 Evaluation of the experiments

The concentration of particles in the equilibration tank must be known in order to compare the results of the deposition and evaluated the size dependent deposition efficiency of the TP2. The concentration of particles in the equilibration tank was calculated from the size distribution measurements performed with the SMPS during sampling (Fig. 6.8 and Fig. 6.10). The SMPS gives as output on the lognormal x-axis of Fig. 6.8 and Fig. 6.10, the electrical mobility diameter of the particles and on the y-axis, the normalized lognormal concentration with respect to the number of size bins (channels) of the instrument used. The SMPS used for these experiments had a size resolution of 64 size channels per decade. When calculating the concentration of the monodisperse section of such an SMPS spectrum, the width of the

transfer function is considered. Since the SMPS was operated with 64 channels per decade, the normalized concentration values of a narrow section of electrical mobility as shown in Fig. 6.8 are summed up and divided by 64 to get the concentration of the primary particles. For each experiment the measured concentration of primary particles is assumed to be the concentration of particles at the inlet of the TP2 and hence be used for comparative studies.
For the experiments with soot agglomerates, due to the undefined morphology of the particles, there is no direct comparison of the diffusion equivalent diameters and electrical mobility diameters as with PSL particles; it is difficult to calculate the particle number concentration of different size classes for comparison with SEM counts. For this reason, the size range shown in Fig. 6.10 was chosen as one size class.

6.3.1 SEM examination of the TP2 Substrates

After sampling, the substrates were examined using an SEM. SEM images were taken from various sections of the substrate with special emphasis made on the 6.5 mm section (Fig. 4.18) of expected homogeneous particle deposition as shown by the model. Fig. 6.11 shows the locations on the TP2 substrates where SEM images were taken and examined.

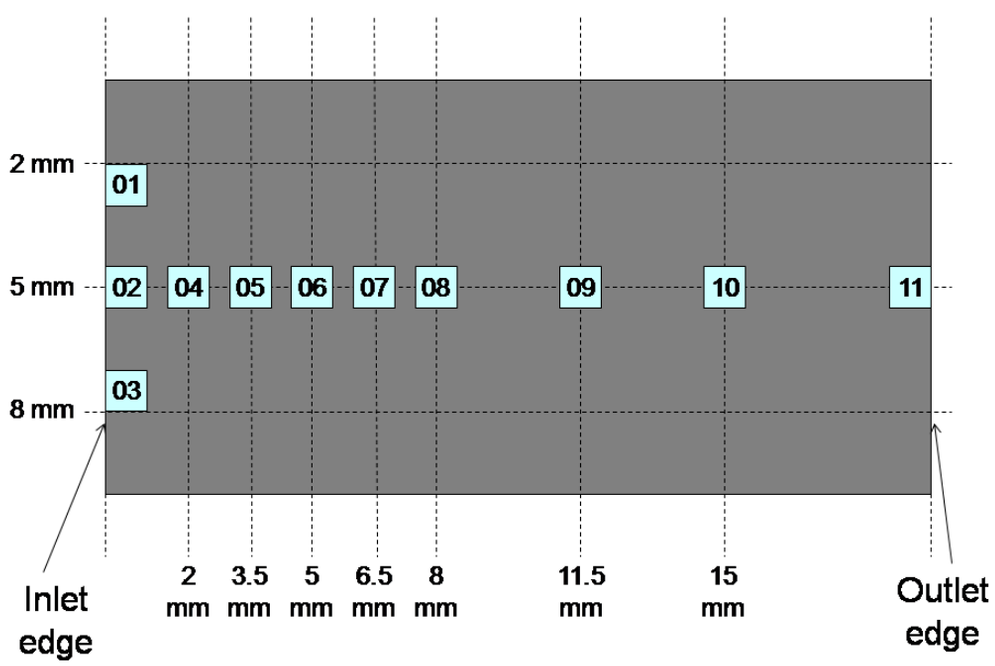

Fig. 6.11 locations on the TP2 substrate which were examined by SEM

Typically, 158 SEM images were taken for each substrate. One overview image is taken for each of the eleven positions shown in Fig. 6.11. More detailed images are then taken in all the positions listed. The magnification of the images taken is dependent on the size of the primary particles which are being examined. The magnification was chosen to be sufficiently large such that the primary particles could be clearly distinguished from any other impurity which may have been present on the substrate prior to sampling. The magnification was however not chosen to be larger than necessary in order to have a bigger surface area and hence higher number of particles to examine. For the primary particle size of 305 nm, a magnification of 10,000 was chosen. Fig. 6.12 shows an example of an SEM image taken with a magnification of 10,000. The particle size of the primary particles on the substrate agrees well with 305 ± 8 nm.

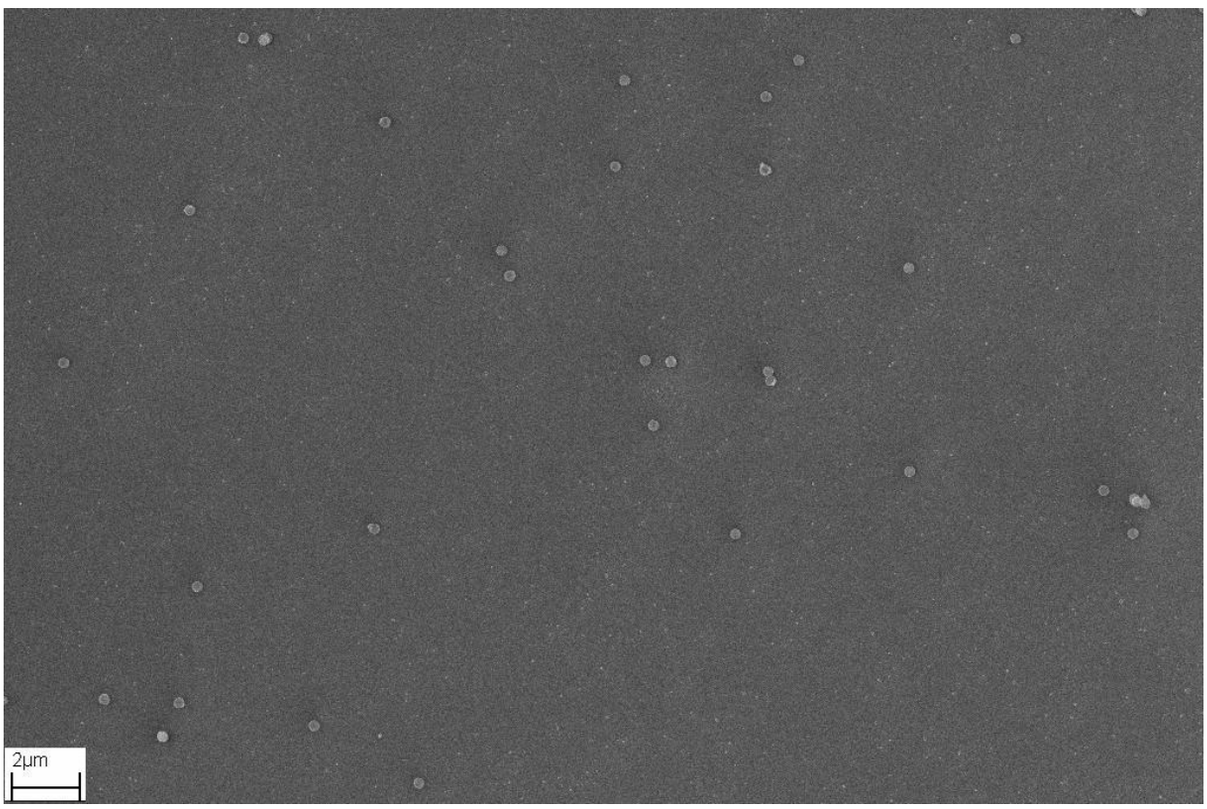

Fig. 6.12 Example of an SEM image taken with a magnification of 10,000. PSL particle size of 305 ± 8 nm.

Nine such images (Fig. 6.12) were taken of positions 01, 02 and 03 to investigate the homogeneity at the inlet. Nine images were also taken for positions 09, 10 and 11. For positions 04, 06 and 08, in the section where homogeneous deposition is expected, 25 images each were taken and nine images were each taken for positions 05 and 07. Fig. 6.13 further illustrates the pattern with which the SEM images were taken. This pattern of evaluation was chosen for the section where a homogeneous deposition is predicted by the model in order to examine homogeneity of the deposition, dependent on the number of

images evaluated. The number of particles deposited is a function of the particle number concentration at the inlet, the flow rate and the sampling time. For the case of Fig. 6.12, the mean particle number concentration calculated from the SMPS measurements was about $2.25*10^{10}$ 1/m³ for a flow rate of 2 ml/min and sampling time of 4 hours. The number of particles deposited as shown by the image makes it more efficient to count the particles per hand rather than using any of the available analysis software.

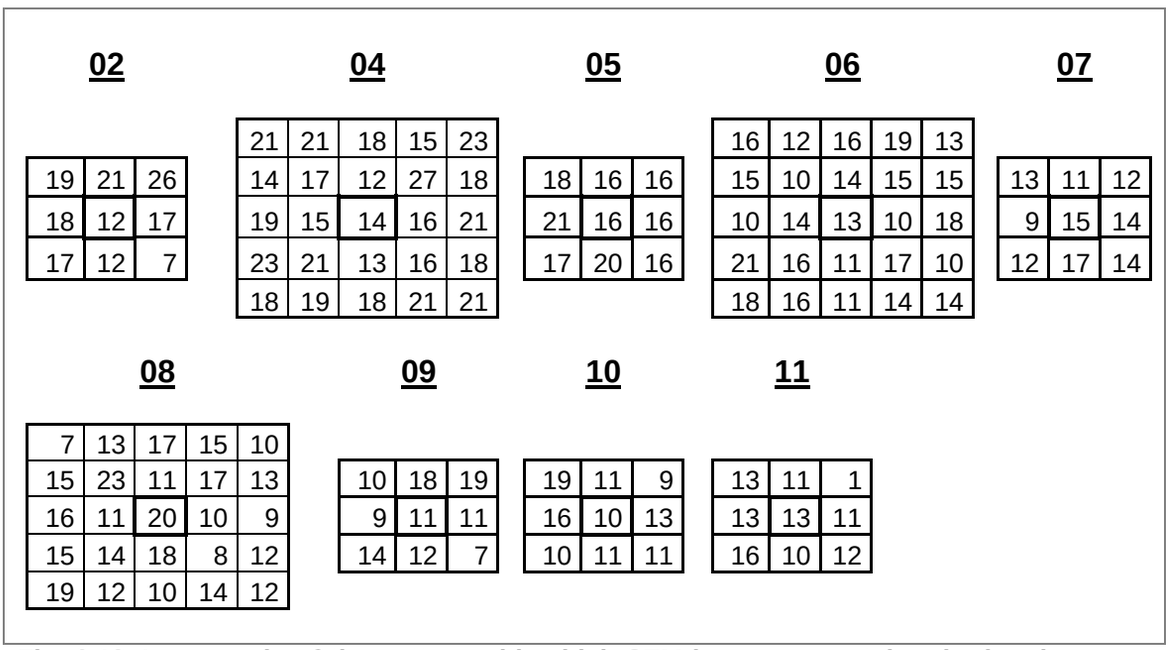

Fig. 6.13 An example of the pattern with which SEM images were taken in the chosen positions on the substrate. The numbers in the boxes represent the number of particles counted on the SEM images for this example for PSL particles with a size of 305 nm

From the mean SMPS particle number concentration, C, which is taken to be the particle number concentration at the inlet of the TP2, the sampling time, t, and the volumetric flow rate, Q, the total number of particles, N, which flow into the TP2 can be calculated as follows:

$$N = CtQ \qquad (6.2)$$

Since the SMPS-measured particle number concentration and sample time are not the same for all experiments, results of the deposition are normalized with respect to the number of particles that flow into the TP as calculated by equation 6.2.

6.4 Experimental Results

A total of 18 experiments were carried out to evaluate the TP2 in a desired size range up to 300 nm, where a device-orientation-independent representative deposition is expected. A summary of the validation experiments is shown in Table 6.1. For experiments 1 to 11, an

SEM magnification of 10,000 was chosen given an image size of $7.74*10^{-10}$ m². For experiments 12 to 14 with 95.6 nm PSL particles, a magnification of 25,000 (SEM image size: $1.09*10^{-10}$ m²) was chosen and for experiments 15 to 18 with soot agglomerates in the size range of 14 to 98 nm, a magnification of 100,000 (SEM image size: $8.02*10^{-12}$ m²) was chosen. The mean particle counts given in Table 6.1 are with respect to the chosen magnification (image size).

Table 6.1 Summary of TP2 evaluation experiments with PSL particles for a size range > 95 nm and soot agglomerates with an electrical mobility size range of 14 – 98 nm.

Particle size (type) [nm]	Device orientation	Particle number concentration (SMPS) [1/m³]	Sampling period [min]	Mean particle count	Std. dev.
305 (PSL)	Case 1	$2.52*10^{10}$	92	12.44	3.59
305 (PSL)	Case 1	$1.86*10^{10}$	92	9.35	3.53
305 (PSL)	Case 1	$1.16*10^{10}$	90	5.10	2.10
305 (PSL)	Case 1	$6.07*10^{10}$	150	4.68	1.76
305 (PSL)	Case 1	$1.54*10^{9}$	180	15.32	3.20
305 (PSL)	Case 2	$2.11*10^{10}$	90	11.66	3.02
305 (PSL)	Case 2	$7.43*10^{9}$	92	4.31	1.58
305 (PSL)	Case 2	$2.25*10^{10}$	240	30.79	4.59
305 (PSL)	Case 3	$2.67*10^{10}$	120	17.74	4.61
305 (PSL)	Case 3	$2.34*10^{10}$	240	24.50	6.07
305 (PSL)	Case 3	$2.30*10^{10}$	180	20.19	4.28
95.6 (PSL)	Case 1	$8.19*10^{10}$	300	20.30	3.49
95.6 (PSL)	Case 1	$3.64*10^{10}$	300	10.89	2.78
95.6 (PSL)	Case 1	$1.00*10^{11}$	300	24.78	3.96
14 – 98(soot)	Case 1	$1.08*10^{12}$	240	23.06	4.64
14 – 98(soot)	Case 1	$1.26*10^{12}$	332	34.64	4.30
14 – 98(soot)	Case 1	$1.03*10^{12}$	368	25.40	5.92
14 – 98(soot)	Case 1	$1.10*10^{12}$	248	17.93	3.75

6.4.1 Deposition rates in comparison to modelling results

Substrates were evaluated by SEM according to the pattern described in Fig. 6.11. A comparison of the mean particle count on SEM images and the calculated values using equation 4.2 is shown in Fig. 6.14.

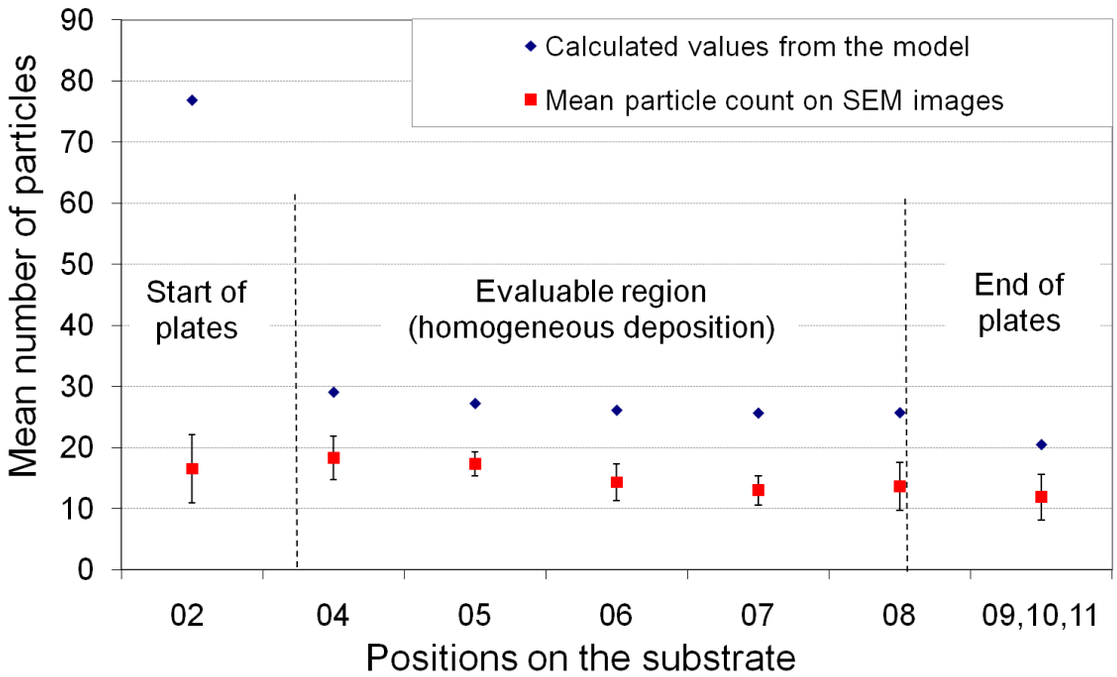

Fig. 6.14 Mean particle count on the SEM images taken on positions along the length of the substrate, in comparison to calculated values from the numerical model. This experiment was performed with monodisperse particles with a size of 305 ± 8 nm. An inlet particle number concentration of $1.55*10^{10}$ $1/m^3$ was measured for this experiment for a sampling period of 180 minutes.

Fig. 6.14 shows a homogeneous deposition of particles along positions 04 to 08 which represent the 6.5 mm section where homogeneous deposition was predicted by the model. Quantitative comparison in deposition between the experiment and the numerical model is not directly possible because the numerical model was an idealized two dimensional model which neglects the effect of walls as well as other constructive and physical non-conformities.. In all experiments however, it was shown that in the 6.5 mm x 6 mm section of the substrate where homogeneous particle deposition is expected, a size-independent representative sample of particles is deposited. Subsequent SEM evaluation of TP2 samples can therefore be performed with only about 5 to 10 SEM images taken in this section.

In the model, it is assumed that the inlet region of the TP2 has a constant temperature value which is exactly equal to the ambient temperature and the temperature of the warm plate is constantly 15 K warmer than this inlet region as well as the colder plate (substrate) which is also constantly at ambient temperature. Heat transfer to the inlet region is neglected. A sudden temperature jump at the start of the plates is modelled which causes a sudden inhomogeneous increase in the temperature gradient at the start of the plates. In reality, heat transfer to the inlet tunnel from the warm plate, creates a temperature gradient towards the inlet and eliminates the sudden temperature jump as given by the model. The large difference

in the number of particles actually deposited in this inlet region compared to the predicted deposition is due to this reason.

6.4.2 Deposition rates with respect to particle size

For all experiments, the deposition in the sections 04 to 08 was determined to be homogeneous and reproducible. Fig. 6.15 shows the percentage of particles that flow into the TP that are deposited in the five different positions analysed (Fig. 6.12) in the 6.5 mm*6 mm section where homogeneous deposition as predicted by the model and for the size classes investigated. Because of differences in the sizes of SEM images all particle counts per SEM image surface area, were projected to a surface area of 1 mm^2. It is shown that particles are deposited homogeneously in this section which implies that SEM analysis of TP samples can therefore be performed with only a low number of, e.g. about five to ten SEM images taken in this section. For samples taken at high concentrations and/or for long sampling periods, fewer images are sufficient to evaluate the sample while more images may be needed in cases of low particle number concentration (low particle deposition density on the substrate.

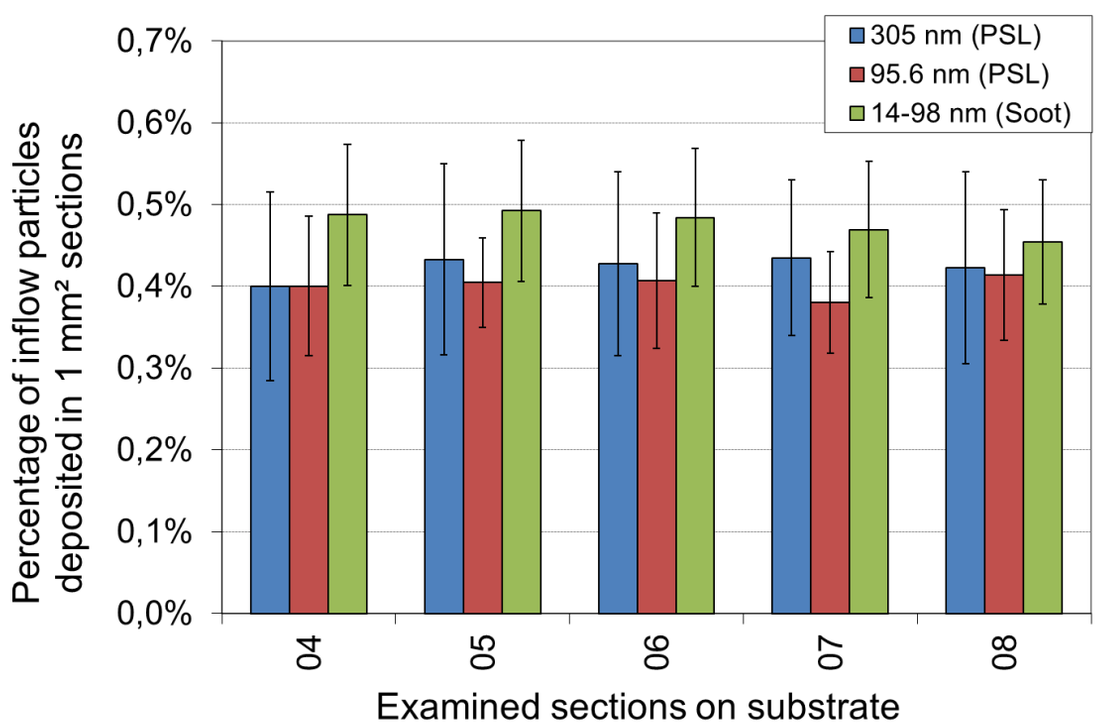

Fig. 6.15 Percentage of particles that flow into the TP, that are deposited in 1 mm2 sections in the region of the TP where homogeneous deposition was predicted by the numerical model.

6.5 Calculating particle number concentration from mean particle count on evaluated SEM images

From the mean count on examined SEM images, it is possible to calculate the number size distribution as well as an average particle number concentration which a worker carrying the TP, was exposed to for an entire shift. The calculation of the number size distribution and particle number concentration is made easier by the homogeneous nature of the deposition whereby only a few SEM images can representatively reproduce the number size distribution and particle number concentration during sampling. The following expression was used to calculate the particle number concentration from the mean count on the SEM images whereby, the *TP deposition rate per unit area = β * Particle number concentration*.

$$\frac{\overline{N}}{A_{SEM} * t} = \beta * C \qquad (6.3)$$

Where, $\overline{N}$ is the mean count on the examined SEM images, A_{SEM} (m²) is the surface area of the examined SEM image, t (s) is the sampling period, C (1/m³) is the particle number concentration and β (m/s) is an experimentally determined calibration factor, which converts the deposited particles per surface area and time into a volumetric particle number concentration. By introducing the SMPS measured particle number concentration as C in equation 6.3, the value of β can be derived which is the gradient of the fit in the graph plotting the TP deposition rate per unit area against the measured particle number concentration. Fig. 6.17 shows the correlation between the TP deposition rate per unit area and the SMPS-measured particle number concentrations.

The results in Fig. 6.17 show a very good correlation coefficient of $R^2 = 0.98$ between the TP deposition rates and the SMPS measured concentrations for all experiments and this for all particle sizes. This shows that a representative deposition for all particle sizes has been established. From Fig. 6.17 one can calculate the real particle number concentration by using the slope of the linear trend line to get the value of the correction factor β, which is 0.00016 m/s. Fig. 6.17 furthermore proves that by operating the TP with a temperature gradient of 15 K/mm, and flow rate of 2 ml/min, a representative, particle size-independent (<300 nm), homogeneous deposition is achieved.

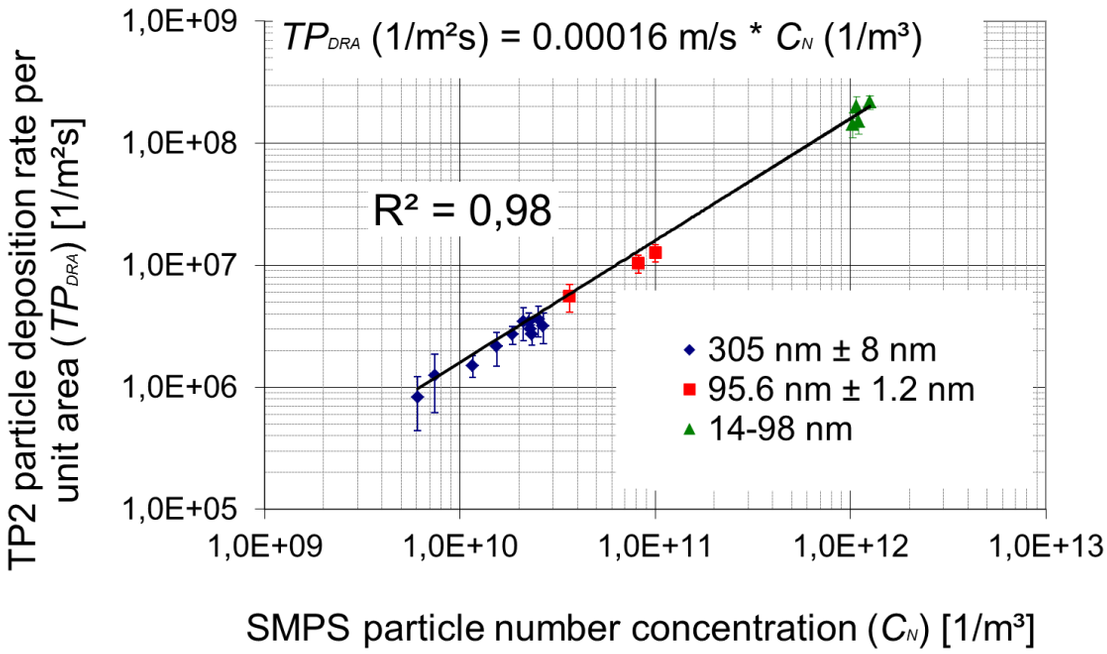

Fig. 6.16 Correlation between TP2 particle deposition rate per unit area and SMPS particle number concentrations for the evaluation experiments performed using mean particle count and sampling time as listed in Table 4.1

The particle number concentration during sampling can be calculated using the mean particle count on about 5 SEM images taken of the substrate on a stretch between 1.5 mm to 8 mm from the start of the substrate. Operating the TP under the abovementioned conditions, a correlation factor (β) of 0.00016 m/s can be used with equation 6.3 to calculate the particle number concentration during sampling.

6.6 Uncertainty Analysis

The process of evaluating the performance of the TP2 was carried out as shown in Fig. 6.17. During the evaluation of the TP2, there were some uncertainties in some of the processes shown in Fig. 6.17. The uncertainties may more or less affect the results of the experiments, which is the deposition rate on the TP2 substrate. The uncertainties in some process e.g. the sampling efficiency of the SMPS system have been described. Uncertainty in other processes such as the aerosol motion and general uniformity over time in the aerosol equilibration tank cannot be quantified. This chapter analyses the uncertainties in the evaluation process.

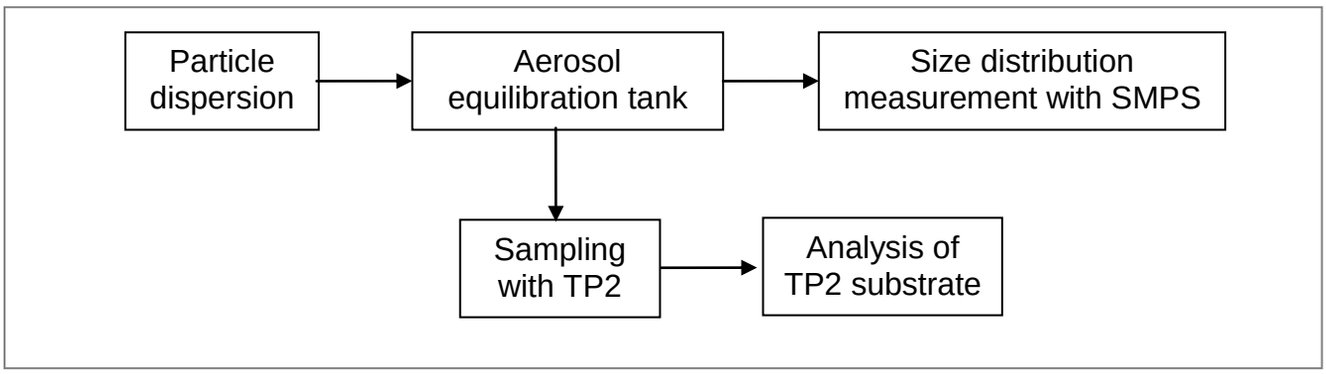

Fig. 6.17 Experimental setup and evaluation scheme of TP2

Effects of cross flow on sampling efficiency

Modelling results showed that the velocity of the cross flow at the inlet of the TP2 can affect the number of particles which are drawn into the TP2 inlet (This is described in detail in Appendix B). For particles in the size range of interest (< 300 nm), the effect of the cross flow was shown to be size-independent. Operating the TP2 at steady flow conditions with a cross flow velocity of at most 10 times the velocity of flow in the TP2 ensures that at least 90 % of particles are drawn into the TP2. This is however the result of an idealised CFD model and has not been experimentally verified.

Measurement uncertainty of the SMPS

A recent comparability study (Kaminski et. al., 2012) was conducted with 8 SMPS systems amongst eleven electrical mobility based instruments for the measurement of particle number size distribution. Except for two SMPSs using an older data acquisition and evaluation software version, the SMPSs agreed well with CPC concentration measurements with Sodium Chloride particles in the size range of about 10 – 100 nm with a small deviation of about ±5%. The exact concentration of an aerosol is not known and cannot be directly (manually) verified. The results of these measurements are therefore trusted due to the theory behind the techniques which agrees for the several instruments in which it is implemented in.

Possible errors during SEM image analysis

The Pattern of SEM images taken for analysis ensured that the images are representative of the deposit (Fig. 6.11). Counting of deposited particles on SEM images was performed manually which cancels out the possibility of a systematic error as one would expect with a particle counting software. The manual count on the SEM images was repeated to eliminate the possibility of counting errors.

7 Summary and Outlook

The goal of this work was to develop a new Thermal Precipitator (TP) as a personal sampler, using an earlier version (TP1) developed by the German Federal Institute for Occupational Safety and Health (BAuA) for occupational particle exposure studies (Plitzko, S. BIA Report 7/2003e), as a basis. The new thermal precipitator (TP2) was developed to sample sub-micron particles homogeneously on silicon substrates in order to simplify subsequent Scanning Electron Microscopic (SEM) examinations (Azong-Wara et al, 2009). An inhomogeneous particle deposition caused by an inhomogeneous temperature gradient in the TP1 required extensive and expensive SEM analysis. This was a major drawback with the TP1. Uncertainty about the temperature gradient and flow rate also made subsequent characterization of the deposition very difficult. A need for optimization was therefore identified and the TP2 was developed with a uniform temperature gradient, together with measurable and controllable temperature gradient and flow rate which resulted in a homogeneous quantifiable particle deposition on the substrate. Subsequent SEM evaluation was therefore made much easier because only a few images of the deposit are now needed for a quantitative analysis of the deposition.

A uniform temperature gradient was achieved in the TP2 by introducing two parallel plates of different but uniform temperatures in the TP2 with an appropriate gap distance between the plates, the colder plate acting as the substrate for particle deposition. Analytical calculations were conducted in order to determine the appropriate gap distance and temperature gradient between the plates which is necessary to achieve a representative deposition of particles on a 20 mm long substrate. 20 mm long plates were chosen because it was the diameter of the substrates of the TP1, which was seen size-wise to be optimal for a personal sampler. A temperature gradient of 15 K/mm and a gap distance of 1 mm in combination with a flow velocity of 5.5 mm/s (flow rate = 2 ml/min) were found to be optimal. The small flow rate which was adopted from the TP1 was found to be ideal in order to maintain a desired laminar flow and to enable particles to be deposited by the weak perpendicularly acting thermophoretic force and avoid being carried out with the flow.

Numerical simulations (2-D) were carried out with the CFD software ANSYS® FLUENT in connection with the Fine Particle Model (FPM) to investigate the deposition characteristics of the TP2. The effect of gravity on the particle deposition was also investigated by considering three different orientations of the TP2 during sampling. Results from the numerical simulations confirmed analytical calculations with a uniform deposition in a 6.5 mm section (length) on the

substrate. This 6.5 mm section is sufficient for subsequent evaluation as according to the simulations more that 33 % of all particles are deposited homogeneously in this section. Numerical simulations further showed that particle deposition in the TP2 for particles less than 300 nm in size is nearly independent of factors such as device orientation, particle density and particle thermal conductivity. For particles above 300 nm, the deposition pattern differs depending on the orientation of the TP2, and/or the density of the particles collected. For the three different orientations of the TP2 considered; case 1 (worker in upright position with the TP2 hanging on his chest pocket or helmet and gravity working in the direction of the flow), case 2 (gravity working perpendicular to the flow and in the direction of particle deposition) and case 3 (gravity working perpendicular to the flow and against the direction of particle deposition) differences caused by particle density for particle sizes up to 300 nm are in the order of ± 8.4 % for modelling with an extreme case of iron particles with a density of 7.9 g/cm³, for which the effect of gravity is more pronounced. Particle sizes up to 300 nm are however of particular interests in particle exposure studies as the size range of about 300 nm represents the minimum of the lung deposition curves. Furthermore larger particles are usually removed from the lungs by macrophages and are therefore of lower importance for personal exposure assessment.

Taking the results of these simulations as a basis, the TP2 was designed to represent this deposition characteristic. In order to create a uniform temperature on the parallel plates, Peltier elements were employed on both plates. The required temperature difference of 15 K between the inner surfaces could be achieved and held constant, by applying a heat sink to the warmer side of the Peltier element used for cooling and then actively cooling the heat sink with a small fan. The total power consumption was in the order of 2 W, which can be provided for several hours by modern batteries. These preliminary experiments showed that the use of Peltier elements was feasible for designing the TP2.

The inlet tunnel of the device was shortened from 8 mm as in the TP1 to 2 mm in the TP2 in order to minimize particles losses in that area, caused by Brownian diffusion. The particle loss in this section was thereby halved.

The TP2 was graphically designed with the 3D-CAD Software CoCreate Modeling, with a novel Substrate Insertion Unit (SIU) designed to easily introduce and retrieve the substrate into and out of the TP2 before and after sampling respectively, without having to dismantle the device as was the case with some previous versions.

A first prototype of the TP2 was built in the university workshop having dimensions of 50 mm x 58.7 mm x 99 mm and weighing about 185 grams. Preliminary tests were carried out

with this first prototype and it was found that the miniature fan which was built into the TP2 to help regulate the temperature gradient as predicted by preliminary tests was not necessary. By taking out the fan, the new TP2 built became smaller with dimensions of 45 mm x 32 mm x 97 mm weighing 45 grams less than the first prototype at 140 grams. The power consumption also dropped to about 1.5 W.

The TP2 was extensively evaluated and validated using monodisperse Polystyrene Latex (PSL) particles of sizes 95.6 ± 1.2 nm and 305 ± 8 nm as well as soot agglomerate particles in the electrical mobility diameter range of 14 – 98 nm. Experimental evaluation of the TP2 showed very promising results. The predicted homogeneous deposition from the model could be qualitatively validated. Overall, the deposition of particles up to the evaluated size of 305 ± 8 nm was found to be particle size-independent and therefore representative of the sampled aerosol. By comparing the particle deposition rate per unit area on the TP substrate with the SMPS measured particle number concentration which was performed parallel to sampling, an expression for calculating the airborne particle number concentration was derived, which takes into account the sampling period and the size of the SEM image examined.

In order to increase the deposition density of the TP2, a higher temperature gradient can be used. The use of a higher temperature gradient however has to be experimentally validated. Modelling results show that for a higher temperature gradient of about 18 K/mm and for the same flow rate of 2 ml/min, the section of homogeneous particle deposition is reduced from about 6.5 mm to about 4.5 mm. About the same number of particles is deposited in this section and therefore a higher deposition density is achieved. The use of a higher temperature gradient however increases the power consumption of the TP2.

Due to the gentle nature of thermophoretic sampling as well as the fact that particles are not conditioned or charged prior to sampling, the TP2 can be used to simulate particle deposition in the lungs by sampling particles directly on living cells and examining the effect of the deposit on the cells.

Overall, the TP2 is a huge improvement from the TP1, with the subsequent SEM analysis immensely simplified.

Outlook

It is planned to use the TP2 in extensive field tests in order to evaluate the performance under non-laboratory conditions. The effects of wind velocity and relative humidity on the deposition characteristics on the TP2 are still to be investigated. Field tests shall also provide more information on the general handiness of the device. The warm plate of the TP2 is expected to reach up to 70°C at work places with temperatures above 50°C. It has to be evaluated if the heat generated is uncomfortable for the worker carrying the device. The constant noise made by the pump also has to be evaluated for its tolerability over an entire working shift. For the purpose of field tests, a controller unit is being developed to power and regulate the TP2. This unit includes a small pump for creating the small flow rate as well as a module with batteries for powering and regulating the Peltier elements. The TP2 was extensively operated for long hours in the laboratory under near ideal conditions. The TP2 was usually not mobile during laboratory tests. As a (mobile) personal sampler, the durability of the device still needs to be tested in the field.

Due to the relatively low temperature gradient applied in the TP2 as well as the gentle nature of thermophoretical particle deposition, the TP2 can be used as the basis to develop a sampler which samples particles directly on living cells for toxicological analysis. For this the colder plate of the TP can be operated at body temperature in order to keep the cells alive and the warm plate operated at a temperature which is 15°C higher than the colder plate (cells). Information about the region of homogeneous particle deposition in the TP2 helps scale such a TP correctly including the position where the cells can be placed.

Bibliography

Asbach, C., Kuhlbusch, T.A.J., Fissan, H. (2005): Effect of corona discharge on the gas composition of the sample flow in the gas particle partitioner, *J. Environ. Mon.* **7**: 877-882.

Azong-Wara, N., Asbach, C., Stahlmecke, B., Fissan, H., Kaminski, H., Plitzko, S., Kuhlbusch, T.A.J. (2009): Optimisation of a thermophoretic personal sampler for nanoparticle exposure studies. *J Nanoparticle Res.* **11**:1611-1624.

Bang, J.J., Elizabeth, A.T., Lawrence, E.M. (2003): Utilization of Selected Area Electron Diffraction Patterns for Characterization of Air Submicron Particulate Matter Collected by a Thermophoretic Precipitator, *J. Air and Waste Manage. Assoc.*, **53**: 227-236.

Batchelor, G.K., Shen, C. (1985): Thermophoretic Deposition of Particles in Gas Flowing over Cold Surfaces, *Journal of Colloid and Interface Science, Vol.* **107***,* No. 1.

Boelter, K.J., and Davidson, J.H. (1997): Ozone generation by indoor, electrostatic air cleaners, *Aerosol Sci. Technol.* **27**: 689-708.

Borm, P.J.A., Robbins, D., Haubold, S., Kuhlbusch, T., Fissan, H., Donaldson, K., Schins, R., Stone, V., Kreyling, W., Lademann, J., Krutmann, J., Warheit, D., and Oberdorster, E. (2006): The potential risks of nanomaterials: a review carried out for ECETOC. *Particle and Fibre Toxicology,* **3** (14 August), 11.

Brock, J.R. (1962): On the theory of thermal forces acting on aerosol particles, *J. Colloid Sci.* **17**: 768-770.

Brouwer, D., van Duuren-Stuurman, B., Berges, M., Jankowska, E., Bard, D., Mark, D. (2009): From workplace air measurement results towards estimates of exposure? Development of a strategy to assess exposure to manufactured nano-objects, *J. Nanopart. Res.,* **11**:1867-1881.

Brouwer, D. (2010): Exposure to manufactured nanoparticles in different workplaces, Toxicology, 269:120-127.

Cardello, N., Volckens, J., Tolocka, M.P., Wiener, R., Buckley, T.J. (2002): Technical Note: Performance of a personal electrostatic precipitator particle sampler, *Aerosol Sci. Technol.* **36**: 162-165.

Cherrie, J. W. (2003): The Beginning of the Science Underpinning Occupational Hygiene, *Ann. occup. Hyg.,* Vol. **47**, No. 3, 179–185.

Cunningham, E. (1910): On the velocity of steady fall of spherical particles through fluid medium. *Proc. R. Soc. London* Ser. A **83**: 357-365.

Dixkens J. and Fissan H. (1999): Development of an Electrostatic Precipitator of Off-Line Particle Analysis. *Aerosol Science and Technology* **30**: 438-453.

Donaldson, K., Li, X.Y., MacNee, W. (1998): Ultrafine (nanometer) particle mediated lung injury. *Journal of Aerosol Science,* **29** (5-6): 553-560.

Donaldson, K., Brown, D., Clouter, A., Duffin, R., MacNee, W., Renwick, L., Tran, L., Stone, V. (2002): The pulmonary toxicology of ultrafine particles. *Journal of Aerosol Medicine,* **15** (2): 213-220.

Demou, E., Stark, W.J., Hellweg, S. (2009): Particle emission and exposure during nanoparticle synthesis in research laboratories, *Ann. Occup. Hyg*., **53**: 829-838.

Engelke, T., van der Zwaag, T., Asbach, C., Fissan, H. Kim, J.H., Yook, S. Pui, D.Y.H. (2007): Numerical Evaluation of Protection Schemes for EUVL Masks in Carrier Systems Against Horizontal Aerosol Flow, *Journal of The Electrochemical Society,* **154** (3).

Epstein, P.S.: (1929): "Zur Theorie des Radiometers," *Zeitschrift für Physik, vol.* **54**: 537-563.

Evans, D.E., Heitbrink, W.A., Slavin, T.J., Peters, T.M. (2008): Ultrafine and Respirable Particles in an Automotive Grey Iron Foundry, *Ann. Occup. Hyg.*, **52**(1): 9-21.

Fissan, H., Neumann, S., Trampe, A., Pui, D.Y.H., Shin, W.G. (2007): Rational and principle of an instrument measuring lung deposited nanoparticle surface area, Journal of Nanoparticle Research **9:** 53 – 59.

Fissan, H. (2008): Nachhaltige Nanotechnologie, Nordrhein-Westfälische Akademie der Wissenschaften – Vorträge I 21, Ferdiand Schöningh, Paderborn (ISBN 978-3-506-76565-9).Fuchs, N. A. (1963): On the stationary charge distribution on aerosol particles in a bipolar ionic atmosphere. *Geofisica Pura e Applicata*, **56**: 185 – 193.

Fuchs, N.A. (1963): On the stationary charge distribution on aerosol particles in a bipolar ionic atmosphere. *Geofisica Pura e Applicata*, **56**: 185 – 193.

Furuuchi, M., Choosong, T., Hata, M., Otani, Y., Tekasakul, P., Takizawa, M Nagura, M. (2010): Development of a Personal Sampler for Evaluating Exposure to Ultrafine Particles, *Aerosol and Air Quality Research*, **10**: 30–37.

Gilmour, P.S., Ziesenis, A., Morrison, E.R. Vickers, M.A., Drost, E.M., Ford, I., Karg, E., Mossa, C., Schroeppel, A., Ferron, G.A., Heyder, J., Greaves, M., MacNee, W., Donaldson, K. (2004): Pulmonary and systemic effects of short-term inhalation exposure to ultrafine carbon black particles, *Toxicology and Applied Pharmacology*, **195** (1): 35-44.

Görner, P., Simon, X., Bémer, D., Lidén, Göran. (2011): Workplace aerosol mass concentration measurement using optical particle counters, *J. Environ. Monit.*, **14**: 420 - 428

Gnewuch, H., Muir, R., Gorbunov, B., Priest, N.D., Jackson, P.R. (2008): A novel size-selective airborne particle sampling instrument (WRAS) for health risk evaluation. In Linkov, I. and Steevens, J. (eds.), Nanotechnology: Risks and *Benefits,* Springer, Dordrecht.

Gonzalez, D., Nasibulin, A.G., Baklanov, A.M., Shandakov, S.D., Brown, D.P., Queipo, P. Kauppinen, E.I. (2005): A new thermophoretic precipitator for collection of nanometer-sized aerosol particles, *Aerosol Sci. Technol.* **39**: 1064-1071.

Green, H.L., Watson, H.H. (1935): Medical Research Council Special Report Series. 199. *KMS, London*.

Hering, S.V., Flagan, R.C., Friedlander, S.K. (1978): Design and evaluation of new low-pressure impactor 1, *Env. Sci. Technol.* **12**: 667-673.

Hering, S.V., Friedlander, S.K., Collins, J.J., Richards, L.W. (1979): Design and evaluation of new low-pressure impactor 2, *Env. Sci. Technol.* **13**: 184-188.

Hermann, M., Wehner, B., Bischof, O., Han, H.-S., Krinke, T., Lui, W., Zerrath, Wiedensohler, A. (2007): Particle counting efficiencies of new TSI condensation particle counters, *J. Aerosol Sci.* **38**: 674-682.

Hinds, W.C. (1999): Aerosol Technology; Properties, Behavior and Measurement of Airborne Particles. *Second Edition.*

Kaminski, H., Kuhlbusch, T.A.J., Rath, S., Götz, U., Sprenger, M., Wels, D., Polloczek, J., Bachmann, V., Dziurowicz, N., Kiesling, H.-J., Schwiegelshohn, A., Monz, C., Dahmann, D., Asbach, C. (2012): Comparability of Aerosol Measurement Instruments for Submicron Particles. (submitted).

Keskinen, J., Pietarinen, K., Lehtmäki, M. (1992): Electrical low pressure impactor, *J. Aerosol Sci.* **23**: 353-360.

Kethley, T.H., Gordon, M.R., Orr, C. (1952): A thermal precipitator for aerobacteriology, *Science* **116**: 368-369.

Kim, J.H., Mulholland, G.W., Kukuck, S.R., Pui, D.Y.H (2005): Slip correction measurements of certified PSL nanoparticles using a nanometer differential mobility analyzer (Nano-DMA) for Knudsen number from 0.5 to 83. *J. Res. Natl. Inst. Stand. Technol.* **110**: 31.

Knutson, E.O. and Whitby, K.T. (1975): Aerosol Classification by Electric Mobility: Apparatus Theory and Applications, *Journal of Aerosol Science*, **6**:443.

Kodas, T., Hampden-Smith, M. (1999): Aerosol processing of materials. Willey, New York.

Kuhlbusch, T.A.J., Fissan, H., Neumann, S. (2004): Number size distribution, mass concentration, and particle composition of PM 1, PM 2.5 and PM 10 in bag filling areas of carbon black production, ICBA-Study, *J. Occup. Env. Hygiene* **1**: 660-674.

Kuhlbusch, T.A.J., Fissan, H. (2006): Particle Characteristics in the Reactor and Pelletizing Areas of Carbon Black Production, *J. Occup. Env. Hygiene* **3:** 558-567.

Kuhlbusch, T.A.J., Fissan, H., Asbach, C. (2008a): Measurement and detection of nanoparticles in the environment, in Nanotechnology, Volume 2: Environmental Aspects, Ed. H. Krug, ISBN 978-3-527-31735-6, Wiley-VCH, Weinheim, p. 229-266.

Lee, J., Altman, I., Choi, M. (2008): Design of a thermophoretic probe for precise particle sampling, *J. Aerosol Sci.* **39**: 418-431.

Lee, S.J., Demokritou, P., Koutrakis, P., Delgado-Saborit, J.M. (2006): Development and evaluation of personal respirable particulate sampler, *Atm. Environ.* **40**: 212-224.

Manodori, L. & Benedetti, A. (2009): Nanoparticles monitoring in workplaces devoted to nanotechnologies, *J. Phys. Conf. Ser*., **170**: 012001.

Martinez, P., Brandvold, D.K. (1996): Laboratory and field measurements of NO_x produced from corona discharge, *Atm. Environ.* **30**: 4177-4182.

Maynard, A.D. (1995): The Development of a New Thermophoretic Precipitator for Scanning Transmission Electron Microscope Analysis of Ultrafine Aerosol Particles, *Aerosol Science and Technology,* **23**: 4, 521-533

Maynard, A.D., Kuempel, E.D. (2005): Airborne nanostructured particles and occupational health, *J. Nanopart. Res.* **7**: 587-614.

Mirme, A., Noppel, M., Peil, I., Salm, J., Tamm, E., Tammet, H. (1984): Multi-channel electric aerosol spectrometer. *In 11th International Conference on Atmospheric Aerosols, Condensation and Ice Nuclei, Budapest* **2**, 155-159.

Misra, C., Singh, M., Shen, S., Sioutas, C., Hall, P.M. (2002): Development and evaluation of a personal cascade impactor (PCIS), *J. Aerosol Sci.* **33**: 1027-1047.

Möhlmann, C., (2005): Vorkommen ultrafeiner aerosole an arbeitsplätzen, *Gefahrstoffe – Reinhaltung der Luft* **65 (11/12)**: 469 – 471.

Möhlmann, C., Welter, J., Klenke, M., Sander, J. (2009): Workplace exposure at nanomaterial production processes, *J. Phys. Conf. Ser*., **170**: 012004.

Montassier, N., Boulaud, D., Renoux, A. (1991): Experimental study of thermophoretic particle deposition in laminar tube flow, *J. Aerosol Sci.* **22**: 677-687.

MSP (2008): *Model 200 Personal Environmental Monitor*, MSP Corp., Shoreview, MN, USA.

Oberdörster, G. (2001): Pulmonary effects of inhaled ultrafine particles, *In. Arch. Occup. Environ. Health*, **74**: 1-8.

Oberdörster, G., Sharp, Z., Atudorei, V., Elder, A., Gelein, R., Lunts, A., Kreyling, W., Cox, C. (2002): Extrapulmonary translocation of ultrafine carbon partikcles following whole-body inhalation exposure of rats, *J. Toxicol. Environ. Health A,* **65**: 1531-1543.

Ono-Ogasawara, M., Serita, F., Takaya, M. (2009): Distinguishing nanomaterial particles from background airborne particulate matter for quantitative exposure assessment, *J. Nanopart. Res.,* **11:**1651-1659.

Orr, C., Martin, R.A. (1958): Thermal precipitator for continuous aerosol sampling, *Rev. Sci. Instr.* **29**: 129-130.

Page, S.J. Volkwein, J.C., Vinson, R.P., Joy, G.J., Mischler, S.E., Tuchmann, D.P., McWilliams, L.J. (2008): Equivalency of a personal dust monitor to the current United States coal mine respirable dust sampler, *J. Environ. Mon.* **10**: 96-101.

PALAS (2003). *Model GFG-1000, Aerosol Generator Instruction Manual.* PALAS® GmbH, Karlsruhe.

Peters, T.M., Heitbrink, W.A., Evans, D.E., Slavin, T.J., Maynard, A.D. (2006): The mapping of fine and ultrafine particle number concentrations in an engine machining and assembly facility, *Ann. Occup. Hyg.* **50**: 249-257.

Patashnick, H., Rupprecht, G., Wang, J.C.F (23 March 1980): New real-time monitoring instrument for suspended particulate mass concentration: the TEOM, *Journal Volume: 25:1; Conference: 179. national meeting of the American Chemical Society, Houston, TX, USA*.

Plitzko, S. (2003): A thermal precipitator as a personal sampler, *BIA Report 7/2003e:* 133-135

Qi, C., Chen, D.R., Greenberg, P. (2008a): Fundamental study of a miniaturized disk-type electrostatic aerosol precipitator for a personal nanoparticle sizer, *Aerosol Sci. Technol.* **42**: 505-512.

Qi, C., Chen, D.R., Greenberg, P. (2008b): Performance study of a unipolar aerosol mini-charger for a personal nanoparticle sizer, *J. Aerosol Sci.* **39**: 450-459.

Roach, S.A. (1959) Measuring Dust Exposure with the Thermal Precipitator in Collieries and Foundries, *Brit. J. industr. Med.,* 1959, 16, 104.

Romay F.J., Takagaki S.S., Pui D.Y.H., Liu B.Y.H. (1998): Thermophoretic deposition of aerosol particles in turbulent pipe flow, *J. Aerosol Sci*. **29**: 943-959

Rubow, K.L., Marple, V.A., Olin, J., McCawley, M.A. (1987): A personal cascade impactor – design, evaluation and calibration, *Am. Ind. Hyg. Assoc. J.* **48**: 532-538.

Schneider, T. (2007): Evaluation and control of occupational health risks from nanoparticles. www.norden.org/pub/sk/showpub.asp?pubnr=2007:581.

Sherwood, R.J., Greenhalgh, D.M.S. (1960): A personal air sampler, *Ann Occup Hyg;* **2**: 127–32.

Sioutas, C., Chang, M.C., Kim, S., Koutrakis, P., Ferguson, S.T. (1999): Design and experimental characterization of a PM1 and a PM2.5 personal sampler, *J. Aerosol Sci.* **6**: 693-707.

Stratmann, F., Otto, E., Fissan, H. (1994): Thermophoretical and diffusional particle transport in cooled laminar tube flow, *J. Aerosol Sci.* **25**: 1305-1319.

Talbot, L., Cheng, R.K., Schefer, R.W., Willis, D.R. (1980): Thermophoresis of particles in a heated boundary layer, *J. Fluid. Mech., vol.* **101,** part 4:737-758.

Tsai, C.-J. and Lu, H.-C. (1995): Design and Evaluation of a Plate-to-Plate Thermophoretic Precipitator, *Aerosol Science and Technology*, **22** (2), 172-180.

Tsai, C.-J., Lin, J.-S., Aggarwal, S.G., Chen, D.-R. (2004): Thermophoretic deposition of particles in laminar and turbulent flows, *Aerosol Sci. Tech.* **38**: 131-139.

Tsai, S.J., Ashter, A., Ada, E., Mead, J.L., Barry, C.F., Ellenbecker, M.J. (2008): Airborne nanoparticle release associated with the compounding of nanocomposites using nanoalumina as fillers, *Aerosol Air Qual. Res*., **8**: 160-177.

TSI (2008). *Model 3076, Constant Output Atomizer Instruction Manual.* TSI Inc., St. Paul, MN.

TSI (2003). *Model 3062, Diffusion Dryer Instruction Manual.* TSI Inc., St. Paul, MN.

TSI (2003). *Model 3936, Scanning Mobility Particle Sizer (SMPS) Instruction Manual.* TSI Inc., St. Paul, MN.

TSI (2007). *Model 3776, Condensation Particle Counter (CPC) Instruction Manual.* TSI Inc., St. Paul, MN.

TSI (2007). *Model 3077/3077A, Aerosol Neutralizer Instruction Manual.* TSI Inc., St. Paul, MN.

Tyndall, J. (1870): On dust and disease, Proc. R. Inst. **6**: 1 – 14.

Viner, A.S., Lawless, P.A., Ensor, D.S., Sparks, L.E. (1992): Ozone generation in DC-energized electrostatic precipitators, *IEEE Trans. Ind. Applicat.* **28**: 504-512.

Wake, D., Mark, D., Northage, C., (2002): Ultrafein aerosols in the workplace, Ann. Occup. Hyg. **46** (Suppl. 1): 235 – 238.

Waldmann, L., Schmitt, K.H. (1966): Thermophoresis and diffusiophoresis of aerosol, Davis, C.N. (Ed), Aerosol Science, Academic Press, London.

Wang, B., Ou, Q., Tao, S., Chen, D.-R. (2012): Performance study of a disk-to-disk thermal precipitator, Journal of Aerosol Science, 52: 45-56.

Wang, S. C. and Flagan, R. (1990): Scanning Electrical Mobility Spectrometer, *Aerosol Science and Technology* **13**: 230 – 240.

Wang, Y.F., Tsai, P.J., Chen, C.W., Chen, D.R. Hsu, D.J. (2010): Using a modified electrical aerosol detector to predict nanoparticle exposure to different regions of the respiratory tract for workers in Carbon Black manufacturing industry, *Environ. Sci. Technol.*, **44**: 6767-6774.

Watson, H.H. (1937): *Trans. Inst. Min. Metall. 46*: 155.

Woodrow Wilson database: http://www.nanotechproject.org/inventories/consumer/analysis_draft/

Wright, B.W. (1953): Gravimetric Thermal Precipitator, *Science, New Series,* Vol. **118** (3059): p. 195.

Wu, Y.-H., Vincent, J. (2007): A Modified Marple-Type Cascade Impactor for Assessing Aerosol Particle Size Distributions in Workplaces, *Journal of Occupational and Environmental Hygiene*, **4** (10): 798-807.

Zheng, F. (2002): Thermophoresis of spherical and non-spherical particles: A review of theories and experiments, *Adv. Colloid. Interfac.* **97**: 255-278

Appendix

Appendix A

A simulation grid was developed to model the sampling section of the TP1 (Fig. 3.3).

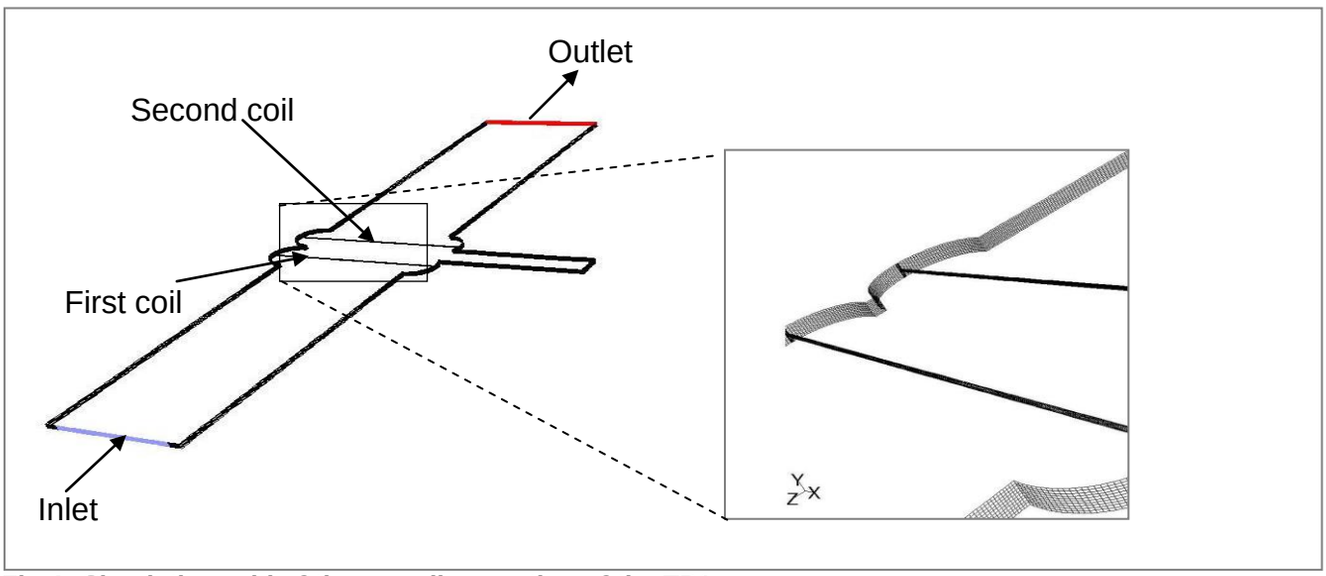

Fig A. Simulation grid of the sampling section of the TP1

Measuring the temperatures of the heating coils was not possible without influencing the values of the temperatures. The temperatures were therefore calculated considering the changing of the electrical resistance of the coils upon application of an electric current as follows.

$$\Delta T = \frac{R(T) - R(T_0)}{\alpha \cdot R(T_0)} \qquad \text{(A)}$$

Where *R(T)* is the electrical resistance of the heating coil at a given temperature, $R(T_0)$ is the electrical resistance of the heating coil at room temperature and α is the linear temperature coefficient. *R(T)* is calculated (*R(T)* = U/I) from the measured value of the voltage (U) for a given applied current (I). When a current is applied, the temperature of the wire and thus *R(T)* also increases. $R(T_0)$ is calculated similarly for a small applied current (up to about 10 mA) and measured voltage, when no substantial temperature rise in the wire is expected. Heat losses were neglected. A temperature increase of about 5 K and 7 K were calculated for the first and second heating coils respectively and these values were used as boundary conditions in the numerical model.

Particle deposition in the TP1 was investigated for five monodisperse particle sizes from 20 nm to 1 µm each with a particle number concentration of 10^{10} 1/m³ at the inlet. Fig B shows results of the numerical modelling of the TP1. An inhomogeneous deposition of particles was found at the region of the heating coils caused by the inhomogeneous temperature gradient at these regions for every investigated particle size.

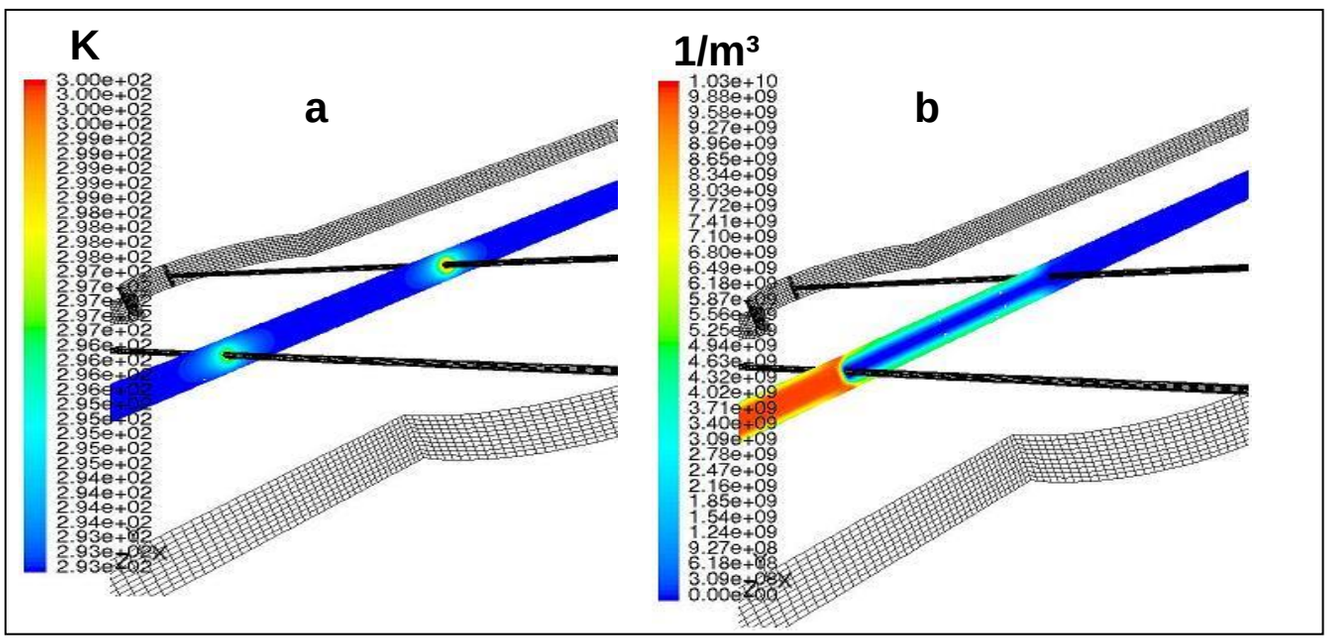

Fig B. a: Temperature profile in the TP1, ambient temperature: 293 K; first coil: 298 K; second coil: 301 K.

b: Concentration profile in the TP1 for 1µm particles with an inlet concentration of 10,000 cm³

Appendix B

Numerical Modelling of the TP2 Inlet

Depending on surrounding conditions, particularly the flow conditions at the inlet of the TP2, the number of particles that flow into the TP2 may vary for the same ambient aerosol concentration. The TP2 samples with a flow rate of 2 ml/min creating a flow velocity of 5.5 mm/s in the TP2. This small flow velocity may be compromised by much larger cross flow velocities and turbulent flows at the inlet of the TP2 preventing many particles from being sucked into the TP2. Numerical simulations were performed with FLUENT using the Discrete Phase Model (DPM) to investigate how cross flows at the inlet of the TP2 affects the inflow of particles into the TP2. The DPM was used because it includes the effect of inertia which is important in determining if particles (especially the larger particles) flow into the TP2. A two dimensional grid was developed to model the inlet region of the TP2 (Fig C). The grid was developed to investigate particle flow into the TP2 at different cross flow velocities. The 2-D grid had a total of 89,000 rectangular cells with 300 grid elements along the cross flow inlet width and 280 elements along the length. The section of the grid representing the TP2 tunnel had a total of 50 grid elements along the inlet and 100 grid elements along the length. For a constant TP2 inlet velocity (v_f) of 5.5 mm/s, cross flow inlet velocities (v_{cf}) of 0.55 mm/s, 5.5 mm/s, 55 mm/s, 110 mm/s, 165 mm/s and 275 mm/s were set in the model giving ratios (TP2 inlet velocity to cross flow inlet velocity) of 10/1, 1/1, 1/10, 1/20 1/30 and 1/50 respectively.

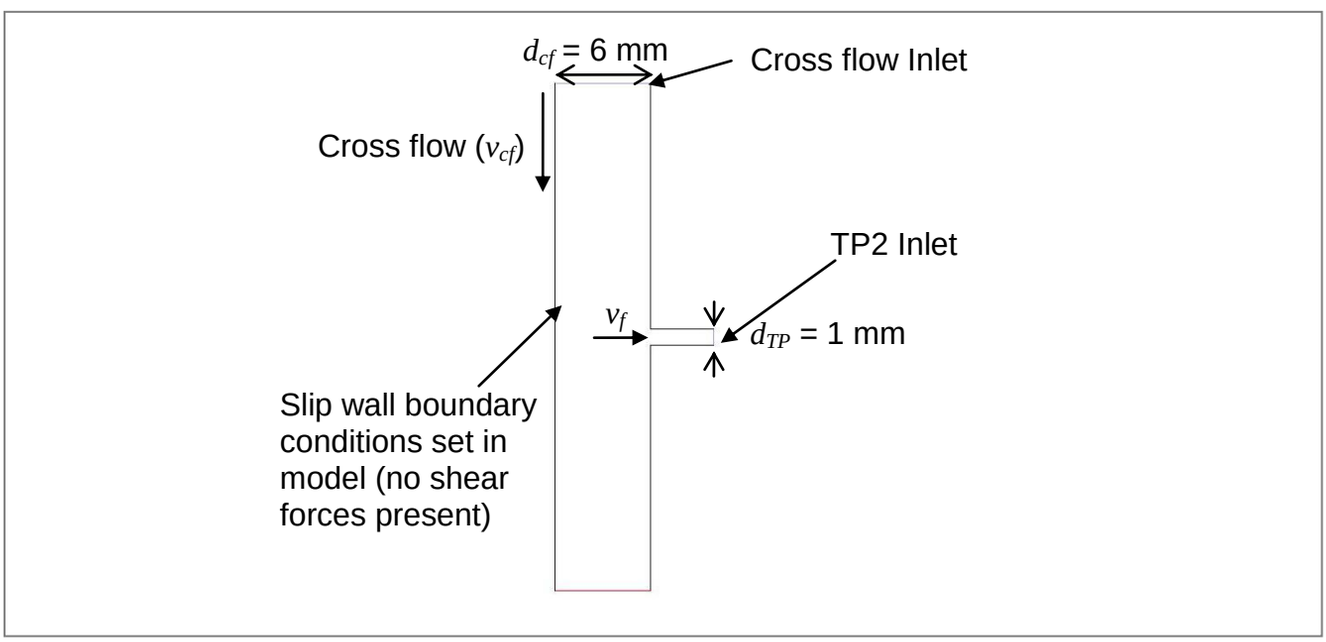

Fig C. 2-D Grid for numerical simulations of the inlet of the TP2 with 89,000 rectangular grid elements

For the same ambient aerosol concentration (C_{cf}) and a TP2 inlet aerosol concentration (C_{TP}), the number of particles that flow into the TP2 can be calculated analytically from the ratio of the volumetric flow rates of the cross flow and the TP2.

$$C_{cf} = \frac{N_{cf}}{t \cdot Q_{cf}} = C_{TP} = \frac{N_{TP}}{t \cdot Q_{TP}} \quad \text{(B)}$$

Where N_{cf} and N_{TP} are the number of particles that flow into the cross flow inlet and TP2 inlet respectively in time t; Q_{cf} and Q_{TP} are the flow rates of the cross flow and the TP2 flow respectively with:

$$Q_{cf} = v_{cf} \cdot d_{cf} \cdot h \quad \text{(C)}$$

and

$$Q_{TP} = v_f \cdot d_{TP} \cdot h \quad \text{(D)}$$

Where v_{cf} and v_f are the flow velocities of the cross flow and TP2 inlet respectively, d_{cf} and d_{TP} are the lengths of the cross flow inlet and TP2 inlet respectively and h is the width of an imaginary third dimension which is equal for both cases. From Equation B, assuming that all cross flow inflowing particles follow the streamlines, the number of particles which flow into the TP2 can be calculated as follows:

$$N_{TP} = N_{cf} \frac{v_f \cdot d_{TP}}{v_{cf} \cdot d_{cf}} \quad \text{(E)}$$

Numerical modelling was performed for particle sizes of 20 nm, 300 nm, 1000 nm and 3000 nm. The effect of Brownian diffusion was not included in these simulations and gravity was initially not included. Fig D shows an example of particle trajectories tracked from the cross flow inlet.

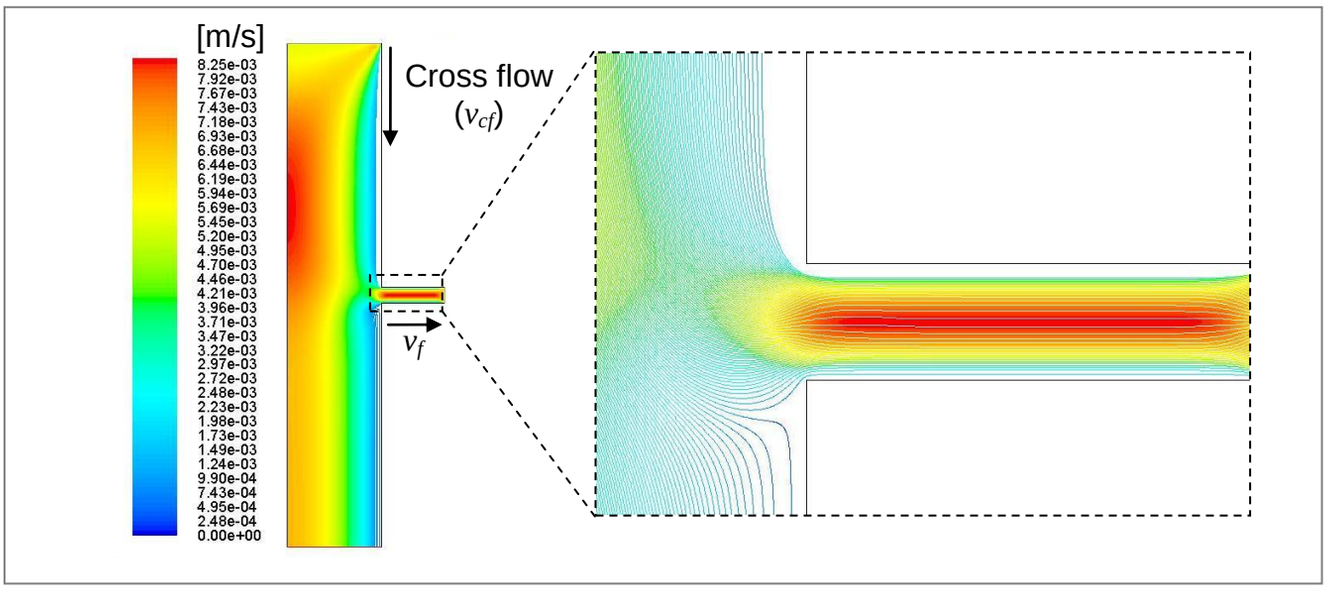

Fig D. Particle trajectories tracked from the cross flow inlet and coloured by flow velocity. Particle trajectories simulated for 20 nm particles and for a cross flow inlet velocity $v_{cf} = v_f$ = 5.5e-3 m/s

A comparison of the number of particles (N_{mod}) that flow into the TP2 as given by the numerical model and the number of particles (N_{TP}) calculated from Equation 6.5, for all investigated particle sizes was carried out to investigate the effect of the cross flow on the number of particles that are actually sucked into the TP2 and thus the concentration of particles flowing into the TP2. Table A. shows the number of particle trajectories into the TP2 with respect to the number of particles expected to flow into the TP2, for a total number of particle tracks from the cross flow inlet N_{cf} = 10,000.

Table A.: Comparison of the number of particle trajectories into the TP2 given by the numerical model (N_{mod}) compared to the analytically calculated particle tracks (N_{TP}) neglecting shear forces and inertia. N_{cf} = 10,000 Paticles tracked from the cross flow inlet. For all simulations, an inlet TP2 velocity v_f is set at 5.5e-3 m/s

Ratio of v_f/v_{cf}	v_{cf} (m/s)	Total number of particle trajectories (N_{TP}) using equation 3.15	Number of particle trajectories into the TP2 (N_{mod})					
			20 nm	300 nm	1 µm	3 µm	6 µm	3 µm
10/1	5.5e-4	10000	10000	10000	10000	10000	10000	10000
1/1	5.5e-3	1667	1644	1664	1644	1644	1642	1640
1/10	5.5e-2	167	148	148	148	148	145	142
1/20	1.1e-1	84	49	49	49	48	44	38
1/30	1.65e-1	56	12	12	12	11	5	0
1/50	2.75e-1	33	0	0	0	0	0	00

Ideally, the ratio of N_{mod} to N_{TP} is equal to 1, which means that the sampled concentration is not affected by the cross flow. The ratio N_{mod}/N_{TP} is plotted in Fig E with respect to particle size, for all modelled TP to cross flow velocity ratios (v_f/v_{cf}).

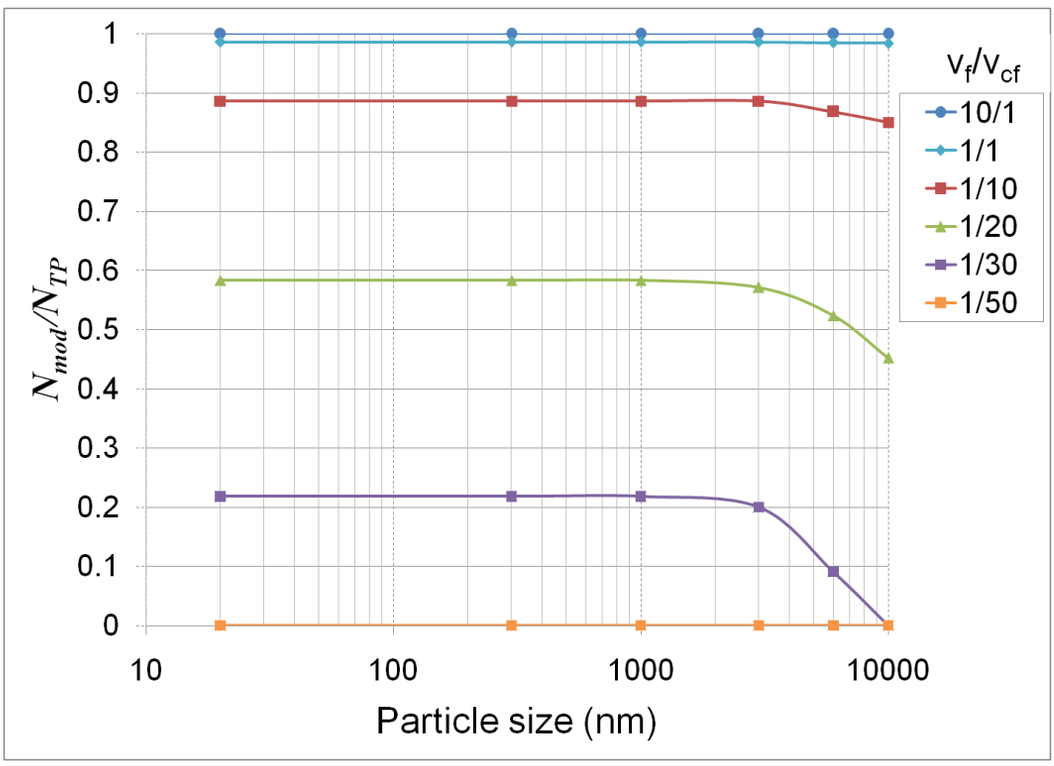

Fig E. Ratio of modelled particle trajectories Nmod to analytically calculated particle trajectories N_{TP} with respect to particle size and for different flow ratios (v_f/v_{cf}), for a total number (N_{cf}) of 10,000 particle trajectories tracked from the cross flow inlet

It can therefore be concluded that the TP2 can effectively (> 90%) sample ambient or workplace aerosol concentrations for surrounding (cross flow) velocities up to 10 times the sampling inlet velocity of the TP. Higher wind velocities at the inlet of the TP2 shall cause the TP2 to sample a concentration which is lower that the ambient aerosol concentration. It must however be noted that these simulations are very idealized. In the case of toxicological studies where the TP2 samples reproduce particle exposure of a worker, in case of extreme cross wind conditions at work places, the same effect can be seen in the particle number concentration up through the nostrils of a worker.

Lebenslauf:

Nkwenti Azong-Wara

Berufliche Erfahrung

Seit 07.2011	**Systemingenieur** bei Siemens AG im Bereich Auslegung von Klimatisierungssysteme für Schienenfahrzeuge.
12.2007 – 06.2011	**Wissenschaftlicher Mitarbeiter** im Bereich "Luftreinhaltung und Nachhaltige Nanotechnologie" am Institut für Energie- und Umwelttechnik (IUTA e.V.), Duisburg.
	Promotionsthema: “Development and Evaluation of a Thermophoretic Personal Sampler for Nanoparticle Exposure Studies“

Veröffentlichungen (als Erstautor)

1. N. Azong-Wara, C. Asbach, B. Stahlmecke, H. Fissan, H. Kaminski, S. Plitzko, T.A.J. Kuhlbusch. **Optimisation of a thermophoretic personal sampler for nanoparticle exposure studies**. *In J Nanoparticle Res.* **11**:1611-1624, 2009

2. N. Azong-Wara, C. Asbach, B. Stahlmecke, H. Fissan, H. Kaminski, S. Plitzko, T.A.J. Kuhlbusch. **Design and experimental evaluation of a thermophoretic personal sampler**. *In J Nanoparticle Res*. DOI 10.1007/s11051-013-1530-8

Akademischer Werdegang

10.1999 – 10.2007 **Studium:** Informations- und Kommunikationstechnik (auslandsorientierter Master Studiengang), Schwerpunkt: Kommunikationstechnik, Universität Duisburg – Essen.

04.2007 – 10.2007 **Masterarbeit:** ***"Entwicklung einer Software zur Dateninversion einer Mobilitätsanalyse"***
Eine ausgewählte Methode aus der Studienarbeit zur Dateninversion für DMA-basierte Größenbestimmungen wurde in einer Software implementiert. Die Dialogsfeldbasierende Software wurde mit Visual C++ entwickelt.

12.2006 – 03.2007 **Studienarbeit:** ***"Entwicklung einer Methode zur Dateninversion eines Differentiellen Mobilitätsbasierten Partikelgroßenerfassungssystems (DMPS)***
Literaturrecherche und Vergleich der existierenden Methoden zur Dateninversion für DMA-basierte Größenbestimmungen. Die beste Methode wurde ausgewählt und die notwendigen mathematischen Formeln hergeleitet.

Schulausbildung

09.1995 – 06.1997 S.H.C Bda (entspr. Oberstufe), Kamerun **(G.C.E. A-Level)**
09.1990 – 06.1995 S.H.C Bda (entspr. Gymnasium), Kamerun **(G.C.E. O-Level)**

Nkwenti Azong-Wara